

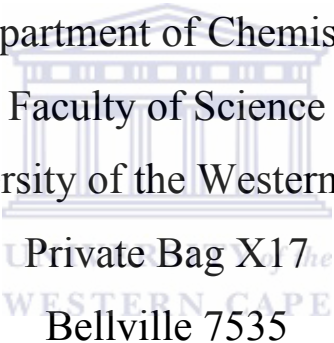
Metal Complexes based on Monomeric and Dendrimeric Pyrrole-  
Imine Ligands as Catalytic Precursors

By

Jane Ngima Mugo

A thesis submitted in partial fulfillment of the requirements for the  
ward of Masters of Science degree.

Department of Chemistry  
Faculty of Science  
University of the Western Cape  
Private Bag X17  
Bellville 7535

The logo of the University of the Western Cape, featuring a stylized classical building with columns and a pediment, with the text 'UNIVERSITY OF THE WESTERN CAPE' overlaid in a light blue color.

Supervisor: Prof Selwyn Mapolie

June 2007

---

## Declaration

I declare that the thesis, **Metal Complexes based on Monomeric and Dendrimeric Pyrrole-Imine Catalytic Precursors**, is my original work and has never been presented for the award of any degree at any other university before and that all the information sources used and or quoted have been indicated and acknowledged by means of complete reference.

Name: Jane Ngima Mugo

Signature:



UNIVERSITY of the  
WESTERN CAPE

Date:

---

## Table of Contents

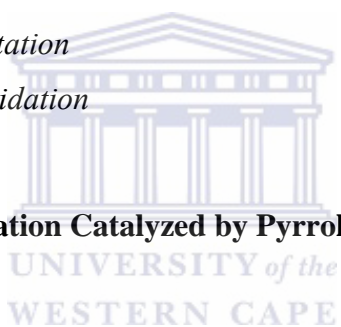
<i>Declaration</i>	<i>ii</i>
<i>Table of Contents</i>	<i>iii</i>
<i>List of Figures</i>	<i>vii</i>
<i>List of Schemes</i>	<i>xi</i>
<i>Abbreviations</i>	<i>xii</i>
<i>Acknowledgement</i>	<i>xiv</i>
<i>Abstract</i>	<i>xv</i>
<b>Chapter 1 : Review of Isolated as well as Immobilized Schiff Base Complexes and their Application as Oxidation Catalysts</b>	<b>1</b>
<i>1.1: General</i>	<i>2</i>
<i>1.2: Schiff base ligands and other N, N-chelates</i>	<i>3</i>
<i>1.2.1: Catalytic application of pyrrolylaldiminato metal complexes</i>	<i>6</i>
<i>1.3: Immobilization of Schiff base metal complexes</i>	<i>10</i>
<i>1.3.1: Mesoporous silicate MCM-41</i>	<i>14</i>
<i>1.4: Alkene epoxidation</i>	<i>15</i>
<i>1.4.1: Active species in oxidation of alkenes</i>	<i>17</i>
<i>1.4.2: Homogeneous catalysts for alkene epoxidation</i>	<i>18</i>
<i>1.4.3: Heterogeneous catalysts for alkene epoxidation</i>	<i>23</i>
<i>1.4.4: Epoxidation of alkenes with hydrogen peroxide as oxidant</i>	<i>27</i>
<i>1.5: Phenol oxidation</i>	<i>28</i>
<i>1.5.1: Homogeneous catalytic oxidation</i>	<i>29</i>
<i>1.5.2: Heterogeneous catalytic oxidation</i>	<i>32</i>
<i>1.6: Aim and scope of this thesis</i>	<i>34</i>
<i>1.7: References</i>	<i>35</i>

---

<b>Chapter 2 : Synthesis and Characterization of Pyrrole–imine Based Ligands, their Cu(II), Co(II) and Ni(II) Complexes and the Immobilization of Cu(II) and Ni(II) Complexes onto mesoporous MCM-41</b>	<b>38</b>
<i>2.1: Introduction</i>	39
<i>2.1.1: Dendrimers</i>	40
<i>2.1.2: Metallodendrimers</i>	42
<i>2.1.3: Highly ordered MCM-41</i>	44
<i>2.2 Results and discussion</i>	45
<i>2.2.1 Synthesis and characterization of the aliphatic substituted pyrrole-imine ligand and its Cu(II), Co(III) and Ni(II) complexes</i>	45
<i>2.2.2: Synthesis and characterization of the aromatic substituted pyrrole-imine ligand and its Cu(II) and Ni(II) complexes</i>	51
<i>2.2.3: Synthesis and characterization of the dendrimeric pyrrole-imine ligand and its Cu(II), Ni(II) and Co(II) complexes</i>	58
<i>2.2.4: Synthesis and characterization of the 3-aminopropyltriethoxysilane functionalized pyrrole-imine ligand and its Cu(II) and Ni(II) complexes</i>	61
<i>2.2.5: Synthesis of MCM-41, immobilization and characterization of the Cu(II) and Ni(II) complexes</i>	65
<i>2.3: Experimental</i>	71
<i>2.3.1: Materials and instrumentation</i>	71
<i>2.3.2: Molecular structure determination using single crystal X-ray analysis</i>	72
<i>2.3.3: Ligand synthesis</i>	73
<i>2.3.4: Synthesis of complexes</i>	75
<i>2.3.5: Synthesis of mesoporous MCM-41</i>	78
<i>2.3.6: Immobilization of the metal complexes</i>	79
<i>2.4: Conclusion</i>	80
<i>2.5: References</i>	81

---

<b>Chapter 3 : Cyclohexene Oxidation Mediated by Pyrrole–imine based Catalyst</b>	
<b>Precursors</b>	<b>83</b>
<i>3.1: Introduction</i>	84
<i>3.2: Results and discussion</i>	85
<i>3.2.1: Oxidation of cyclohexene</i>	85
<i>3.2.2: Catalytic oxidation of cyclohexene using mononuclear catalysts</i>	88
<i>3.2.3: Catalytic oxidation of cyclohexene using dendrimeric and MCM-41 immobilized catalysts</i>	98
<i>3.2.4: Homogeneous versus heterogeneous catalysts</i>	108
<i>3.3: Conclusions</i>	109
<i>3.4: Experimental</i>	109
<i>3.4.1: Materials and instrumentation</i>	109
<i>3.4.2: Catalytic cyclohexene oxidation</i>	110
<i>3.5: References</i>	110
<b>Chapter 4 : Phenol Hydroxylation Catalyzed by Pyrrole-imine Complexes</b>	<b>112</b>
<i>4.1: Introduction</i>	113
<i>4.2: Results and discussion</i>	116
<i>4.2.1: Hydroxylation of phenol</i>	116
<i>4.2.2: The effect of pH on phenol conversion using mononuclear catalysts</i>	119
<i>4.2.3: The effect of pH on phenol conversion using dendrimeric catalysts</i>	120
<i>4.2.4: The effect of pH on phenol conversion using MCM-41 supported catalysts</i>	122
<i>4.2.5: The effect of pH on catalyst selectivity</i>	123
<i>4.2.6: Effect of the nature of the metal on</i>	128
<i>4.2.7: Heterogeneous versus homogeneous catalyst</i>	128
<i>4.2.8: Effect of H<sub>2</sub>O<sub>2</sub> concentration on</i>	130
<i>4.3: Conclusion</i>	131
<i>4.4: Experimental</i>	131
<i>4.4.1: Materials and instrumentation</i>	131
<i>4.4.2: Phenol hydroxylation</i>	132



---

<i>4.5: References</i>	<i>132</i>
<b>Chapter 5 : Summary and Future Work</b>	<b>134</b>
<i>5.1: Summary</i>	<i>135</i>
<i>5.2: Future work</i>	<i>136</i>



---

## List of Figures

Figure 1.1: Some examples of pyrrole-imine Schiff bases	3
Figure 1.2: General structure of a pyrrolyaldiminato complex	4
Figure 1.3: General structure of a salicyaldiminato complex	5
Figure 1.4: Example of a Ru(II) pyrrole-imine complex	6
Figure 1.5: Cr(II) pyrrolyaldiminato complex	6
Figure 1.6: Neutral Ni(II) complexes of pyrrole imine ligands	7
Figure 1.7: Ti(IV) complex of pyrrole-imine ligands	8
Figure 1.8: Pyrrolyaldiminato Nickel complex	9
Figure 1.9: Dibenzyl Hf(IV) pyrrolyaldiminato complexes	10
Figure 1.10: Cu(II) Schiff base complex immobilized onto MCM-41	12
Figure 1.11: MCM-41 immobilized Ru(II) complex	13
Figure 1.12: Mn(III) complex (t-salpr) tethered on MCM-41	13
Figure 1.13: Diagrammatic representation of MCM-41	14
Figure 1.14: General structure of metalloporphyrin complexes	19
Figure 1.15: A model for oxygen transfer showing the less-hindered approach for cis-alkenes than for trans-alkenes	20
Figure 1.16: Iron porphyrin complexes	21
Figure 1.17: N,N-bis(salicylidene)ethylene diamine metal complex	22
Figure 1.18: N, N'-bis (2-hydroxyphenyl) ethylenediimine	23
Figure 1.19: Co(II) N-alkyl salicyaldiminato complex	23
Figure 1.20: Diagrammatic representation of Co(II) N-alkyl salicyaldiminato complex supported on MCM-41	25
Figure 1.21: Mn(III) salen type complex (CAT1) anchored onto the AMPTSi/HMS material	26
Figure 1.22: Mn(III) salen type complex (CAT2) anchored onto the AMPTSi/HMS material	27
Figure 1.23: General structure of metalloporphyrin (ML)	30
Figure 1.24: Structure of $[\text{Ni}(\text{Me}_4\text{R}_2\text{Bzo}[14]\text{tetraeneN}_4)]$ , (R= H, CH <sub>3</sub> , Cl, NO <sub>2</sub> )	30
Figure 1.25: Structure of metal complex of N,N'-bis(salicylidene)ethane-1, 2-diamine	31

Figure 1.26: Structure of H <sub>2</sub> salpn ligand	32
Figure 1.27: Structure of H <sub>2</sub> saldien ligand	33
Figure 2.1: Different dendritic architectures of catalyst located at the (a) periphery, (b) core (c) focal point of a wedge, (d) and periphery of a wedge	41
Figure 2.2: Poly (propylene imine) 1st generation dendrimer, DAB-PPI-(NH <sub>2</sub> ) <sub>4</sub>	42
Figure 2.3: Palladium metallodendrimer	43
Figure 2.4: <sup>1</sup> H-NMR spectrum of N-[-1H-pyrrol-2-ylmethylene]propan-1-amine, <b>L1</b>	46
Figure 2.5: Molecular diagram of complex <b>C3</b> drawn with 30% probability ellipsoids	49
Figure 2.6: <sup>1</sup> H-NMR Spectrum of N-(2,6-diisopropylphenyl)-N-[(1E)-1H-pyrrol-2-ylmethylene]amine, <b>L2</b>	52
Figure 2.7: Molecular diagram of <b>C4</b> drawn with 50% probability ellipsoids	54
Figure 2.8: Molecular structure of <b>C5</b> shown with 50 % probability ellipsoids	55
Figure 2.9: <sup>1</sup> H-NMR Spectrum of DAB-PPI-(N=CH(C <sub>4</sub> H <sub>3</sub> NH) <sub>4</sub> ), <b>L3</b>	59
Figure 2.10: ESI-MS spectrum of DAB-PPI-(N=CH(C <sub>4</sub> H <sub>3</sub> NH) <sub>4</sub> ), <b>L3</b>	60
Figure 2.11: ESI-MS spectrum of <b>L4</b>	63
Figure 2.12: Condensation and hydrolysis of <b>C9</b>	64
Figure 2.13: FT-IR spectrum of MCM-41	65
Figure 2.14: XRD patterns of calcined MCM-41, <b>Cu-MCM-41</b> and <b>Ni-MCM-41</b>	66
Figure 2.15: Nitrogen sorption isotherm of MCM-41, <b>Cu-MCM-41</b> and <b>Ni-MCM-41</b>	68
Figure 2.16: The Powder XRD pattern of <b>Co-MCM-41</b>	70
Figure 2.17: The Powder XRD patterns of <b>L4-MCM-41</b> and <b>Na-MCM-41</b>	70
Figure 3.1: Mononuclear pyrrolyaldiminato complexes	86
Figure 3.2: Dendrimeric pyrrolyaldiminato complexes	86
Figure 3.3: MCM-41 immobilized pyrrolyaldiminato complexes	87
Figure 3.4: Product distribution of the mononuclear pyrrolyaldiminato catalysts, [M <sup>2+</sup> ] = 6.0 x 10 <sup>-3</sup> molL <sup>-1</sup> ; M: H <sub>2</sub> O <sub>2</sub> : cyclohexene = 1:400:400.	93
Figure 3.5: Product distribution of the mononuclear pyrrolyaldiminato catalysts, [M <sup>2+</sup> ] = 1.2 x 10 <sup>-2</sup> molL <sup>-1</sup> ; M: H <sub>2</sub> O <sub>2</sub> : cyclohexene = 2:400:400.	94
Figure 3.6: Product distribution of the mononuclear pyrrolyaldiminato catalysts, [M <sup>2+</sup> ] = 3.0 x 10 <sup>-3</sup> molL <sup>-1</sup> ; M: H <sub>2</sub> O <sub>2</sub> : cyclohexene = 0.5:400:400.	95



Figure 3.7: Product distribution of the mononuclear pyrrolyaldiminato catalysts, $[M^{2+}] = 6.0 \times 10^{-3} \text{ molL}^{-1}$ ; M: $\text{H}_2\text{O}_2$ : cyclohexene = 1:200:400.	96
Figure 3.8: Product distribution of the mononuclear pyrrolyaldiminato catalysts, $[M^{2+}] = 6.0 \times 10^{-3} \text{ molL}^{-1}$ ; M: $\text{H}_2\text{O}_2$ : cyclohexene = 1:800:400.	96
Figure 3.9: Product distribution of the mononuclear pyrrolyaldiminato catalysts, $[M^{2+}] = 6.0 \times 10^{-3} \text{ molL}^{-1}$ ; M: $\text{H}_2\text{O}_2$ : cyclohexene = 1:200:200.	97
Figure 3.10: Product distribution of the supported pyrrolyaldiminato catalysts, $[M^{2+}] = 6.0 \times 10^{-3} \text{ molL}^{-1}$ ; M: $\text{H}_2\text{O}_2$ : cyclohexene = 1:400:400.	103
Figure 3.11: Product distribution of the supported pyrrolyaldiminato catalysts, $[M^{2+}] = 1.2 \times 10^{-2} \text{ molL}^{-1}$ ; M: $\text{H}_2\text{O}_2$ : cyclohexene = 2:400:400.	104
Figure 3.12: Product distribution of the supported pyrrolyaldiminato catalysts, $[M^{2+}] = 3.0 \times 10^{-3} \text{ molL}^{-1}$ ; M: $\text{H}_2\text{O}_2$ : cyclohexene = 0.5:400:400.	104
Figure 3.13: Product distribution of the supported pyrrolyaldiminato catalysts, $[M^{2+}] = 6.0 \times 10^{-3} \text{ molL}^{-1}$ ; M: $\text{H}_2\text{O}_2$ : cyclohexene = 1:400:200.	105
Figure 3.14: Product distribution of the supported pyrrolyaldiminato catalysts, $[M^{2+}] = 6.0 \times 10^{-3} \text{ molL}^{-1}$ ; M: $\text{H}_2\text{O}_2$ : cyclohexene = 1:800:400.	106
Figure 3.15: Product distribution of the supported pyrrolyaldiminato catalysts, $[M^{2+}] = 6.0 \times 10^{-3} \text{ molL}^{-1}$ ; M: $\text{H}_2\text{O}_2$ : cyclohexene = 1:200:200.	107
Figure 3.16: 7-oxabicyclo[4,1,0]hepta-2-one	107
Figure 4.1: Mononuclear pyrrolyaldiminato complexes	115
Figure 4.4.2: Dendrimeric pyrrolyaldiminato complexes	115
Figure 4.3: MCM-41 immobilized pyrrolyaldiminato complexes	116
Figure 4.4: Phenol conversion for the catalysts evaluated	117
Figure 4.5: Catechol and hydroquinone ratio for the mononuclear copper catalyst, <b>C1</b>	125
Figure 4.6: Catechol and hydroquinone ratio for the mononuclear nickel catalyst, <b>C2</b>	125
Figure 4.7: Catechol and hydroquinone ratio for the dendrimeric copper catalyst, <b>C6</b>	126
Figure 4.8: Catechol and hydroquinone ratio for the dendrimeric nickel catalyst, <b>C7</b>	126
Figure 4.9: Catechol and hydroquinone ratio for the MCM-41 supported copper catalysts, <b>Cu-MCM-41</b>	127
Figure 4.10: Catechol and hydroquinone ratio for the MCM-41 supported nickel catalysts, <b>Ni-MCM-41</b>	127

---

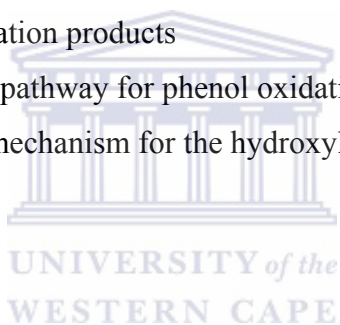
## List of Tables

Table 1.1: Summary of common methodologies for metal complex immobilization	11
Table 2.1: Characterization data for <b>L1</b> , <b>C1</b> , <b>C2</b> and <b>C3</b>	47
Table 2.2: Crystal data and structure refinement parameters for <b>C3</b>	50
Table 2.3: Selected bond lengths and angles for <b>C3</b>	51
Table 2.4: Characterization data for <b>L2</b> , <b>C4</b> , and <b>C5</b>	53
Table 2.5: Summary of crystal data and structure refinement parameters for <b>C4</b> and <b>C5</b>	56
Table 2.6: Selected bond lengths and angles for <b>C4</b>	57
Table 2.7: Selected bond lengths and angles for <b>C5</b>	58
Table 2.8: Characterization data for <b>L3</b> , <b>C6</b> , <b>C7</b> and <b>C8</b>	61
Table 2.9: Characterization data for <b>L4</b> , <b>C9</b> and <b>C10</b>	65
Table 2.10: Characterization data for MCM-41, <b>Cu-MCM-41</b> and <b>Ni-MCM-41</b>	67
Table 3.1: Cyclohexene oxidation catalyzed by mononuclear complexes in CH <sub>3</sub> CN	91
Table 3.2: Oxidation of cyclohexene by dendrimeric complexes in CH <sub>3</sub> CN	99
Table 3.3: Oxidation of cyclohexene MCM-41 immobilized complexes in CH <sub>3</sub> CN	102
Table 4.1: Effect of pH on catalytic activity of mononuclear catalysts	120
Table 4.2: Effect of pH on catalytic activity of dendrimeric catalysts	121
Table 4.3: Effect of pH on catalytic activity of MCM-41 immobilized catalysts	123
Table 4.4: Effect of H <sub>2</sub> O <sub>2</sub> concentration (PhOH:H <sub>2</sub> O <sub>2</sub> ) on phenol hydroxylation	130

---

## List of Schemes

Scheme 1.1: Stoichiometric or catalytic alkene epoxidation	15
Scheme 1.2: Possible reaction pathways in the epoxidation of alkenes	18
Scheme 1.3: Proposed pathway for the oxidation of phenol	29
Scheme 2.1: Synthetic route to N-[(1E)-1H-pyrrol-2-ylmethylene]propan-1-amine, <b>L1</b>	45
Scheme 2.2: Fragmentation pattern for <b>L1</b>	47
Scheme 2.3: Synthetic route of Cu(II) complex, <b>C1</b>	48
Scheme 2.4: Synthetic route to (2,6-diisopropylphenyl)-N-[(1E)-1H-pyrrol-2-ylmethylene]amine, <b>L2</b>	52
Scheme 2.5: Synthetic route to dendrimeric ligand, DAB-PPI-(N=CH(C <sub>4</sub> H <sub>3</sub> NH)) <sub>4</sub> , <b>L3</b>	59
Scheme 2.6: Synthetic route to triethoxysilane functionalized pyrrole-imine ligand, <b>L4</b>	62
Scheme 3.1: Cyclohexene oxidation products	88
Scheme 4.1: Proposed reaction pathway for phenol oxidation in the aqueous phase	114
Scheme 4.2: Proposed radical mechanism for the hydroxylation of phenol to catechol and hydroquinone	118



---

## Abbreviations

AMPTSi	3-aminopropyltriethoxysilane
AAS	Atomic absorption spectrometry
BQ	Benzoquinone
CT	Catechol
CTAB	Cetyltrimethylammonium bromide
C	Complex
CH	Cyclohexene
Cp	Cyclopentadiene
eV	Electron volt
ESI-MS	Electrospray ionization mass spectrometry
FT-IR	Fourier transform infrared spectroscopy
GC	Gas chromatography
GC-MS	Gas chromatography mass spectrometry
HMS	Hexagonal mesoporous silica
Hq	Hydroquinoline
HQ	Hydroquinone
L	Ligand
LCT	Liquid crystal templating mechanism
ML	Metalloporphyrin
MAO	Methylaluminoxane
$M_w/M_n$	Molecular weight distribution
Saldien	N,N'-bis(salicylidene)diethylenetriamine
Salen	N,N'-bis(salicylidene)ethane-1,2-diamine
Salpn	N,N'-bis(salicylidene)propane-1,3-diamine
t-Salpr	3-[N,N'-bis-3-(3,5-di-tert-butylsalicylidemino)propyl]amine
NMR	Nuclear magnetic resonance
PDI	Poly dispersity index
PE	Polyethylene
i-Bu <sub>3</sub> Al	Triisobutylaluminium
TOF	Turn over frequency

---

TON	Turn over number
TEOS	Tetraethyl orthosilicate
XRD	X-ray diffraction



---

## Acknowledgement

I would like to thank my supervisor Prof. Selwyn Mapolie for his professional guidance and support through the research project and advice that shaped this thesis. I extend my sincere appreciation to Dr. Ilia A. Guzei, for solving the crystal structures, Ms. Juanita Van Wyk for running the NMR spectra and Mr. Timothy Lesch for the assistance with the instruments especially the HPLC and GC. I am also very thankful to WRC-SA and NRF-SA for the funding. To my colleagues in the UWC organometallic research group, thank you for the useful discussions.

My gratitude also goes to Prof. G. C. Mwangi and Prof. O. Yoshiko for financial support, my thanks to my family for their prayers, support and encouragement – mum, dad, Nyaguthii, Mutugi, Gituru and Wairiuko. And to my friends Ng'ang'a Kibandi, Irene Wangui, James Kariuki, Edwin Kimathi, Lydia and Gerald Chege, Mary and Patrick Ndururi, Frankline Keter, Stephen Ojwach, and Dr. Gitari, I appreciate your support through this processes. Finally I thank God for the gift of life, guidance and protection.



UNIVERSITY *of the*  
WESTERN CAPE

---

## Abstract

Pyrrole–imine ligands were prepared by condensation of pyrrole-2-carboxylaldehyde with propyl amine, 2,6-diisopropylaniline, poly(propylene) imine dendrimer and 3-aminopropyl-triethoxysilane to give the desired ligands in good yields. These ligands were characterized via combination of techniques to establish the molecular structure. These include  $^1\text{H-NMR}$ ,  $^{13}\text{C-NMR}$ , and FT-IR spectroscopy and ESI-MS spectrometry. Microanalysis was performed to confirm the purity of the product. Complexes of these ligands were then prepared from  $\text{Cu}(\text{OAc})_2 \cdot \text{H}_2\text{O}$ ,  $\text{Ni}(\text{OAc})_2 \cdot 4\text{H}_2\text{O}$  and  $\text{Co}(\text{OAc})_2 \cdot 4\text{H}_2\text{O}$ . The complexes were also characterized by electrospray ionization mass spectrometry (ESI-MS), FT-IR and the purity also confirmed by microanalysis. Single crystal X-ray crystallography of complexes  $(\text{C}_3\text{H}_7)\text{N}=\text{CH}(\text{C}_4\text{H}_3\text{N}-2)_3\text{Co}$  (**C3**),  $(2,6-i\text{-Pr}_2\text{C}_6\text{H}_3)\text{N}=\text{CH}(\text{C}_4\text{H}_3\text{N}-2)_2\text{Cu}$  (**C4**) and  $2,6-i\text{-Pr}_2\text{C}_6\text{H}_3)\text{N}=\text{CH}(\text{C}_4\text{H}_3\text{N}-2)_2\text{Ni}$  (**C5**) was performed to determine the molecular structure. The three structures show that the complexes formed are mononuclear. The structures reveal that the ligands are bidentate coordinated with a *trans*-geometry.

The inorganic support MCM-41 was prepared by the hydrolysis of tetraethylorthosilicate in the presence of a templating agent cetyltrimethylammonium bromide. The triethoxysilane functionalized complexes of copper and nickel were then covalently anchored onto this support and characterized by FT-IR spectroscopy,  $\text{N}_2$  sorption and X-ray diffraction. Highly crystalline MCM-41 material was obtained and the crystallinity was retained after the immobilization of the metal complexes as evident from the XRD results.  $\text{N}_2$  sorption studies showed that the MCM-41 material synthesized was of high surface area.

These catalysts showed moderate to high activity efficiency in the oxidation of cyclohexene with  $\text{H}_2\text{O}_2$  as oxidant in an oxygen atmosphere. The copper catalysts were the most active with low product selectivity. However, the nickel systems were the most selective with only two products, 2-cyclohexene-1-one and cyclohexene oxide, being the only observed products. The homogeneous systems were found to be more active than the heterogeneous ones.

---

In the oxidation of phenol to the dihydroxylbenzenes (catechol and hydroquinone), the activity of the nickel and copper catalysts were found to be highly dependent on the pH of the system. The optimal pH was established to be between 3 and 4 for all the catalysts. At pH lower than 3, all the catalysts showed dramatic reduction in activity while at higher pH the activity initially reduced after which it leveled out. With regard to selectivity, all the catalysts were more selective for catechol over hydroquinone.





**Chapter 1 : Review of Isolated as well as  
Immobilized Schiff Base Complexes and their  
Application as Oxidation Catalysts**



## 1.1: General

Over the recent past, organometallic chemistry has grown and the impact of catalytic applications in various chemical technologies has rapidly evolved from the realm of academic laboratories into full-scale industrial processes.<sup>1</sup>

Nowadays it is generally agreed that the key step in catalytic reactions is the interaction of reactive molecules with the active sites of homogeneous, heterogeneous or biological (enzyme) catalysts<sup>2</sup>. Development of well-defined catalysts that enable rapid and selective chemical transformations and which can be separated completely from the products is still an unresolved challenge.<sup>3</sup>

Homogeneous and heterogeneous catalysts are both widely utilized for laboratory scale chemical reactions. However, in large scale commercial operations, heterogeneous catalysts are more frequently used due to the ease of separating the solid catalyst from the fluid media. The advantages of homogeneous catalysis are the inherent higher catalytic activity and selectivity, whereas those of most solid, heterogeneous catalysts are the relatively low cost and ease of catalyst and product separation. Ideally, a catalyst that can combine the recoverability/recyclability of heterogeneous systems with the selectivity of homogeneous catalysts is desired.<sup>4</sup>

Modern catalytic science faces even more complicated and challenging problems. These are concerned with the urgent necessity to create new effective industrial processes, which are selective, ecologically pure and consume minimum energy.<sup>5</sup> Environmental issues and recent developments in chemistry have introduced a number of compelling requirements that must be met in the development of practical catalysts, and in this context, recyclability is an important attribute.<sup>6</sup>

Oxidation is one of the most important reactions for the metabolism of biotic substrates and many enzymes are known to catalyze various types of oxidation. The search for new oxidation catalysts and improving existing technologies is one of the most important concerns for both industrial and academic research.<sup>7</sup>

This chapter is a review of the development of pyrrolyaldimine ligands, their late transition metal complexes and the applications thereof in various catalytic processes. It includes Schiff base metal complexes anchored onto inorganic supports such as MCM-41, which have been evaluated as catalyst carriers. In addition it covers homogeneous and heterogeneous catalytic oxidation of olefins and phenols.

## 1.2: Schiff base ligands and other N, N-chelates

Schiff bases are typically formed by the condensation of a primary amine and an aldehyde<sup>8</sup> (ketones will also form imines of type  $R_1R_2C=N-R_3$ , but the reaction tends to occur less rapidly than with aldehydes). The presence of a dehydrating agent normally favours the formation of the Schiff bases. The resultant functional group  $R_1HC=N-R_2$  is called an imine and is capable of binding metal ions via the N atom, especially when used in combination with one or more other donor atoms to form a chelating ligand. The R groups may be aryls or alkyls. Examples of a few pyrrole-based Schiff base compounds are shown in Figure 1.1.

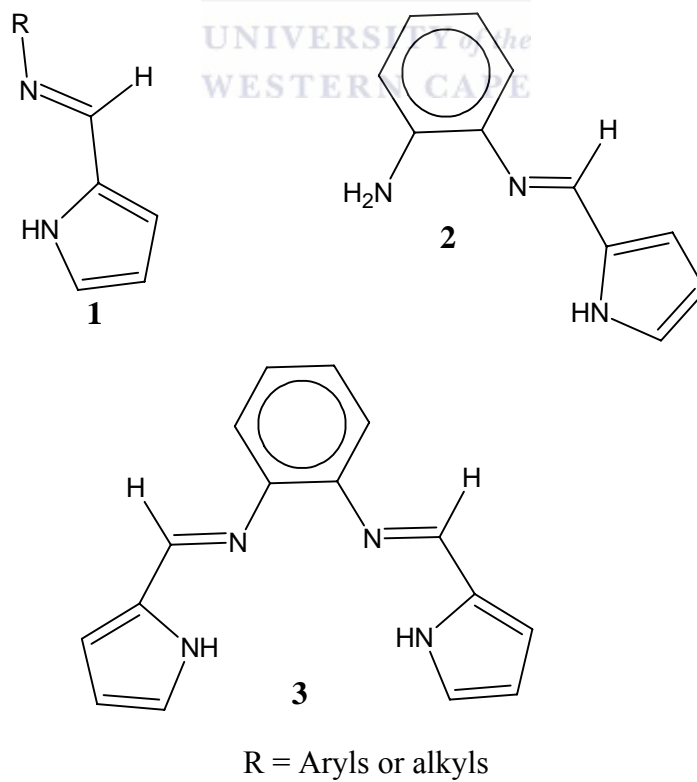
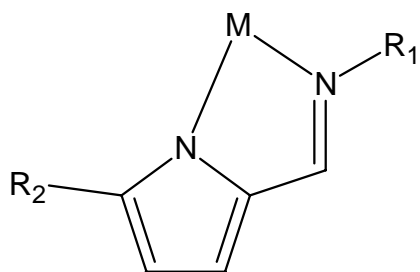


Figure 1.1: Some examples of pyrrole-imine Schiff bases

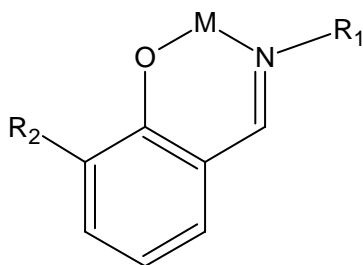
The synthetic flexibility of these compounds has resulted in their diverse structural designs.<sup>9</sup> Active and well designed Schiff bases are considered useful ligands that are able to stabilize many different metals in various oxidation states. Steric and electronic properties of these ligands may be varied by simply changing the substituents. This facilitates controlling of the performance of the metal complexes in variety of useful catalytic transformations and transmits chiral information to produce non-racemic products through a catalytic process. Either chiral aldehydes or amines can also be used.<sup>10</sup> Metal complexes of Schiff base ligands have played an important role in the development of coordination chemistry because of the structural and electronic versatility they offer.<sup>11</sup>

Mono-anionic bidentate nitrogen ligands are of current interest particularly for the preparation of low-valent, low coordinate metal complexes of hard transition and main group elements, for which intriguing structure and reactivity patterns have emerged.<sup>12</sup> Pyrrolylaldimine ligands are closely related to salicylaldimine ligands, which often yield metal complexes that exhibit specific chemical transformations in both a stoichiometric and a catalytic manner. Both pyrrolylaldimine and salicylaldimine ligands are easily prepared and have similar steric demands; their steric and electronic properties may be varied by simply changing the substituents (R groups). The chelating pyrrolylaldiminato ligand forms five-membered ring systems with metal ions, Figure 1.2, whereas salicylaldiminato complexes tend to form six-membered rings, Figure 1.3.



4

Figure 1.2: General structure of a pyrrolylaldiminato complex



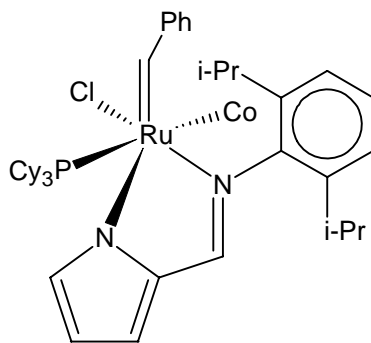
5

 $R_1 = \text{Aryl or alkyl}, R_2 = \text{alkyl}$ 

Figure 1.3: General structure of a salicylaldiminato complex

However metal complexes containing the pyrrolyl moiety (pyrrolylaldiminato) have received much less attention. Only a few examples have been reported. Bis-chelating pyrrolylaldiminato ligands with bulky substituents have not drawn as much attention either as salicylaldiminato ligands, which have been shown to be excellent ligands for transition metals e.g. Zr, and Ni, that act as catalysts for various catalytic transformations e.g. olefin polymerization. Very recently, salicylaldiminato zinc compounds have been reported to be active for the copolymerization of  $\text{CO}_2$  and epoxides.<sup>13</sup>

The pyrrolylaldiminato complexes may either be formed by *in situ* formation of the pyrrole-imine and concomitant complexation to metal center via template-type synthesis, or by prior formation of the imine ligand and subsequent reaction to form the desired metal complex. The later synthetic method being most favourable because ancillary ligands can also be attached to the metal center Ru(II)<sup>14</sup>, Cr(II)<sup>15</sup>, and Ni(II)<sup>16</sup> whilst with the former, template-type synthesis; bis (pyrrole-imine) metal complexes appear to be the favoured product.

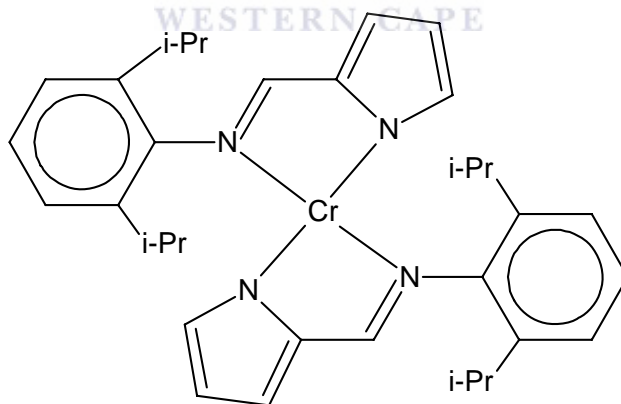


6

Figure 1.4: Example of a Ru(II) pyrrole-imine complex

### 1.2.1: Catalytic application of pyrrolyaldiminato metal complexes

The main application for the reported pyrrolyaldiminato metal complexes is in polymerization and oligomerization of olefins. These complexes exhibit high activity and are based on main group metals<sup>13</sup>, early and late transition metal complexes. Gibson *et al.*<sup>15</sup> reported activity of up to  $1.2 \times 10^2 \text{ gmmol}^{-1}\text{h}^{-1}\text{bar}^{-1}$  in ethylene polymerization with a Cr(II) complex bearing two bulky N,N-chelating monoanionic pyrrole-imine ligands  $\{\text{ArN}=\text{CH}(\text{C}_4\text{H}_3\text{N}-2)\}_2\text{Cr}$  where  $\text{Ar} = 2,6\text{-}i\text{-Pr}-(\text{C}_6\text{H}_3)$  as shown in Figure 1.5.

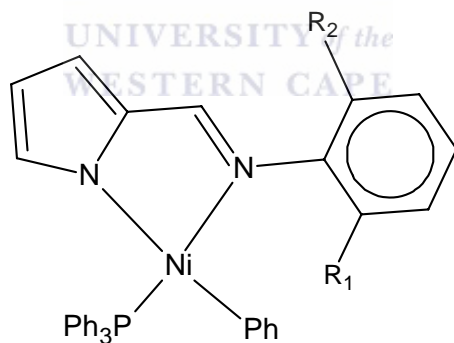


7

Figure 1.5: Cr(II) pyrrolyaldiminato complex

Li *et al.*<sup>16</sup> reported neutral Ni(II) complexes (Figure 1.6) that exhibit extremely high catalytic activities for the vinylic polymerization of norbornene and produced high molecular weight polynorbornene, in the presence of methylaluminoxane (MAO) under

moderate conditions similar to the neutral salicylaldiminato Ni(II) complexes. The yields, molecular weights as well as catalyst activities depended significantly on the reaction conditions. Variation of the molar ratios of Al:Ni, using **8a** showed considerable effects on the polymer yields, molecular weights and catalyst activities. The activity ranged from  $3.6 \times 10^6$  g polym (mol Ni)<sup>-1</sup>h<sup>-1</sup> at Al:Ni, 1000:1 to  $8.8 \times 10^6$  g polym (mol Ni)<sup>-1</sup>h<sup>-1</sup> at Al:Ni, 2000:1. It was also observed that the structure of the neutral Ni(II) complexes had an effect on the polymer yields and activities under the same experimental conditions. Bulky substituents in the ortho position of the aromatic group attached to the imino nitrogen atom hinder the insertion of norbornene. The decrease of steric hindrance is favorable to the insertion reaction of norbornene. Hence, **8a** in Figure 1.6 with two large substituents displays the lowest catalytic activity and produces polymers with the lowest molecular weight. **8d** with only one substituent displayed the highest catalytic activity and produces polymers with the highest molecular weight among the four catalysts. All polymers display relatively high molecular weights of up to  $1.3 \times 10^6$  g (mol Ni)<sup>-1</sup>.



**8a:** R1 =R2 = *i*-Pr

**8b:** R1=*i*-Pr. R2=Me

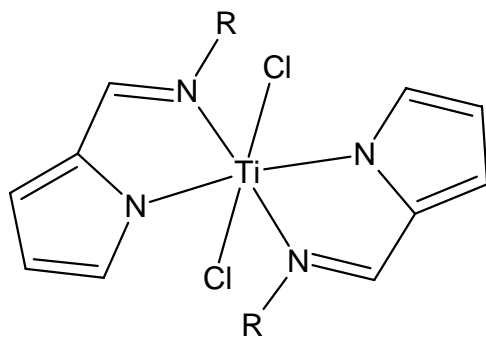
**8c:** R1 = R2 = Et

**8d:** R1=*t*-Bu, R2=H

Figure 1.6: Neutral Ni(II) complexes of pyrrole imine ligands

Yoshida *et al.*<sup>17</sup> reported a Ti(IV) complex having two non-symmetrical bidentate pyrrole-imine chelate ligands, Figure 1.7. These complexes were evaluated in the

polymerization of ethylene with MAO as cocatalyst. They displayed very high activities and produced high molecular weight polyethylene. Activities of  $1.4 \times 10^4$  kg polymer  $(\text{mol Ti})^{-1}\text{h}^{-1}$  were obtained and these are comparable to what was obtained using  $\text{Cp}_2\text{TiCl}_2$ . High molecular weight ( $M_w$ ) polyethylene of up to  $2.6 \times 10^6$  was obtained. Alternatively, using  $[\text{Ph}_3\text{C}]\text{B}(\text{C}_6\text{F}_5)_4/i\text{-Bu}_3\text{Al}$  as a co-catalyst, ultrahigh molecular weight polyethylene ( $M_w > 4.0 \times 10^6$ ) and activities of  $1.5\text{-}2.0 \times 10^3$  kg polymer  $(\text{mol Ti})^{-1}\text{h}^{-1}$  were reported. The molecular weight distribution ( $M_w/M_n$ ) of the polyethylene was 2.21 indicating that the polymer is produced by a single-site catalyst. Complexes **9b** and **9c** exhibited lower activities of  $4.0 \times 10^2$  and  $8.0 \times 10^2$  kg polymer  $(\text{mol Ti})^{-1}\text{h}^{-1}$  with high  $M_w$  values of  $4.12 \times 10^5$  and  $4.41 \times 10^5$  respectively. Complex **9d** showed very high activity of  $1.4 \times 10^4$  kg polymer  $(\text{mol Ti})^{-1}\text{h}^{-1}$  with a very high  $M_w$  value of  $2.6 \times 10^6$ . These are the highest activities reported for homogeneous titanium complexes which do not contain cyclopentadiene (Cp) ligands. It was observed that an increase in the bulkiness of the R group resulted in enhanced activity. This activity enhancement was attributed to the effective separation between the cationic active species and the anionic co-catalyst as a result of the attachment of bulkier alkyl substituents to the imino nitrogen.



**9a:** R=Ph

**9b:** R=Et

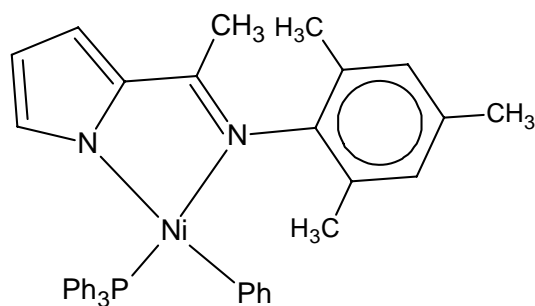
**9c:** R=*n*-hexyl

**9d:** R=cyclohexyl

Figure 1.7: Ti(IV) complex of pyrrole-imine ligands



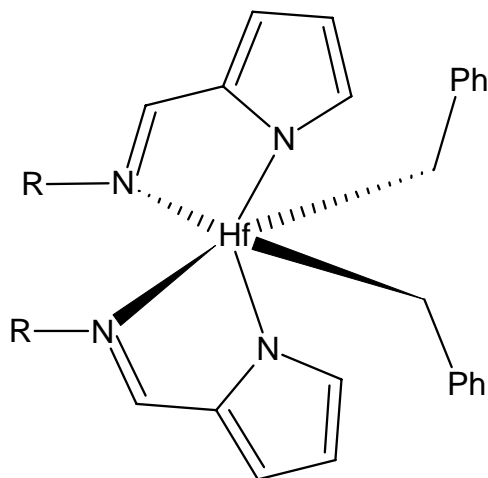
Bellarbarba *et al.*<sup>18</sup> also reported a Ni(II) complex, **10**, and preliminary test for catalytic ability in the oligomerisation of olefins in the presence of a phosphine scavenger such as [Ni(COD)<sub>2</sub>]. An activity at 25° C was estimated to be  $1.3 \times 10^3$  g oligomer (mol Ni)<sup>-1</sup>h<sup>-1</sup>bar<sup>-1</sup>. This value corresponds to non-optimized oligomerisation conditions.



**10**

Figure 1.8: Pyrrolylaldiminato Nickel complex

Dibenzyl hafnium(IV) complexes with pyrrole-imine ligands as shown in Figure 1.9 were reported by Matsui *et al.*<sup>19</sup>. Complex **11c** showed activity of up to  $2.2 \times 10^3$  g (PE) (mmol Hf)<sup>-1</sup>h<sup>-1</sup>bar<sup>-1</sup> with a M<sub>w</sub> value of  $8.8 \times 10^4$  in the presence of triisobutylaluminium (i-Bu<sub>3</sub>Al) in ethylene polymerization. When [Ph<sub>3</sub>C]B(C<sub>6</sub>F<sub>5</sub>)<sub>4</sub> was used as a co-catalyst in the presence of (i-Bu<sub>3</sub>Al), a polymer with a PDI of 2.07 was obtained. This compares favorably with PDI values normally obtained from other single site catalysts. In the case where MAO was used as the cocatalyst, activity of  $1.2 \times 10^3$  g (PE) (mmol Hf)<sup>-1</sup>h<sup>-1</sup>bar<sup>-1</sup> with **11c** was reported. This activity is of the same order of magnitude as that found using titanium complexes with pyrrole-imine ligands under the same polymerization conditions.



**11a:** R=1-*i*-Pr-4-methylbenzene

**11b:** R= *i*-Pr

**11c:** R=*t*-Bu

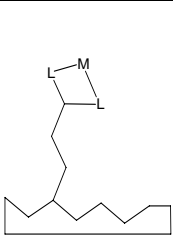
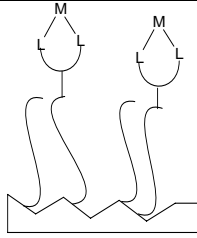
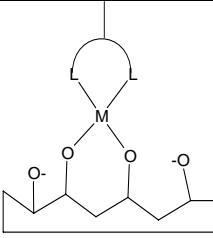
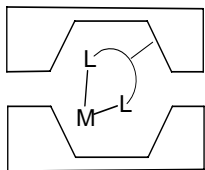
Figure 1.9: Dibenzyldi Hf(IV) pyrrolylaldiminato complexes

### 1.3: Immobilization of Schiff base metal complexes

Catalytic transition metal complexes tethered to organic or inorganic supports have received much attention in the past few decades because they can, in principle, combine the advantages of homogeneous and heterogeneous catalysts. There are many synthetic techniques that have been utilized to immobilize molecular homogeneous catalysts onto supports.

These complexes can be tethered on silica surfaces through a ligand in the complex which has alkoxy- or chlorosilane functional groups (ion pair) that react with surface hydroxyl groups on the SiO<sub>2</sub> or by impregnating the homogeneous catalyst onto a solid support.<sup>20</sup> This may be achieved by using an ion-exchange resin to bind anionic catalysts, encapsulating inorganic complexes into pores of chemically modified silica such as MCM-22, MCM-41 and MCM-48 or zeolites, or covalently binding coordination complexes onto modified silica as illustrated in Table 1.1. At present there is considerable academic and commercial interest in the immobilization of well-defined homogenous catalysts.<sup>21-24</sup>

Table 1.1: Summary of common methodologies for metal complex immobilization<sup>4</sup>

				
<b>Immobilization method</b>	covalent ligand binding	physisorption	ion pair	encapsulation
<b>Application</b>	broad	restricted	restricted	restricted
<b>Drawbacks</b>	preparation	competition with solvents	competition with polar or ionic substrates	substrate size diffusion

The immobilization results in heterogeneous catalysts that tend to have reduced activity relative to their homogeneous analogues. However, this drawback can be offset by the advantages of simplification of reaction procedures, easy separation of products, catalyst recovery, reduction of trace metal contamination, facile methods for parallel screening, and the possibility to design continuous flow processes. A widely studied approach to facilitate catalyst and product separation is the attachment of metal complexes onto insoluble organic, inorganic or hybrid supports. In an ideal case, the supported complexes can be recovered from reaction mixture by simple filtration, they do not contaminate the product solution by leaching, they can be recycled, and they can help increase selectivity. As transition metal complexes are often expensive to purchase or prepare, immobilization on a support enables simple extraction and recyclability, resulting in commercial advantages as well as ease of manipulation. The transformation from a homogeneous to a heterogeneous catalytic process is achieved by anchoring the active catalytic site on a solid having a large surface area.<sup>4</sup> Schiff bases are of the most versatile and thoroughly studied ligands, but very few reports are available on the polymer anchored Schiff bases and their application in catalysis. The encapsulations in

zeolites, immobilization onto mesoporous silica and polysiloxane membranes of metal complexes have been used with moderate to excellent results.

Singh *et al.*<sup>25</sup> reported copper-Schiff base MCM-41, Figure material, Figure 1.10. They confirmed by argon etching to a depth of 45 Å that the copper Schiff base complex was distributed both on the external surface (pore end) and within the pores of Si-MCM-41.

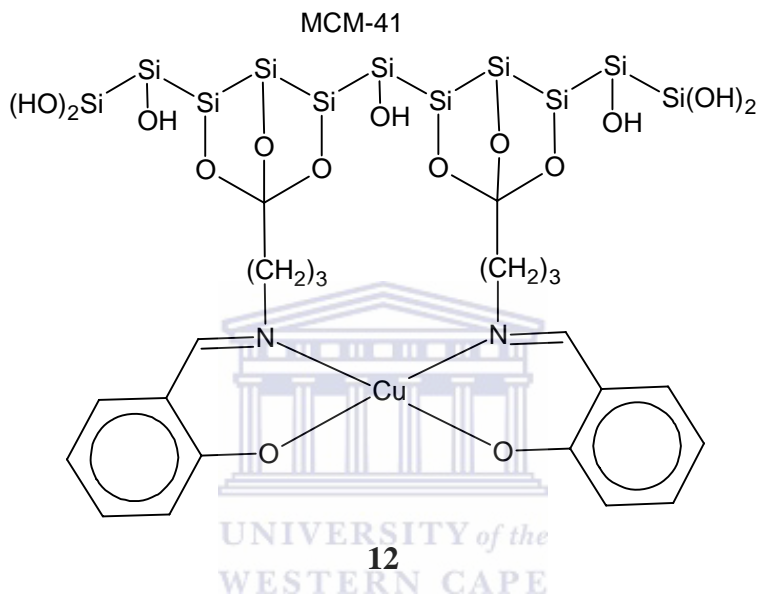


Figure 1.10: Cu(II) Schiff base complex immobilized onto MCM-41

De Clercq *et al.*<sup>5</sup> recently reported a Ru(II) complex that has been covalently anchored on MCM-41 as illustrated by Figure 1.11.

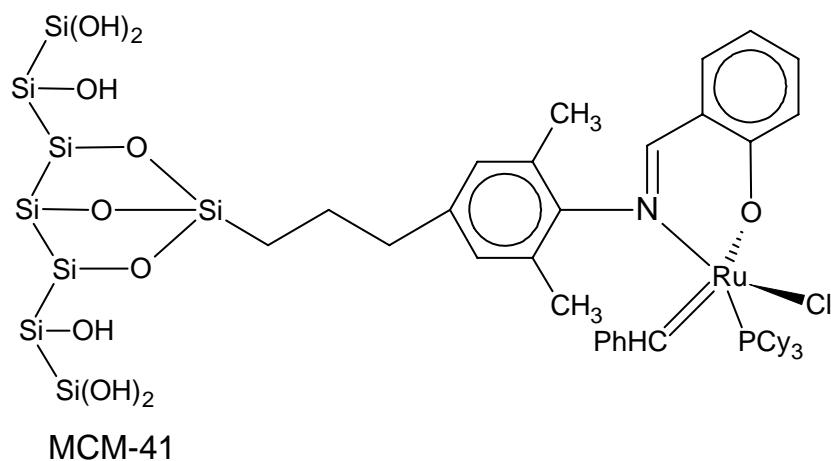
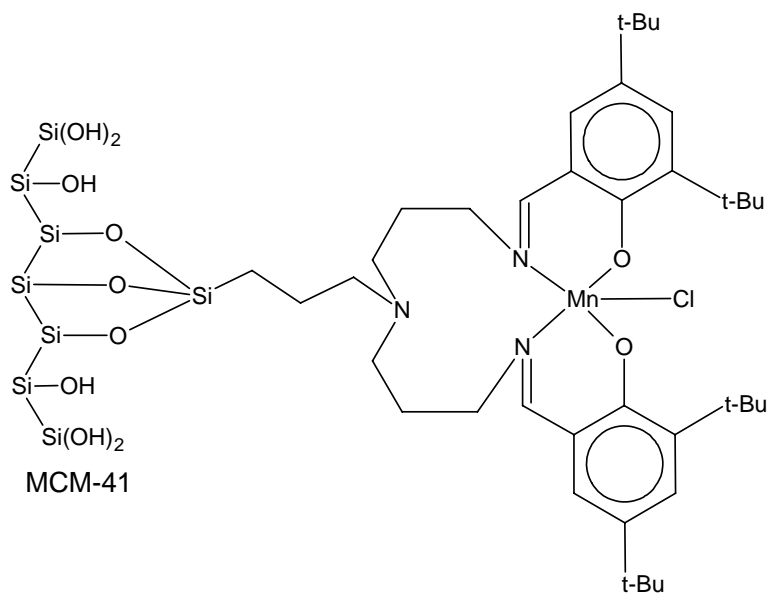


Figure 1.11: MCM-41 immobilized Ru(II) complex

Sutra and Brunel <sup>26</sup> reported a Mn(III) complex, **14**, of the pentadentate, 3-[N,N'-bis-3-(3,5-di-tert-butylsalicylideneamino)propyl]amine, (*t*-salpr), ligand anchored onto the surface of MCM-41. The ligand is linked to the silica surface by stable covalent Si-O-Si bonds. Additional apical ligands are added to tetradentate salen complexes in order to improve their catalytic activity. MCM-41 retained its regular pore structure even after functionalization.

Figure 1.12: Mn(III) complex (*t*-salpr) tethered on MCM-41

### 1.3.1: Mesoporous silicate MCM-41

In search of an appropriate support we were attracted to the inorganic support MCM-41, Figure 1.13. MCM-41 is of great interest in catalysis due to its textural properties: hexagonal array of unidimensional pores of sizes between 20 and 100 Å, specific surface areas of about 1500 m<sup>2</sup>g<sup>-1</sup>, which open the possibility of being used as supports or catalysts in the processing of complex hydrocarbons and pore volume of up to 1.3 cm<sup>3</sup>g<sup>-1</sup>. It is reported that the template free MCM-41 becomes featureless when exposed to moisture and subjected to mechanical compression.<sup>25</sup>

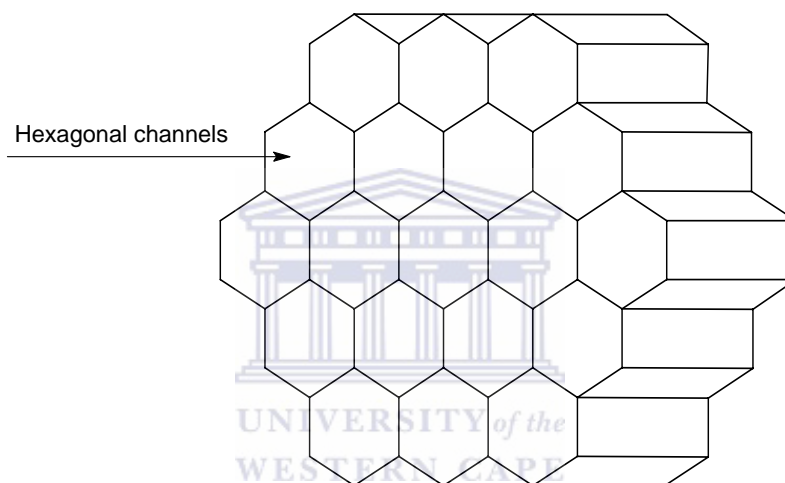


Figure 1.13: Diagrammatic representation of MCM-41

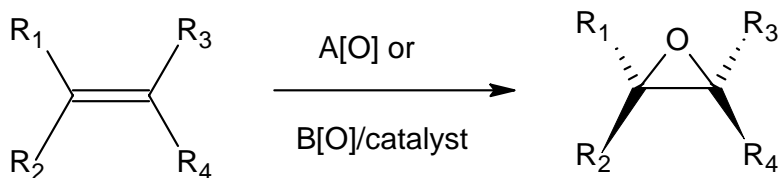
MCM-41 offers several advantages:

- Inorganic solids, particularly those having a structured large surface are more robust than organic polymers, have a considerably larger area and, therefore, larger activity should in principle be achievable with these solids.
- It retains a rigid exposed surface area, whereas conventional polymer beads typically swell and shrink variably in different media, often resulting in unpredictable effects on catalyst activity.
- Anchoring the active catalytic centers on high surface area solids would help to overcome the activity decrease generally found in going from homogeneous to heterogeneous catalysis due to inefficient interfacial mass transfer between the liquid and the solid phase.

- The MCM-41 solid support consists of an ordered array of hexagonal channels with a pore diameter in the mesoporous region, which permits a low diffusional resistance (cf. nanoporous zeolite support) for the reactant molecules to access the metal active site located within the channels.<sup>3</sup>

#### 1.4: Alkene epoxidation

Epoxides are important intermediates in laboratory research and industry.<sup>27</sup> The epoxide ring can readily be opened to produce 1,2-functionalities with a high degree of regio- and steric control (Scheme 1.1). Thus they can be employed as precursors for the development of drugs, agrochemicals and other additives. In other cases they are polymerized to form epoxy resins and used for the synthesis of several perfume materials, anthelmintic preparations, plasticizers, sweeteners and as solvents for synthetic cellulose esters, paints, enamels and lacquers.<sup>28</sup> Propene epoxide is a valuable product which is a strategically important and versatile chemical intermediate and whose manufacture accounts for about 10% of total European usage of propene. Two thirds of propene epoxide is consumed in the manufacture of polyether polyols, the rest being converted to propene glycols, glycol ethers and other materials that have a wide range of applications.



Scheme 1.1: (A) Stoichiometric or (B) catalytic alkene epoxidation<sup>34</sup>

Process A in Scheme 1.1 corresponds to stoichiometric oxidation. Typically this is achieved by transfer of oxygen from a reagent which has excess oxygen content, e.g. peroxyacid, hydrogen peroxide. Process B corresponds to the catalytic reaction. Again an oxygen-rich reagent is used and many catalysts are available based on various transition metals such as V, Mo and Cu complexes with hydroperoxides.<sup>29</sup> Efficient operation of these processes have major commercial and environmental impacts thus the catalyst used should have high efficiency. Most catalysts used in these industrial

processes are based on mixed metal oxides. Direct oxidation of hydrocarbons by  $O_2$  gives poor selectivity at high conversion, which limits conversion to a few percent in most practical situations. The inefficiency associated with low selectivity has motivated the search for solid catalysts with higher activity in selective oxidation.<sup>30</sup> Catalyzing of these reactions by transition metal complexes is an area of intense research. The discovery of group (VIII) transition metals that mediate olefin oxidations with hydroperoxides and other oxidizing agents presented a major breakthrough. Amongst the second row transition metals, ruthenium complexes are well known to catalyze oxidation reactions under mild conditions. But there are only a few industrially and preparatively useful liquid phase catalytic oxidation processes which do not compromise on the selectivity.

Various synthetic porphyrins have been widely used as model catalysts for the oxidation of olefins. Metalloporphyrins of the transition metal ions as well as other transition metal complexes with simple ligands have been used for this catalytic oxidation.<sup>31</sup> New processes for the oxidation of olefins have been developed with respect to environmental considerations to replace the chlorohydrin method. Green chemistry demands chemical processes for epoxide production via direct oxygen insertion into C=C bonds. Oxygen sources currently used include molecular oxygen, hydrogen peroxide, organic hydroperoxides and peracids.

Driving forces for search of new epoxidation catalysts are:

- Selectivity control; currently used catalysts lack selectivity. Conversion in some cases is pushed due to over-oxidation or partially oxidized products. This is caused by the general phenomenon that the said product molecules are more reactive than the reactants being oxidized.
- Environmental constraints; development of processes that produce less waste and have greater safety is essential.

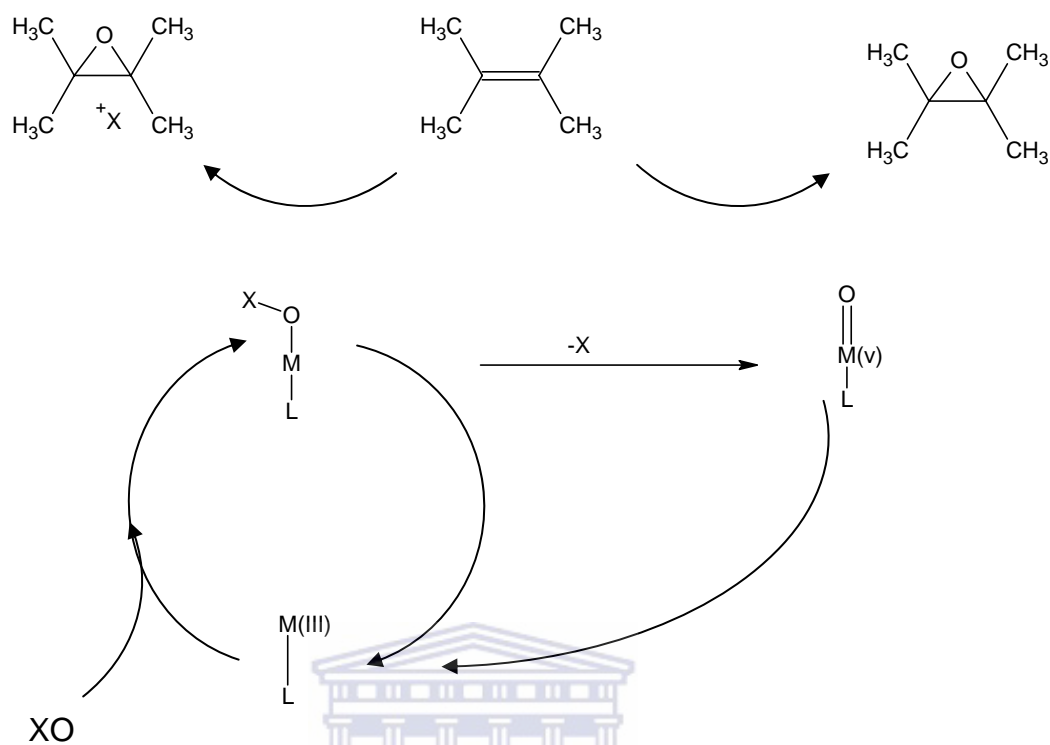


The literature in this area is extensive and difficult to segregate into sharply delineated categories, but a fair way to attempt this is according to the catalyst precursors which could be heterogeneous and homogeneous systems.<sup>32</sup>

#### ***1.4.1: Active species in oxidation of alkenes***

This area has attracted a great deal of interest, and recent studies on the nature of the active species demonstrate that there are still some important issues in need of resolution. In addition, a full understanding of the roles of the various experimentally detected species in the catalytic cycle has not yet been achieved. The study of the catalytic cycle is complicated by the fact that the turnover can be limited by re-oxidation of the catalyst used e.g. Mn (salen) complex. This can manifest itself in two ways, the re-oxidation reaction may be slow and/or in biphasic systems the concentration of oxidant in the organic layer may be limiting. The epoxidation reaction itself can also be extremely rapid.<sup>33</sup>

Adam *et al.*<sup>34</sup> described how the use of a range of oxidants in the epoxidation of *cis*-alkenes changed the ratio of *cis/trans*-epoxide. The fact that significantly different diastereoselectivities were observed with different oxidants caused these workers to propose that there is a second oxidation cycle operating in which the terminal oxidant is involved in substrate oxidation and that this is in competition with oxidation by  $O=Mn^V$  (salen). Scheme 1.2 shows their proposal for the two competing mechanisms. They also noted differences in diastereoselectivity with different counterions but explained these in terms of the two state reactivity hypotheses. Freire and co-workers<sup>35</sup> also observed that the outcome of the reaction was oxidant dependent and proposed that there was a possibility of two competing pathways.



Scheme 1.2: Possible reaction pathways in the epoxidation of alkenes<sup>34</sup>

## 1.4.2: Homogeneous catalysts for alkene epoxidation

### 1.4.2.1: Metalloporphyrin complexes

The first report of the use of metalloporphyrin complexes, the general structure of which is shown in Figure 1.14, as catalysts for epoxidation was by Groves et al.<sup>36</sup>.

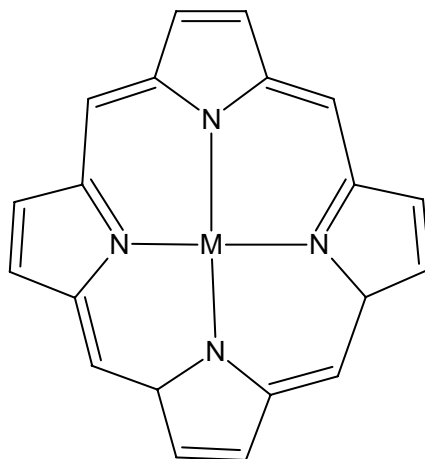


Figure 1.14: General structure of metalloporphyrin complexes

They reported that iron porphyrin complexes, chloro- $\alpha,\beta,\gamma,\delta$ -tetraphenylporphinatoiron (III) and chlorodimethylferriprotoporphyrin (IX), were capable of facilitating oxygen transfer from iodosylbenzene to saturated and unsaturated hydrocarbons. The yield for cyclohexene oxide was 55 % while that of cyclohexanol was 15 %. Traces of cyclohexanone were also detected. Similarly, cyclohexadiene gave 74 % yield of the corresponding epoxide. Oxidation of *trans*- and *cis*-stilbene gave their respective *trans*- and *cis*-stilbene oxides.

Later Groves and Kruper<sup>37</sup> applied the porphyrin chemistry to chromium and prepared the oxoporphinatochromium (V) complex,  $(Cr^{III}TPPCl)$ , [chlorotetraphenylporphinatochromium (III)] capable of epoxidising alkenes giving alcohols and epoxides in fair to excellent yields under catalytic and stoichiometric conditions. Norbonene epoxide was obtained in 99 % yield. It was also observed that metal oxo ( $M=O$ ) species were capable of acting as a staging post for oxygen transfer and these authors termed the process 'oxygen-rebound'. In 1982, Guilmet and Meunier<sup>38</sup> discovered that the reaction rate could be increased by up to 15 times and yields of epoxides improved somewhat by the addition of small amounts of pyridine derivatives in their study of the epoxidation of styrene catalyzed by an iron porphyrin complex. In no case was the pyridine *N*-oxide formed, indicating that the pyridine acts by co-ordinating to the metal centre. Increased reaction rate, chemoselectivity and stereoselectivity in the

presence of pyridine were also observed later on by Meunier *et al.*<sup>39</sup> Pyridine acted as an axial ligand to the metalloporphyrin. The epoxidation of simple alkenes was performed using manganese porphyrin complexes as catalysts and the more convenient bleach as the oxygen source.

In 1983 Groves and Nemo<sup>40</sup> reported their analysis of the mechanism of oxygen transfer from the oxometalloporphyrin to the alkene substrate. They noted that *cis*-alkenes were more reactive than *trans*-alkenes towards epoxidation and that there was a dramatic difference in selectivity. *Cis*-stilbene oxide was obtained in 77 % yield whilst *trans*-stilbene was unreactive towards epoxidation. This degree of selectivity was remarkable since typical epoxidising reagents such as peroxyacids were known to react with *cis*-alkenes twice as fast as the corresponding *trans*-alkene. A mechanism of the *side-on approach* shown in Figure 1.15 was proposed to explain the high degree of selectivity in the metalloporphyrin system.

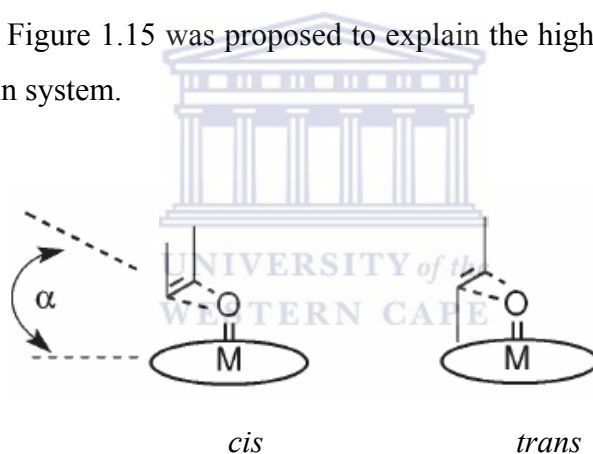


Figure 1.15: A model for oxygen transfer showing the less-hindered approach for *cis*-alkenes than for *trans*-alkenes adapted from ref 27.

This model is best explained as a stereo electronic effect. The incoming alkene approaches the metal oxygen bond from the side at an angle  $\alpha$ . When maximum overlap between the filled  $\pi$  orbitals of the approaching *cis*-alkene occurs with the  $\pi$  antibonding orbital of the metal-oxo group, the epoxide is formed in high yields. However, the approach for a *trans*-alkene involves an unfavourable steric interaction between one of the alkene substituents and the porphyrin plane. The degree of orbital overlap is now considerably less than that of the *cis*-alkene, the yield of epoxide is significantly lower and in some cases it is zero. They proposed that by structural modification of the

porphyrin plane, the angle of approach,  $\alpha$ , could be optimized to provide a high degree of selectivity and even enantioselectivity. Later on, Groves and Myers<sup>41</sup>, presented the catalytic asymmetric epoxidation of alkenes with chiral iron porphyrin complexes, Figure 1.16. Styrene derivatives afforded the highest selectivities in the case of the *cis* isomer.

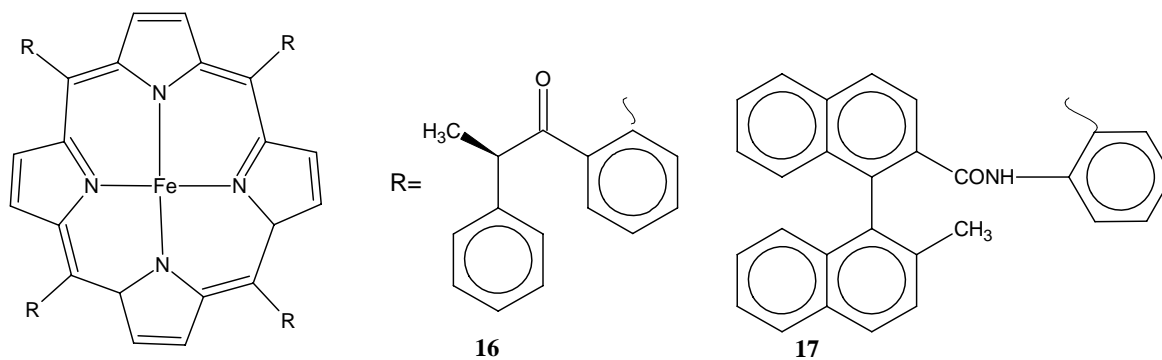


Figure 1.16: Iron porphyrin complexes

Currently manganese and iron porphyrins in the presence of H<sub>2</sub>O<sub>2</sub> are the most important catalyst types for epoxidation reactions. Porphyrins of other metals, such as molybdenum, give inferior conversions and selectivities.

#### 1.4.3.2: Non-porphyrin metal complexes

The tetradentate salen ligand, N,N-bis(salicylidene)ethylene diamine and over 2500 metal complexes of the type, **18**, based on substituted and unsubstituted salens as shown in Figure 1.17 have been described, making the system a standard in co-ordination chemistry. It was Kochi and co-workers who laid the foundation for metal-salen catalyzed epoxidation in a series of papers during the 1980's.<sup>42-44</sup> Their first reports concerned a series of cationic chromium salen complexes and their ability to epoxidise alkenes in both stoichiometric and catalytic reactions.

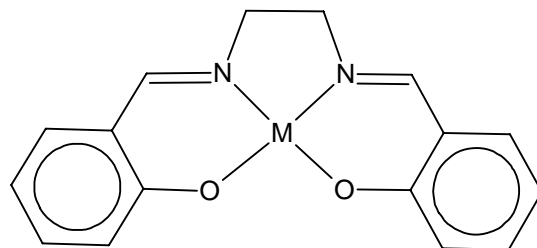
**18**

Figure 1.17: N,N-bis(salicylidene)ethylene diamine metal complex

The catalytic ability of Ni(II) Schiff base or macrocyclic complexes towards hydrocarbon oxidation have been well documented in the literature. It appears that a specific ligand environment is required for the Ni(II) to participate in catalysis with a particular oxidant. Nickel(II) Schiff base complexes based on the ligand, *N,N'*-bis(2-hydroxyphenyl)ethelenediimine (Figure 1.18) was reported by Chatterjee *et al.*<sup>45</sup>. The ability of Ni(II) complex of **19** to catalyze epoxidation of various olefins in the presence of sodium hypochlorite NaOCl was investigated. They observed that cyclohexene epoxide was obtained in 16 %, 1-hexene epoxide at 29 %, while *cis*- and *trans*-stilbene both gave *trans*-stilbene oxide at 13 % and 35 % yields, respectively. Nickel peroxide formation was evident as appearance of a fine black suspension in the reaction mixture was observed. They proposed formation of a high valent Ni(IV)-oxo species in the reaction as intermediate, as proposed by earlier workers.<sup>46</sup> This Ni(IV)-oxo species subsequently transfers its oxo-atom to the olefin. It was also suggested that the epoxide formation probably takes place through an open radical chain pathway as the catalytic system lacks stereospecificity. This could also account for the observation of substantial amounts of benzaldehyde (10 %) as side product in the oxidation of stilbenes. Epoxidation of olefins was found to be ineffective when CH<sub>3</sub>CN was used as solvent. They attributed this to the fact that formation of the Ni(IV)-oxo species (catalytically active intermediate) is not favoured kinetically as it perhaps involves the coordination of OCl<sup>-</sup> through the substitution of axially coordinated CH<sub>3</sub>CN (which is a stronger nucleophile than OCl<sup>-</sup>).

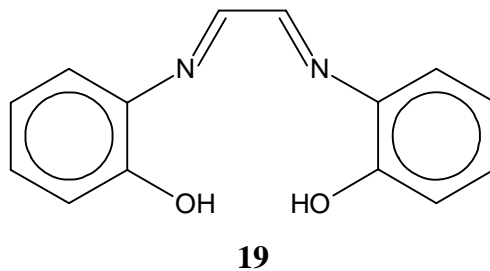


Figure 1.18: N, N' -bis (2-hydroxyphenyl) ethylenediimine

The oxidation reactions based on soluble catalysts Co(II) N-alkyl salicylaldiminato complex, **20**, was reported by Luo and co-workers<sup>47</sup> and showed conversion of about 41.7 % and a turnover frequency (TOF) of 15 mol (styrene) mol (Co)<sup>-1</sup> h<sup>-1</sup>. This was lower than what was observed for the immobilized analogue of **20**. This is probably due to the fact that the loading of active sites in the silica matrix of MCM-41 prevents the dimerization of active centers which happens in the case of the soluble catalyst.

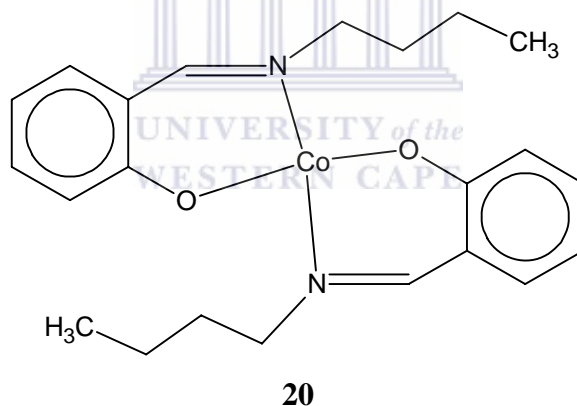


Figure 1.19: Co(II) N-alkyl salicylaldiminato complex

### 1.4.3: Heterogeneous catalysts for alkene epoxidation

Despite the interest, some of the drawbacks of homogeneous transition metal complexes as catalysts for selective epoxidation of olefins are:

- Low selectivity.
- Catalyst deactivation by auto-oxidation and  $\mu$ -dimerization through the formation of oxo bridges.
- High cost of complex preparation.

- Lack of recycling methods makes it difficult for application of this system on a large scale.

To avoid these problems, recent trends in immobilization of transition metal complexes on insoluble supports appear to be a good way of heterogenizing homogeneous catalysts. Such types of heterogenized – homogeneous catalytic systems not only offer the combined advantages of homogeneous catalysis (mild conditions) and heterogeneous catalysis (easier separation of the catalyst from the reaction medium) but also impose extreme shape selectivity in catalytic processes and increasing catalyst life time. Various strategies for immobilization can be employed.<sup>48</sup> Immobilization of Co(II), Ni(II), Mn(II), and Cu(II) complexes of the {H<sub>2</sub>: N,N'-bis(salicylidene)ethane-1,2-diamine} ligand onto alumina carrier has been reported. {H<sub>2</sub>: N,N'-bis(salicylidene)ethane-1,2-diamine} and its other substituted derivatives have also been encapsulated in a zeolite-Y matrix and their catalytic activities have been studied towards the decomposition of H<sub>2</sub>O<sub>2</sub> and selective epoxidation/oxidation of olefins. Luo *et al.*<sup>47</sup> reported a Co(II) N-alkyl salicylaldiminato complex supported onto MCM-41, **21**, that was active for the epoxidation of styrene giving a 56.5 % conversion after an hour with turnover frequencies (TOF) of 36 mol- (styrene) mol (Co)<sup>-1</sup> h<sup>-1</sup> (TOF determined after 1 hour). Recyclability evaluation of the catalyst was also undertaken. On the second run, the catalyst had lost its activity completely, while no leaching of the Co was detected. The reason for the deactivation of the catalyst was thought to probably be due to the dimerization of the Co(II) N-alkyl salicylaldiminato complex groups which are still close enough (1.25 nm apart) in the heterogeneous catalysts.



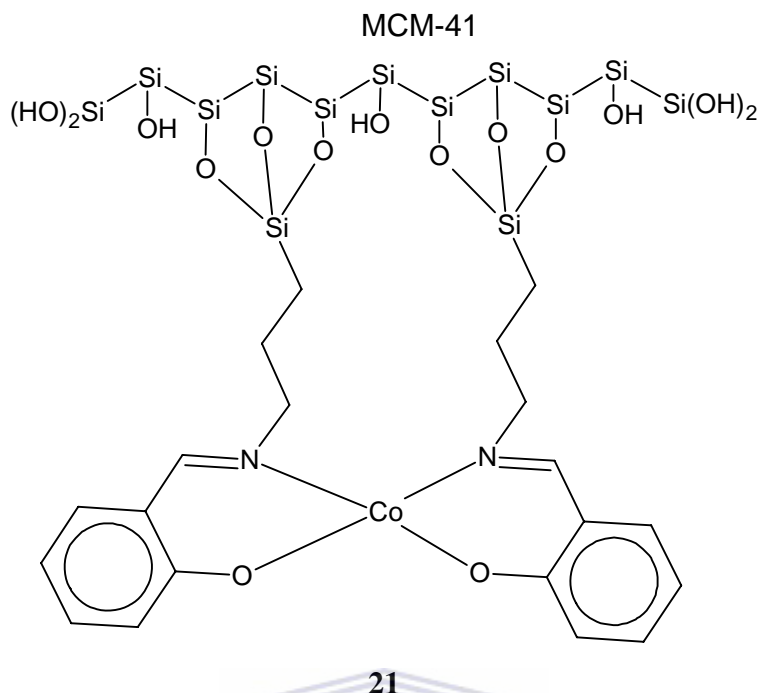


Figure 1.20: Diagrammatic representation of Co(II) N-alkyl salicylaldiminato complex supported on MCM-41

Dasa *et al.*<sup>49</sup> reported the catalytic activity of two Mn(III) salen complexes immobilized on AMPTSi/HMS in the epoxidation of styrene and methylstyrene. The two systems were (1*R*,2*R*)-[Mn(3,5-dtButsalhd)Cl], (CAT1), **22**, and 1*R*,2*R*)-[Mn(3,5-dtButsaldPh)Cl] (CAT2), **23**. CAT1 shows higher asymmetric induction than CAT2. It has been reported that the catalytic activity and enantioselectivity in asymmetric epoxidation of non-functionalized alkenes catalyzed by chiral Mn(III) salen complexes can be tuned by the introduction of groups on the aldehyde fragment and diimine bridge. The diimine bridging groups contribute to stereochemical effects, whereas the groups in the aldehyde fragment are related to electronic effects. Hence, in this case heterogenized CAT2 and the presence of cyanuric chloride probably reduced the electron density of the Mn(III) salen complex, thus leading to a significant decrease in the enantiomeric excess percentage (% ee). In heterogenized CAT1, its anchoring on the solid support probably lead to changes in the steric environment in the diimine bridge, and thus improved % ee was observed. The styrene conversions, turnover numbers (TON) and turnover frequency (TOF) were lower than the corresponding homogeneous phase reactions which

may be attributed to slow diffusion of the reactants into the AMPTSi/HMS porous structure.

Since both heterogeneous catalysts were enantioselective in the epoxidation of  $\alpha$ -methylstyrene, they were re-used in another catalytic experiment using the same epoxidation procedure after a convenient purification process. Similar catalytic results were obtained as in the first catalytic re-use indicating that they are recyclable under the experimental conditions. No significant changes were observed in their FT-IR spectra for the typical bands of the catalysts, indicating that no catalyst or ligand decomposition occurred. Nevertheless, after the epoxidation of  $\alpha$ -methylstyrene with NaOCl new bands appeared in the region of the bands due to the silica backbone in the spectra of both catalysts. This may be due to some extent of hydrolysis of the HMS Si–O–Si bonds because the reactions were performed under alkaline conditions.

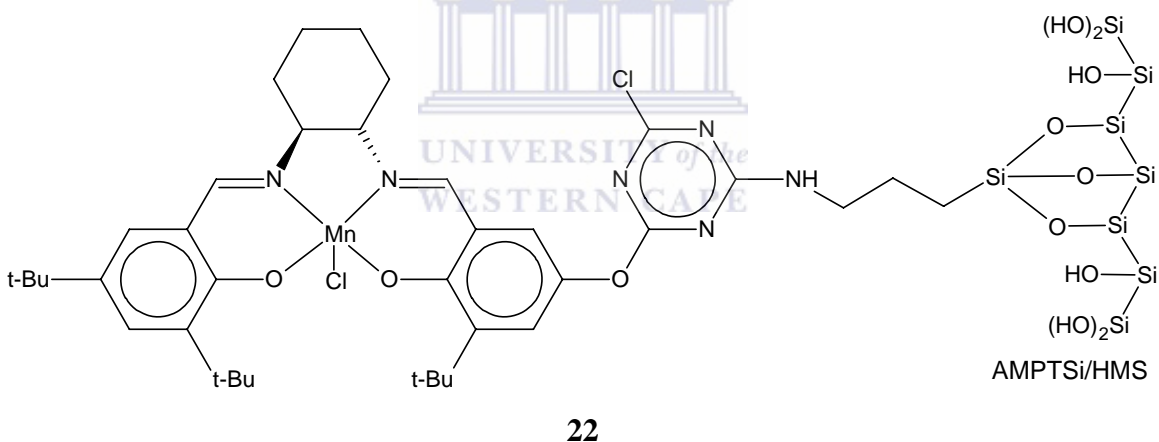
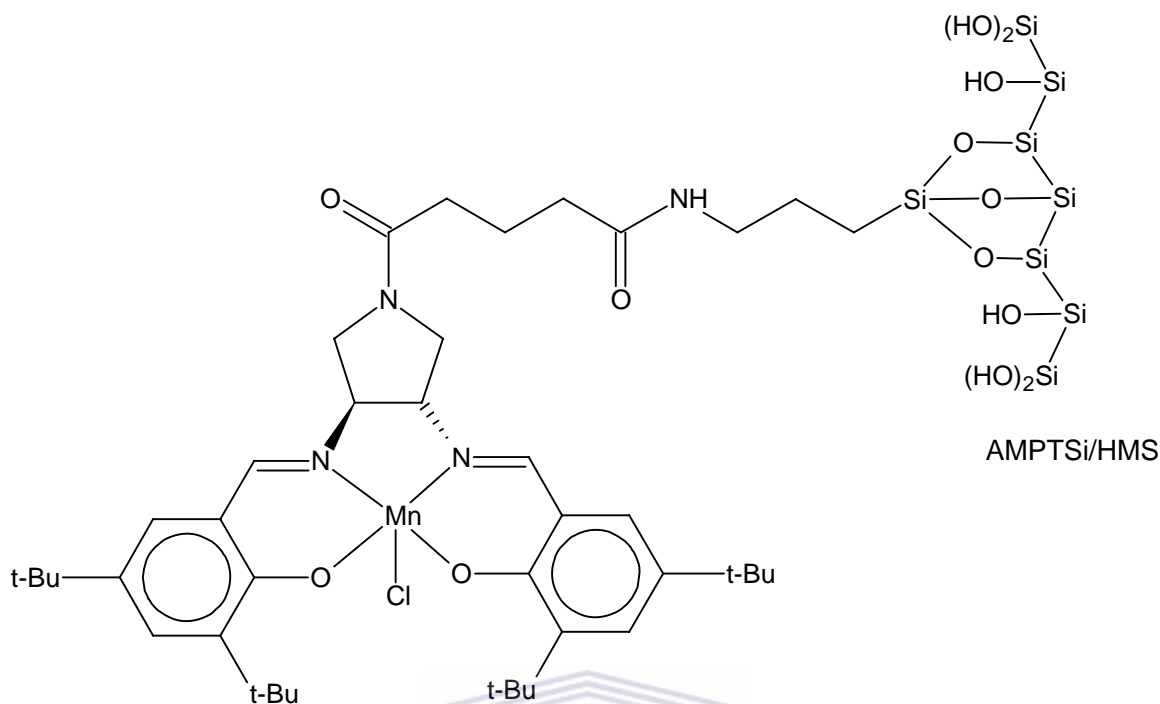


Figure 1.21: Mn(III) salen type complex (CAT1) anchored onto the AMPTSi/HMS material



23

Figure 1.22: Mn(III) salen type complex (CAT2) anchored onto the AMPTSsi/HMS material

UNIVERSITY of the  
WESTERN CAPE

#### 1.4.4: Epoxidation of alkenes with hydrogen peroxide as oxidant

Hydrogen peroxide is probably the best terminal oxidant after dioxygen with respect to environmental and economic considerations because the reaction affords only water as a by-product. Indeed, in certain circumstances, it is better than oxygen insofar as  $O_2$ /organic mixtures can sometimes spontaneously ignite. As a result, epoxidation systems that use hydrogen peroxide in conjunction with catalytic amounts of cheap, relatively nontoxic metals are potentially viable for large-scale productions. Heterogeneous systems for epoxidation of alkenes with  $H_2O_2$  are typically mineral-type catalysts, including zeolites or hydrotalcites. For instance, Ti-MWW (a zeolite having large, 10-membered ring channels in the siliceous framework, also known as MCM-22) mediates epoxidation of C6-C8 linear aliphatic alkenes with 30 %  $H_2O_2$  to produce a 4:1 ratio preference in favor of *E*-alkenes over their *Z*-isomers. This preference is related to the larger pore size, which also allows formation of C6-C8 epoxides in 80-85 % yield.

However, such systems tend to be used at slightly elevated temperatures (e.g., 60-70° C), which may lead to decomposition of sensitive products.<sup>37</sup>

### 1.5: Phenol oxidation

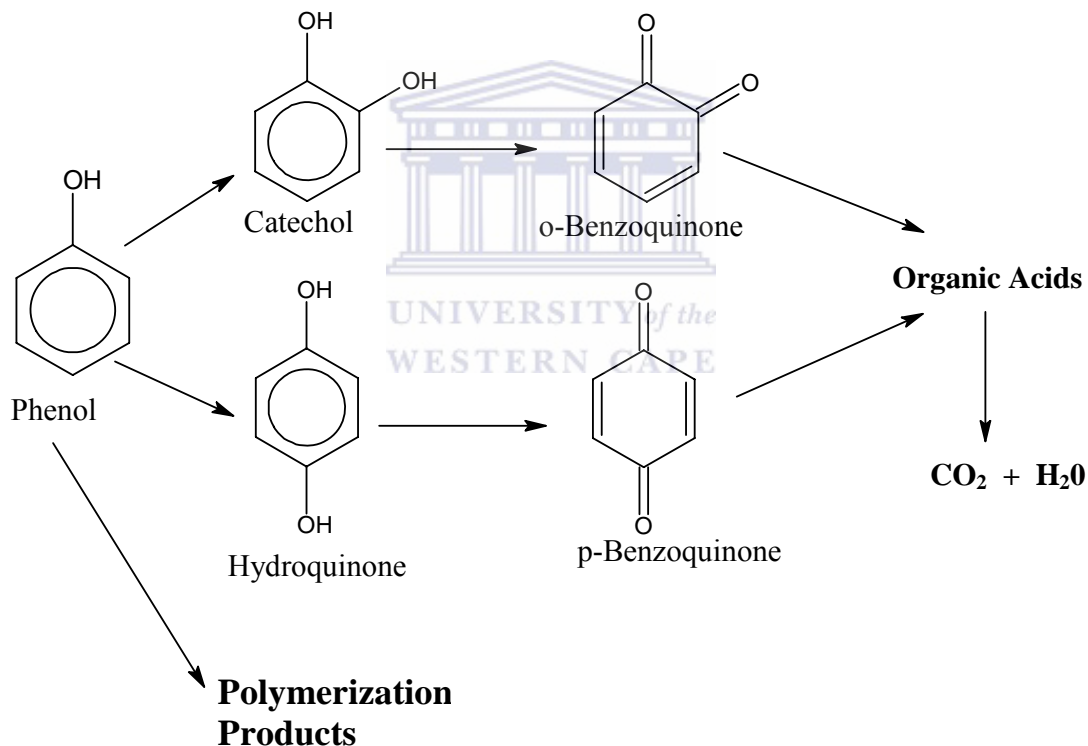
The petrochemical, fine chemical, cellulose and pharmaceutical industries produce waste water containing organics such as phenol, which are extremely toxic to aquatic life and poorly biodegradable.<sup>50</sup> It is difficult to oxidize these organic wastes biologically since they are often in very high concentrations. Biological degradation involves processes that are very time consuming and operate well only in cases of relatively dilute waste or when in very low concentration. Recovery is often not economically feasible.<sup>51</sup> Total oxidation of these organic compounds in water is used to directly eliminate the pollutants or transform them to non-toxic products able to be further eliminated by biological treatment.<sup>52</sup> Chemical oxidation of phenolic waste offers an alternative treatment. The treatments presently used and being studied are:

- Electrochemical treatment;
- Wet oxidation by an oxidant e.g. hydrogen peroxide, ozone, or oxygen in the presence of a catalyst.
- Photo-catalytic oxidation;
- Photo-electrochemical oxidation;
- Processes under supercritical conditions.

The choice of treatment process depends on the level of phenol concentration, economics, easy control, reliability and treatment efficiency. In many cases, severe reaction conditions are required, high temperatures (500-700) K and pressures (70-200) bar, for oxidation to take place. In other cases, higher amounts of energy or chemical products are required. Hence, these expensive methods have lower feasibility e.g. non-catalytic wet oxidation and supercritical oxidation which require high energy consumption and therefore involve increased operational costs. The development of inexpensive and efficient processes for waste-water treatment at intermediate levels of phenol concentration is of considerable interest for industrial activities. The oxidation of dilute aqueous solutions for organic pollutants using air or oxygen over a solid catalyst has been

shown to be a useful and inexpensive alternative process in which the organic compounds are ultimately oxidized to carbon dioxide and water.

The catalytic oxidation of phenol initially gives two main products catechol and hydroquinone as shown in Scheme 1.3. In this initial step they are the only expected products as –OH group of phenol is *ortho* and *para* directing. Maurya *et al.*<sup>2</sup> reported that only the two products are obtained with a mass balance of about 96%. No minor product (e.g. polymeric materials), if any, were detectable in GC under the reported condition. Further oxidation of catechol and hydroquinone to organic acids can also be achieved.



Scheme 1.3: Proposed pathway for the oxidation of phenol

### 1.5.1: Homogeneous catalytic oxidation

Synthetic metalloporphyrins have been demonstrated to be effective catalysts for oxidation reactions using hydrogen peroxide. In many instances metalloporphyrins of the

type in Figure 1.23, catalyzed hydrogen peroxide decomposition and have been coupled with organic substrates that require one pot oxidation producing a single product.

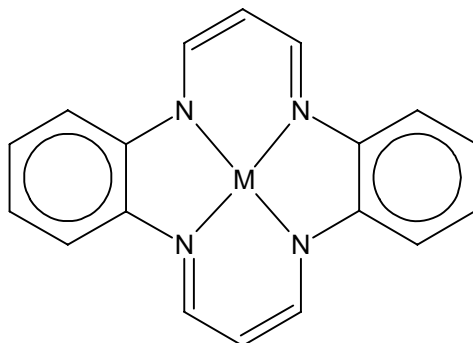


Figure 1.23: General structure of metalloporphyrin (ML)

Salavati-Niasari *et. al.*<sup>53</sup> reported that catechol and hydroquinone were observed with a mass balance of about 95 % when phenol oxidation was catalyzed by a Ni(II) complex of the 14-membered tetraaza macrocyclic ligands, “5,7,12,14-tetramethyldibenzo-1,4,8,11-tetraaza-cyclotetradecine”, [Ni(Me<sub>4</sub>R<sub>2</sub>Bzo[14]tetraeneN<sub>4</sub>)] (R=H, CH<sub>3</sub>, Cl and NO<sub>2</sub>), as shown in Figure 1.24. Hydrogen peroxide was used as an oxidant. Polymeric products were not detected in GC under the conditions used. The unsupported Ni(II) complex showed good activity of up to 33.5 % conversion with the reaction being more selective for catechol formation relative to hydroquinone.

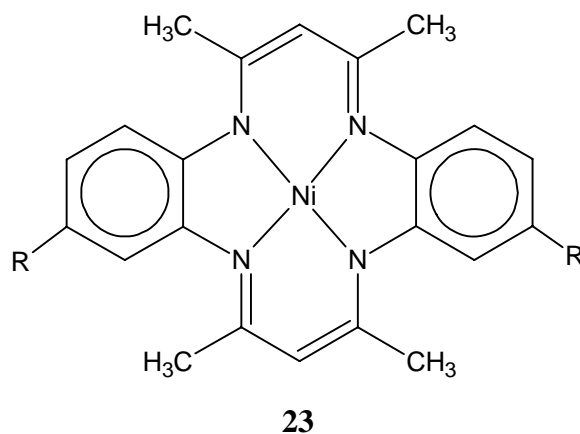
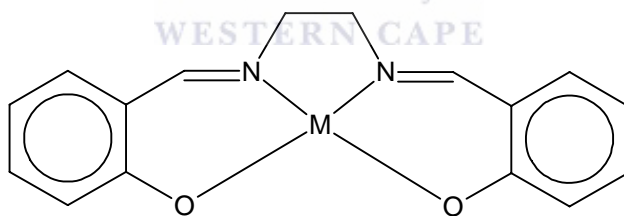


Figure 1.24: Structure of [Ni(Me<sub>4</sub>R<sub>2</sub>Bzo[14]tetraeneN<sub>4</sub>)], (R= H, CH<sub>3</sub>, Cl, NO<sub>2</sub>)

Bolzacchini and co-workers<sup>54</sup> reported the oxidation of propenoidic phenols by molecular oxygen catalyzed by  $[N,N\text{-}9\text{-bis}(\text{salicylidene})\text{ethane-}1,2\text{-diaminato}]\text{Co(II)}$ . The evaluation was done using different solvents and for variously substituted phenols to find processes alternative to those reported for the removal of polyphenols from waste waters in the paper industry. The reaction of methyl *E*-4-hydroxy-3-methoxycinnamate (*E*-methyl ferulate) selectively gave the corresponding 4-hydroxybenzoic acid and 4-hydroxybenzaldehyde. The highest yields were observed in chloroform, while methanol had good yields and pyridine gave very low yields. *E*-methyl ferulate gave the highest conversion, methyl *E*-4-hydroxycinnamate showed low conversion, while the other phenols, methyl *E*-3-hydroxy-4-methoxycinnamate (*E*-methyl isoferulate) and methyl *E*-3-chloro-4-hydroxycinnamate, did not react.

Xie *et al.*<sup>55</sup> reported Schiff base Cu(II) and Co(II) complexes of the ligand,  $N,N'\text{-bis}(\text{salicylidene})\text{ethane-}1,2\text{-diamine}$  shown in Figure 1.25, as well as the Cu(II) derivative of  $N,N'\text{-bis}(\text{salicylidene})\text{benzene-}1,2\text{-diamine}$  as mimetic peroxidases used in phenol oxidation showing good catalytic activity.



24

Figure 1.25: Structure of metal complex of  $N,N'\text{-bis}(\text{salicylidene})\text{ethane-}1,2\text{-diamine}$

The reaction rates with and without catalyst were compared using  $\text{H}_2\text{O}_2$  as an oxidant and in buffered solutions. The reaction rate for the oxidation process increased by a factor of ca.  $1 \times 10^4$  and  $1 \times 10^3$  for the Schiff base complexes containing Co(II) or Cu(II) catalyzed processes, respectively. The catalytic activity of the Schiff base complexes depends on changes of the  $[\text{H}_2\text{O}_2]: [\text{Catalyst}]$  ratio, temperature and pH of the reactive system. This behaviour resembles that of the natural enzyme.

### 1.5.2: Heterogeneous catalytic oxidation

Various transition metal complexes of H<sub>2</sub>salen (H<sub>2</sub>: N,N'-bis(salicylidene)ethane-1,2-diamine) and its substituted derivatives encapsulated in a zeolite matrix have been studied for catalytic activities towards oxidation of phenol. Maurya *et al.*<sup>56</sup> recently reported oxidation of phenol using complexes of Cr(III), Fe(III), Bi(III), Ni(II) and Zn(II) of N,N-bis(salicylidene)propane-1,3-diamine(H<sub>2</sub>salpn), **25**, encapsulated in zeolite-Y as catalyst precursor and H<sub>2</sub>O<sub>2</sub> as oxidant.

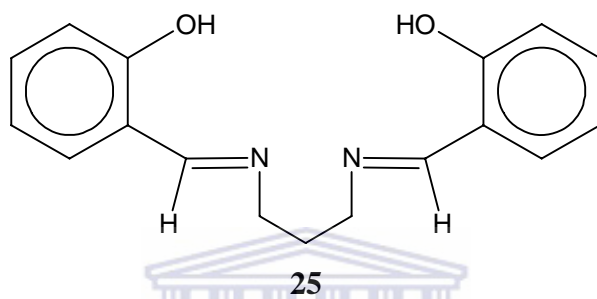


Figure 1.26: Structure of H<sub>2</sub>salpn ligand

The activity as a function of time was studied. Catechol and hydroquinone were identified as the major products. A maximum conversion of about 23 % was observed with zeolite-Fe(H<sub>2</sub>salpn) after 3 hours. Zeolite-Ni(H<sub>2</sub>salpn) showed the poorest performance for the oxidation of phenol as well as the formation of hydroquinone. However, it gave the best selectivity of more than 92 % for catechol formation. The highest selectivity of around 32 % for the formation of hydroquinone was obtained with zeolite-Cr(H<sub>2</sub>salpn) after 3 hours.

Subsequently Maurya *et al.*<sup>2</sup> reported N,N-bis(salicylidene)diethylenetriamine (H<sub>2</sub>saldien), **26**, encapsulated in zeolite matrix. H<sub>2</sub>saldien is a potential dibasic pentadentate ligand with good flexibility and could give stable transition metal complexes. Cr, Fe and Bi analogues were prepared and evaluated as catalytic precursors in phenol oxidation.



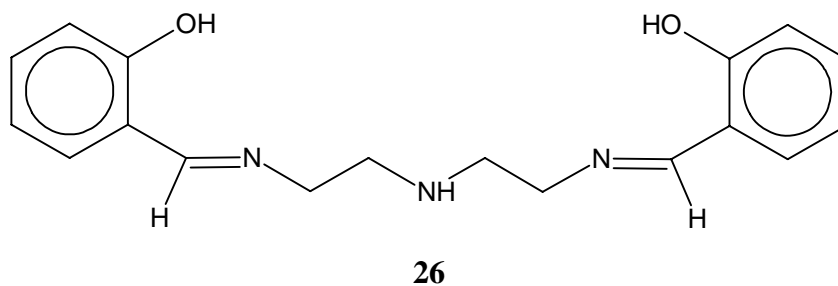


Figure 1.27: Structure of H<sub>2</sub>saldien ligand

The highest phenol oxidation was observed at 1:1 phenol: H<sub>2</sub>O<sub>2</sub> molar ratio as various reaction parameters such as, catalyst amount, H<sub>2</sub>O<sub>2</sub> concentration and volume of solvent were varied at a fixed amount of phenol. However, selectivity towards the formation of catechol and hydroquinone varied with each catalyst. Catalytic oxidation studies were performed using [Cr(saldien)·H<sub>2</sub>O]Cl, [Fe(saldien)·H<sub>2</sub>O]Cl and [Bi(saldien)·H<sub>2</sub>O]Cl all supported on zeolite-Y. H<sub>2</sub>O<sub>2</sub> was used as the oxidant while CH<sub>3</sub>CN was the solvent. Catechol and hydroquinone were again obtained as the major products. zeolite-[Cr(saldien)·H<sub>2</sub>O]Cl was the best catalyst in comparison to zeolite-[Bi(saldien)·H<sub>2</sub>O]Cl, which in turn was better than zeolite-[Fe(saldien)·H<sub>2</sub>O]Cl in terms of phenol transformation as well as formation of catechol and hydroquinone. However, in terms of selectivity, the latter two catalysts were more selective, about 84 %, for catechol. The zeolite-[Cr(saldien)·H<sub>2</sub>O]Cl showed 69 % selectivity for the formation of catechol. The unencapsulated complexes, [Cr(saldien)·H<sub>2</sub>O]Cl, [Fe(saldien)·H<sub>2</sub>O]Cl and [Bi(saldien)·H<sub>2</sub>O]Cl were also studied as catalyst with H<sub>2</sub>O<sub>2</sub> as oxidant in CH<sub>3</sub>CN under similar conditions as those of the encapsulated analogues. A similar trend, i.e. higher conversion of phenol with 0.05 moles of H<sub>2</sub>O<sub>2</sub>, as noted previously was also observed. However, the conversion was considerably lower in comparison to that of encapsulated analogues and followed the order: [Cr(saldien)·H<sub>2</sub>O]Cl (31 %) > [Fe(saldien)·H<sub>2</sub>O]Cl (22 %) > [Bi(saldien)·H<sub>2</sub>O]Cl (21 %) after 6 h of reaction time.

Salavati-Niasari *et al.*<sup>53</sup> also reported [Ni(Me<sub>4</sub>R<sub>2</sub>Bzo[14]tetraeneN<sub>4</sub>)] (R = H, CH<sub>3</sub>, Cl and NO<sub>2</sub>), encapsulated in the nanocavity of zeolite-Y. They evaluated these catalysts for phenol oxidation using H<sub>2</sub>O<sub>2</sub> as oxidant. They observed activity of up to 96 mol (phenol consumed) mol (Co)<sup>-1</sup> h<sup>-1</sup>. In these catalytic systems no polymer products were observed

under the conditions used. Increasing the reaction time from 6 to 12 h showed only a minor increase in the transformation of phenol and percent selectivity for the formation of catechol and hydroquinone. Recovery was attempted at the end of the reaction. The catalyst was separated by filtration, thoroughly washed with solvent and reused under similar conditions. Although the analysis of the recovered catalysts by atomic absorption spectroscopy showed no reduction in the amount of metal ions, they showed slightly lower conversions after subsequent re-use. They also observed that the encapsulated catalysts were more active but less selective for the catechol formation than the unencapsulated ones.

### **1.6: Aim and scope of this thesis**

Heterogenization of homogeneous transition metal catalysts have become an area of interest of research from both academic and an industrial point of view. As part of this ongoing research we are presently engaged in developing non-porphyrinic transition metal complexes. The aim is to develop mononuclear and multinuclear, monoanionic N,N-chelating pyrrole- imine ligands. Cu(II), Co(II), and Ni(II) complexes of these ligand systems will also be prepared. These complexes will then be evaluated as catalyst precursors in the oxidation of alkenes and phenols. Complexes of some of these ligand systems have shown considerable activity in polymerization. Multinuclear systems are expected to show significantly improved catalytic activities.

We will also attempt to prepare, immobilize and characterize new catalysts of copper, cobalt and nickel complexes of bidentate pyrrolide-imine N,N-chelate ligands with covalent attachment onto MCM-41. These immobilized catalyst systems will then be evaluated for the oxidation of olefins and phenols.

**1.7: References**

1. T. V. Laine, U. Piironen, K. Lappalainen, M. Klinga, E. Aitola, M. Leskela, *J. Organomet. Chem.*, **606** (2000) 112.
2. M. R. Maurya, S. J. J. Titinchi, S. Chand, *J. Mol. Cat. A: Chem.*, **193** (2003) 165.
3. R. V. Heerbeek, P. C. J. Kamer, P. W. N. M. van Leeuwen, J. N. H. Reek, *Chem. Rev.*, **102** (2002) 3717.
4. C. W. Jones, M. W. McKittick, J. V. Nguyen, K. Yu, *Top. Catal.*, **34** (2005) 67.
5. B. De. Clercq, F. Lefebvre, F. Verpoort, *Appl. Catal. A: Chem.*, **247** (2003) 345.
6. J. H. Clark, D. J. Macquarrie, *Chem. Soc. Rev.*, **25** (1996) 303.
7. M. H. Peyrovi, V. Mahdavi, M. A. Salehi, R. Mahmoodian, *Catal. Commun.*, **6** (2005) 476.
8. T. Katsuki, *Chem. Soc. Rev.*, **33** (2004) 437.
9. R. L. De, K. Samanta, K. Maiti, E. Keller, *Inorg. Chim. Acta*, **316** (2001) 113.
10. P. G. Cozzi, *Chem. Soc. Rev.*, **33** (2004) 410.
11. J. Lewinski, M. Dranka, I. Kraszewska, W. Sliwinski, I. Justyniak, *Chem. Commun.*, (2005) 4935.
12. L-C. Liang, C-W. Yang, M. Y. Chiang, C-H. Hung, P-Y. Lee, *J. Organomet. Chem.*, **679** (2003) 135.
13. H. Hao, S. Bhandari, Y. Ding, H. W. Roesky, J. Magull, H-G. Schmidt, M. Noltemeyer, C. Cui, *Eur. J. Inorg. Chem.*, (2002) 1060.
14. S. D. Drouin, H. M. Foucault, G. P.A. Yap, D. E. Fogg, *Can. J. Chem.*, **83** (2005) 748.
15. V. C. Gibson, C. Newton, C. Redshaw, G. A. Solan, A. J. P. White, D. J. Williams, *J. Chem. Soc., Dalton Trans.*, (2002) 4017.
16. Y-S. Li, Y-R. Li, X-F. Li, *J. Organomet. Chem.*, **667** (2003) 185.
17. Y. Yoshida, S. Matsui, Y. Takagi, M. Mitani, T. Nakano, H. Tanaka, N. Kashiwa, T. Fujita, *Organometallics*, **20** (2001) 4793.
18. R. M. Bellabarba, P.T. Gomes, S. I. Pascu, *J. Chem. Soc., Dalton Trans.*, (2003) 4431.
19. S. Matsui, T. P. Spaniol, Y. Takagi, Y. Yoshida, *J. Chem. Soc., Dalton Trans.*, (2002) 4529.

20. H. Gao, R. J. Angelici, *J. Am. Chem. Soc.*, **119** (1997) 6937.
21. B. S. Lane, K. Burgess, *Chem. Rev.*, **103** (2003) 2457.
22. T.R. Gaydhankar, U. S. Taralkar, R. K. Jha. P. N. Joshi, R. Kumar, *Catal. Commun.*, **6** (2005) 361.
23. M. Salavati-Niasari, P. Salemi, F. Davar, *J. Mol. Cat. A: Chem.*, **238** (2005) 215.
24. A. Caselli, E. Gallo, F. Ragaini, A. Oppezzo, S. Cenini, *J. Organomet. Chem.*, **690** (2005) 2142.
25. U. G. Singh, R. T. Williams, K. R. Hallam, G. C. Allen, *J. Solid State Chem.*, **178** (2005) 3405.
26. P. Sutra and D. Brunel, *Chem. Commun.*, (1996) 2485.
27. M. Masteri-Farahani, F. Farzaneh, M. Ghandi, *J. Mol. Cat. A: Chem.*, **243** (2006) 170.
28. R. M. Lambert., F. J. Williams, R. L. Cropley, A. Palermo, *J. Mol. Cat. A: Chem.*, **228** (2005) 27.
29. C. T. Dalton, K. M. Ryan, V. M. Wall, C. Bousquet, D. G. Gilheany, *Top. Catal.*, **5** (1998) 75.
30. L. Lefferts, K. Seshan, B. Mojet, J. Ommen, *Catal. Today*, **100** (2005) 63.
31. A. S. Kanmani, S. Vancheesan, *J. Mol Catal. A: Chem.*, **125** (1997)127.
32. S. K. Samantaray, K. Parida, *Catal. Commun.*, **6** (2005) 578.
33. E. M. McGarrigle, D. G. Gilheany, *Chem. Rev.*, **105** (2005) 1564.
34. W. Adam, K. J. Roschmann, C. R. Saha-Möller, D. Seebach, *J. Am. Chem. Soc.*, **124** (2002) 5068.
35. R. A. Silva, C. Freire, B. de Castro, *New J. Chem.*, **28** (2004) 253.
36. J. T. Groves, T. E. Nemo, R. S. Myers, *J. Am. Chem. Soc.*, **101** (1979) 1032.
37. J. T. Groves, W. J. Kruper, *J. Am. Chem. Soc.*, **101** (1979) 7613.
38. E. Guilmet, B. Meunier, *Tetrahedron Lett.*, **23** (1982) 2449.
39. B. Meunier, E. Guilmet, M-S. De Carvalho, R. Poilblanc, *J. Am. Chem. Soc.*, **106** (1984) 6668.
40. J. T. Groves, T. E. Nemo, *J. Am. Chem. Soc.*, **105** (1983) 5786.
41. J. T. Groves, R.S. Myers, *J. Am. Chem. Soc.*, **105** (1983) 5791.

42. T. L. Sidall, N. Miyaura, J. C. Huffmann J. K. Kochi, *J. Chem. Soc., Chem. Commun.*, (1983) 1185.
43. E. G. Samsel, K. Srinivasan, J. K. Kochi, *J. Am. Chem. Soc.*, **107** (1985) 7606.
44. K. Srinivasan, P. Michaud, J. K. Kochi, *J. Am. Chem. Soc.*, **108** (1986) 2309.
45. D. Chatterjee, S. Mukherjee, A. Mitra, *J. Mol. Catal. A: Chem.*, **154** (2000) 5.
46. H. Yoon, C. J. Burrows, *J. Am. Chem. Soc.*, **110** (1988) 4087.
47. Y. Luo, J. Lin., *Micropor. Mesopor. Mater.*, **86** (2005) 23.
48. S. A. Patel, S. Sinha, A. N. Mishra, B. V. Kamth, R. N. Ram, *J. Mol. Cat. A: Chem.*, **192** (2003) 53.
49. P. Dasa, I. Ku'zniarska-Biernacka, A. R. Silva, A. P. Carvalho, J. Pires, C. Freire, *J. Mol. Cat. A: Chem.*, **248** (2006) 135.
50. M. Harmankaya, G. Gunduz, *Tr. J. Engin. Environ. Science*, **22** (1998) 9.
51. A. Alejandre, F. Medina, P. Salagre, A. Fabregat, J. E. Sueiras, *Appl. Catal.: B*, **18** (1998) 307.
52. A. Santos, P. Yustos, A. Quintanilla, F. Garcia-Ochoa, *Top. Catal.*, **33** (2005) 181.
53. M. Salavati-Niasari, M. Bazarganipour, *Catal. Commun.*, **7** (2006) 336.
54. E. Bolzacchini, C. Canevali, F. Morazzoni, M. Orlandi, B. Rindone, R. Scotti, *J. Chem. Soc., Dalton Trans.*, (1997) 4695.
55. J-Q. Xie, J-Z. Li, X-G. Meng, C-W. Hu, X-C. Zeng., *Trans. Met. Chem.*, **29** (2004) 388.
56. M. R. Maurya, S. J. J. Titinchi, S. Chand, I. M. Mishra, *J. Mol. Cat. A: Chem.*, **180** (2002) 201.

**Chapter 2 : Synthesis and Characterization of  
Pyrrole–imine Based Ligands, their Cu(II), Co(II)  
and Ni(II) Complexes and the Immobilization of  
Cu(II) and Ni(II) Complexes onto mesoporous  
MCM-41**

## 2.1: Introduction

Metal complexes containing chelating nitrogen ligands continue to constitute an active area of research.<sup>1</sup> Included amongst these are pyrrole imine ligands. The choice of pyrrole Schiff base systems is based on the fact that deprotonation upon metallation generates a very powerful anionic  $\sigma$ -donor group. This has important applications in stabilizing metals in high oxidation states, an obligatory requirement for certain transition metal and main group metal ion catalysts, or producing neutral complexes of lower oxidation states such as Fe(II) and Ni(II).

The most studied of the above class of ligands are the pyrrole monoanionic ligands.

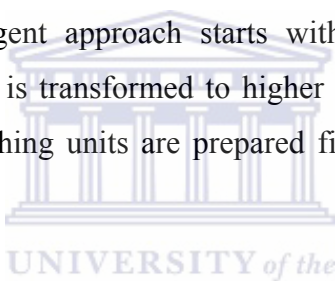
Several structural features of the imino-pyrrolide ligand are attractive for their potential to stabilize  $\sigma$  donation. The enthalpically favoured conjugation of the pyrrolide and olefinic units may also favour retention of planarity in the ligand system. The potential for electronic and steric tuning can be attained via functionalization of the imino moiety.<sup>2</sup> The ligands are also attractive for their ease of access from commercially available precursors and have a narrow chelate bite angle of 70 – 85°. Chelating mono (imino) pyrrolato complexes have indeed been reported for a range of transition metals e.g. Ru(II)<sup>3</sup>, Ti(IV)<sup>4</sup>, Cr(II) and Cr(III)<sup>5</sup> complexes that prove potent polymerization catalysts as discussed in Chapter 1. These complexes are obtained through the treatment of the Schiff-base ligand with the corresponding metal salt.

In this chapter, we report the synthesis and characterization of Cu(II), Co(II), Co(III) and Ni(II) complexes based on monofunctional and multifunctional pyrrole–imine ligands. Different moieties of the imino nitrogen were prepared. The multifunctional ligand is based on the dendrimer framework of poly(propylene imine) that allows multiple metal centers while the different monofunctional ligands are based on aliphatic and aromatic functionalities. The aliphatic monofunctional pyrrole–imine ligands were prepared with the propyl as well as the triethoxysilylpropane functionality at the imino nitrogen. The propyl chain corresponds to the dendrimer backbone, while the triethoxysilane functionality allows for the immobilization onto a siliceous carrier such as MCM-41. In addition the preparation and immobilization onto the inorganic support, MCM-41 of

Cu(II) and Ni(II) pyrrole-imine base complexes as well as their characterization are also discussed.

### ***2.1.1: Dendrimers***

Dendrimers are well defined, highly branched macromolecules consisting of a central core and emanating from this are several branches at specific and regular points leading to a number of successive, well-defined generations.<sup>6</sup> Ideally, they are perfect monodispersed macromolecules with regular highly branched and three dimensional architectures with the ability to carry a number of functional groups depending on the generation.<sup>7</sup> They are produced in an iterative sequence of reactions in either a divergent or convergent synthetic route.<sup>8</sup> The stepwise synthesis gives a controlled architecture, which allows their molecular structure to be precise and unique, in contrast to many other macromolecules.<sup>9</sup> The divergent approach starts with the core molecule then, via multiple reaction sequences, it is transformed to higher generations. In the convergent approach, the peripheral branching units are prepared first and then anchored onto the core molecule.<sup>10</sup>



Dendrimer chemistry has gained importance over the past two decades. Several potential applications of dendrimers, including catalysis, have been explored and are well documented in numerous review articles that have been published in recent years. Advantages of dendritic catalysis include the ability to fine-tune the catalytic centers by ligand design and the ability to perform mechanistic studies on these uniformly distributed catalytic sites attached to the support and in other cases the ability to be used as an immobilization phase for the homogenous catalysts.<sup>11</sup> The catalytic performance, i.e. the activity, selectivity, stability, and recyclability of the system, depends on the dendritic architecture that is used. The possible architectures are periphery-functionalized (of a dendrimer or a dendritic wedge), core-functionalized and focal point-functionalized (on a dendritic wedge) systems, Figure 2.1.<sup>12</sup>



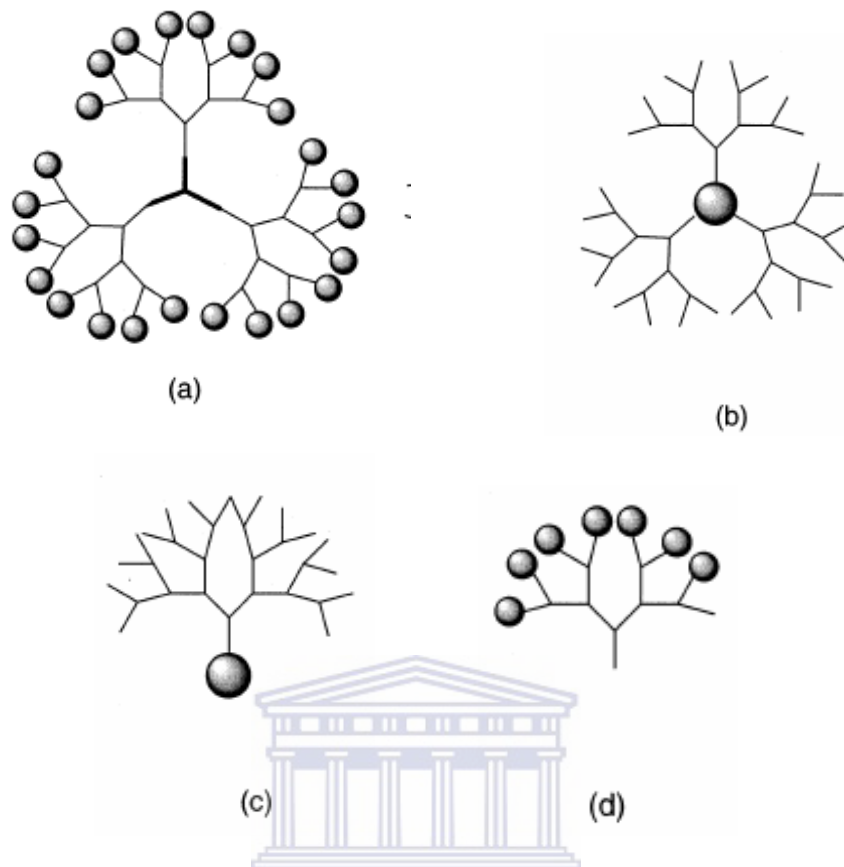
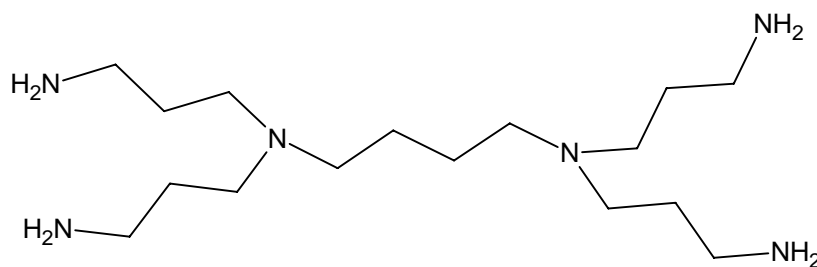


Figure 2.1: Different dendritic architectures of catalyst located at the (a) periphery, (b) core (c) focal point of a wedge, (d) and periphery of a wedge

The dendrimers are named according to their generations. Diaminobutane-poly(polylene imine) or (DAB-PPI-(NH<sub>2</sub>)<sub>n</sub>) dendrimer is commercially available in many generations. The first generation [DAB-PPI-(NH<sub>2</sub>)<sub>4</sub>], Figure 2.2, has a diaminobutane core with 4 terminal amino groups. These amino groups can be functionalized and subsequently converted to metallodendrimers synthesized with appropriate metal precursors.<sup>13, 14</sup> This type of nitrogen rich dendrimers have been characterized by various spectroscopic methods in addition to mass spectrometry.



27

Figure 2.2: Poly (propylene imine) 1st generation dendrimer, DAB-PPI-(NH<sub>2</sub>)<sub>4</sub>

### 2.1.2: Metallodendrimers

From on-going research into dendrimers and their applications in coordination chemistry, it has become clear that the numbers of synthetic routes available to attach a metallic moiety to the branches of a dendrimer are limited.<sup>15</sup> The synthesis of metallodendrimers has in recent years, like the more linear metal-containing polymers, developed at a prolific rate. These materials show potential in a number of industrial applications and are thought to possess interesting electronic, magnetic, optical and catalytic properties.<sup>16</sup> These potential uses are in many instances ascribed to the incorporation of metal centers into the dendrimers or functionalizing the dendrimer giving rise to metallodendrimers. As far as metallodendrimers are concerned, the introduction of metal centers may occur at various branching points within the dendrimers, at the core or on the periphery of the dendritic molecule. Periphery (terminal)-functionalized dendrimers have their catalytic sites located at the surface of the dendrimer supports, and these active sites are therefore directly available to the substrate. Many of these types of dendrimers have been reported. The focus of the work in this chapter is on periphery functionalized metallodendrimers.



Cuadrado, Morán, and co-workers reported ferrocenyl metallodendrimers based on 1<sup>st</sup> and 5<sup>th</sup> generations poly(propyleneimine) dendrimer frameworks. Construction relied on treatment of the requisite polyamine with  $(\eta^5\text{-C}_5\text{H}_5)\text{Fe}-(\eta^5\text{-C}_5\text{H}_4\text{COCl})$  to afford the corresponding polyferrocene.<sup>19</sup> These ferrocenyl metallodendrimers exhibited a single reversible oxidation process suggesting all of the metal centers in a single molecule were electrochemically equivalent. This not only aids in the structural determination but also confirms that the different catalytic sites are equivalent. Other research groups have also functionalized the surface of DAB-PPI-(NH<sub>2</sub>)<sub>n</sub>.<sup>20</sup>

### **2.1.3: Highly ordered MCM-41**

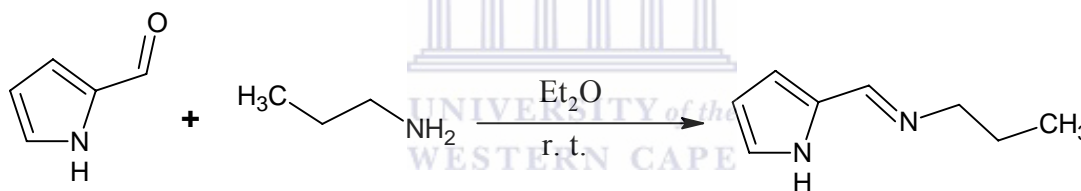
In 1992, Beck *et al.*<sup>21</sup> reported the synthesis, characterization, and proposed a mechanism of formation of a new family of silicate/aluminosilicate mesoporous molecular sieves designated as M41S. MCM-41 is a member of this family and exhibits hexagonal and uniformly arranged mesopores. The dimensions of the mesopores may be engineered in the range of  $\sim 15\text{\AA}$  to greater than  $100\text{\AA}$ . They proposed a liquid crystal templating mechanism (LCT) in which surfactant liquid crystal structures serves as organic templates for the formation of these materials. An intimate link of the structure and pore dimensions of MCM-41 materials to the properties of the surfactant, including surfactant chain length and solution chemistry was also established in this templating mechanism. The presence of variable pore size MCM-41, cubic material, and other phases indicated that M41S is an extensive family of materials. Since 1992, much research has been reported on the synthesis of mesoporous molecular sieves. Morphologies of shape and surface patterns in mesoporous silica MCM-41 have also been widely described.<sup>22, 23</sup> There are many techniques that have been utilized to immobilize molecular metallic catalysts onto these inorganic supports. These as discussed in chapter 1 are physisorption, ion pairing encapsulation and covalent binding. The approach that is, in principle, most widely applicable is ligand tethering (covalent ligand binding). In this methodology, the organic ligand of the metal complex is covalently anchored onto the solid support. In the cases where the ligand does not dissociate in the catalytic cycle, these catalysts can be used as recyclable systems in nearly any solvent. The key drawback to this methodology, however, is in the preparation thus the covalent

supporting of transition Schiff base metal complexes onto these silicate/aluminosilicate mesoporous molecular sieves has not been widely reported.<sup>24</sup>

## 2.2 Results and discussion

### 2.2.1 Synthesis and characterization of the aliphatic substituted pyrrole-imine ligand and its Cu(II), Co(III) and Ni(II) complexes

Ligand **L1** was prepared by reacting pyrrole-2-carboxyaldehyde with propyl amine in the ratio of 1:1 in dry Et<sub>2</sub>O, Scheme 2.1. Glacial acetic acid was added to catalyze the reaction. An orange brown oil was obtained in 56 % yield. The moderate yield can be accounted for due to some loss of product during the purification process. The ligand showed good solubility in common solvents such as dichloromethane, diethyl ether, chloroform, tetrahydrofuran as well as in toluene. Characterization was done by <sup>1</sup>H-, <sup>13</sup>C-NMR and FT-IR spectroscopy, mass spectrometry and microanalysis.



Scheme 2.1: Synthetic route to N-[(1E)-1H-pyrrol-2-ylmethylene]propan-1-amine, **L1**

The <sup>1</sup>H-NMR spectrum obtained in CDCl<sub>3</sub>, Figure 2.4, showed proton signals of the propyl chain at 0.92 ppm for the CH<sub>3</sub>, 1.68 ppm for the CH<sub>2</sub> at the center and that at 3.50 ppm is for the CH<sub>2</sub> adjacent to the imine while in the <sup>13</sup>C-NMR spectrum their signals were observed at 11.7, 24.3, and 62.7 ppm respectively. The most characteristic signal in the <sup>1</sup>H-NMR spectrum is that of the pyrrole N=CH proton observed at 8.04 ppm with a carbon signal at 151.4 ppm from the <sup>13</sup>C-NMR spectrum. The <sup>1</sup>H-NMR spectrum also showed pyrrole ring signals at 6.9 ppm for the CH proton next to NH, 6.2 ppm for the CH next to the carbon bonded to the imine system and 6.5 ppm for the CH in between the two. Their respective carbon signals in the <sup>13</sup>C-NMR spectrum are those at 121.4, 109.5 and 113.7 ppm while that at 130.1 ppm is for the pyrrole ring carbon bonded to the imine system. The NH proton signal was not observed in the <sup>1</sup>H-NMR spectrum. This may be

attributed to the fact that the NH proton is exchangeable and thus may not be observed in the deuterated solvent.

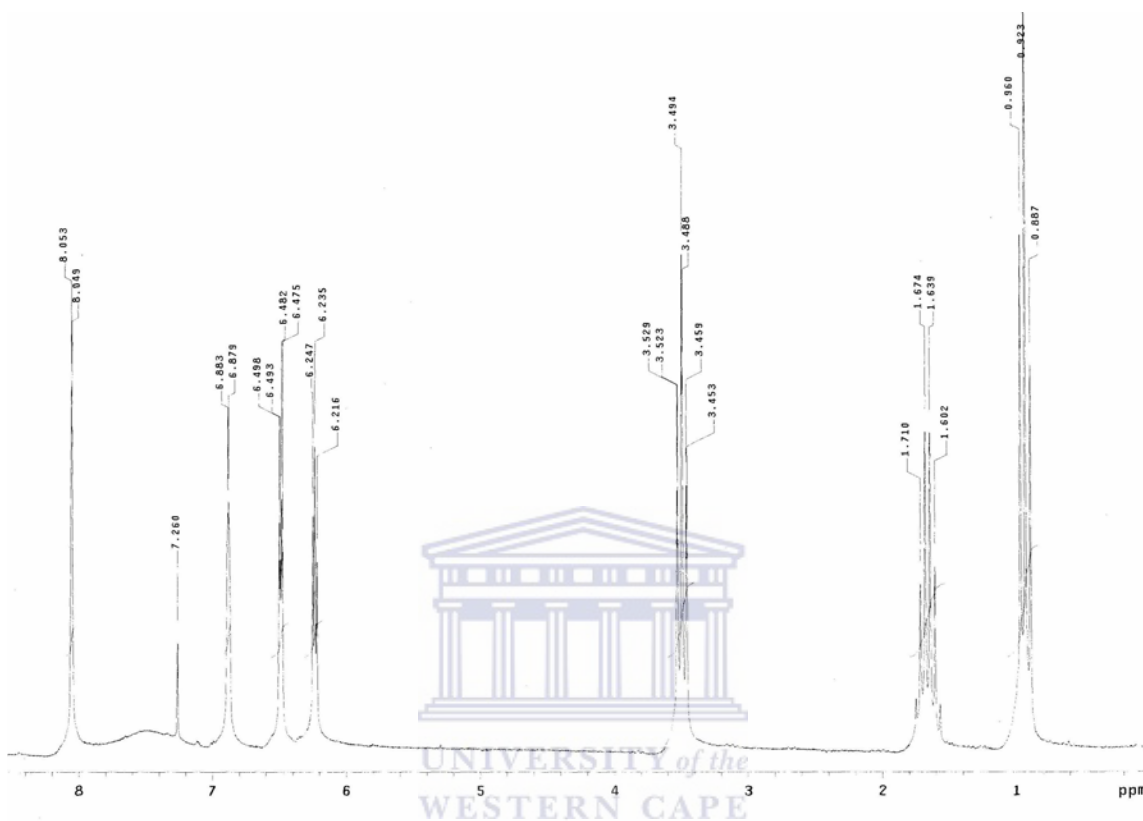
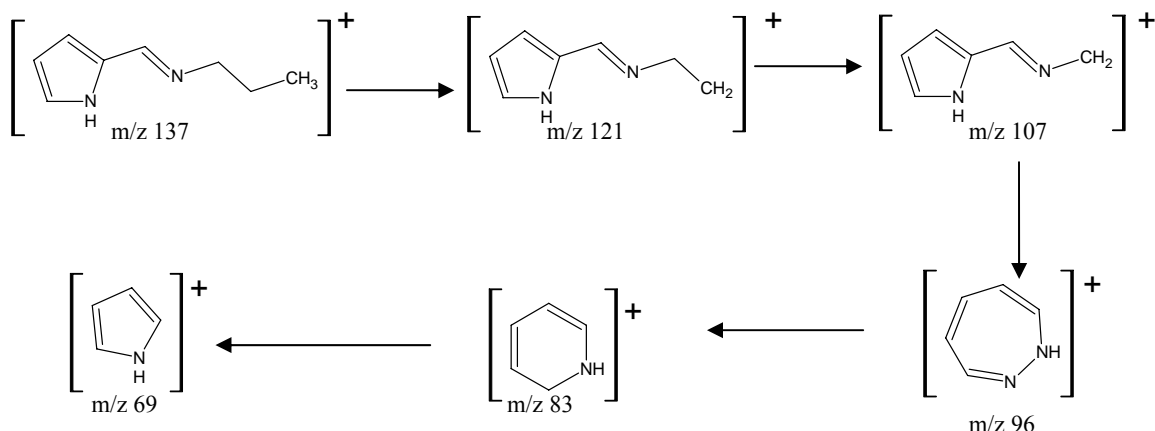


Figure 2.4:  $^1\text{H-NMR}$  spectrum of N-[(1E)-1H-pyrrol-2-ylmethylene]propan-1-amine, **L1**

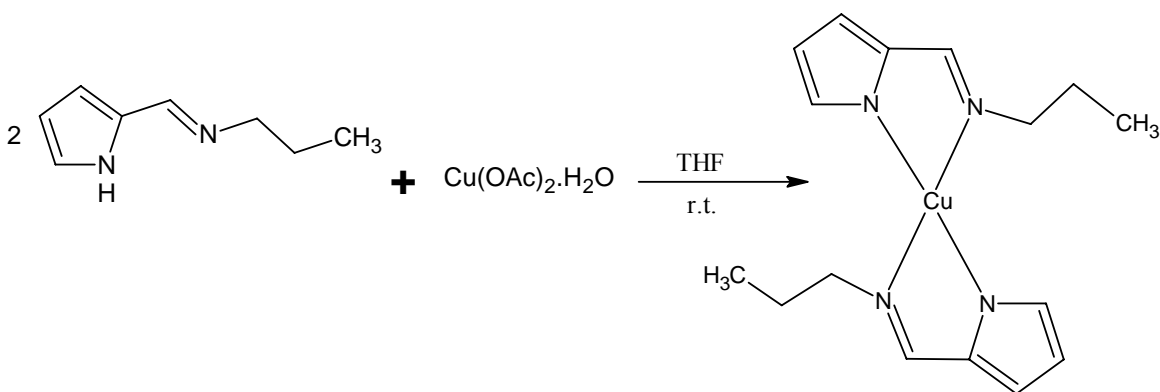
**L1** is relatively stable and does not decompose on exposure to air in solution for prolonged periods. The FT-IR spectrum shows a characteristic band at  $1638\text{ cm}^{-1}$  for the  $\nu_{\text{C=N}}$  functional group as a sharp peak and that of the N-H group at *ca.*  $3100\text{ cm}^{-1}$ . The broadness of the latter peak can be associated with hydrogen bonding of the NH groups.<sup>25</sup> The elemental analysis data obtained agrees with the calculated molecular weight of **L1** associated with 0.25  $\text{H}_2\text{O}$  as shown in Table 2.1. Electron impact mass spectrometry was also used to characterize **L1**. The spectrum obtained exhibited the fragmentation pattern shown in Scheme 2.2. The singly charged ion at  $m/z$  137 corresponds to the molecular mass of **L1**. The fragmentation pattern shows the initial loss of the propyl chain followed by the imine system to produce a fragment at  $m/z$  69 corresponding to the pyrrole group.

Scheme 2.2: Fragmentation pattern for **L1**Table 2.1: Characterization data for **L1**, **C1**, **C2** and **C3**

	m/z [M+H] <sup>+</sup>	FT-IR $\nu_{(C=N)}\text{cm}^{-1}$	Micro analysis, Found (Calc)		
			C	H	N
<b>L1</b> <sup>a</sup>	137	1638	68.11 (68.29)	8.48 (8.95)	19.31 (19.91)
<b>C1</b>	335	1590	57.21 (57.55)	6.73 (6.64)	17.08 (16.78)
<b>C2</b> <sup>b</sup>	330	1596	56.29 (56.84)	6.39 (6.86)	15.89 (16.57)
<b>C3</b> <sup>c</sup>	465	1586	59.90 (59.74)	7.11 (7.31)	16.59 (17.42)

<sup>a</sup> Microanalysis include 0.25 H<sub>2</sub>O<sup>b</sup> Microanalysis include 0.5 H<sub>2</sub>O<sup>c</sup> Microanalysis include H<sub>2</sub>O

The copper complex of **L1** was prepared by the treatment of the ligand with sodium hydride resulting in the formation of pyrrolide-imine sodium salt. Deprotonation of **L1** proceeded cleanly affording a red-brown Na salt. This salt was characterized by <sup>1</sup>H-NMR spectroscopy and a shift of all signals up field was observed. After filtration of the excess NaH under nitrogen, an appropriate amount of Cu(OAc)<sub>2</sub>·H<sub>2</sub>O was added, Scheme 2.3. The acetate dissolved giving a blue colour that changed gradually to deep green over the reaction time. An analytically pure deep green crystalline material was obtained after recrystallization. We were unable to obtain crystals for X-ray analysis. An attempt to carry out the reaction at elevated temperatures did not improve the yields.

Scheme 2.3: Synthetic route of Cu(II) complex, **C1**

An attempt to synthesize the Ni and Co analogues using the same approach as for **C1** proved to be futile. An alternative synthetic method was thus employed. The nickel, **C2**, and cobalt complexes, **C3**, were prepared by *in situ* deprotonation of the ligand by NaOH in the presence of Ni(OAc)<sub>2</sub>·4H<sub>2</sub>O and Co(OAc)<sub>2</sub>·4H<sub>2</sub>O respectively. **C2** and **C3** were obtained in moderate yields. Recrystallization gave analytically pure products as well as crystals good enough for X-ray analysis for **C3**.

According to the FT-IR spectra, the Cu(II), Co(III), and Ni(II) complexes show a significant shift of the C=N stretching frequencies indicating coordination through the azomethine nitrogen as shown in Table 2.1. The absence of the broad band at *ca.* 3200-3084 cm<sup>-1</sup> indicate the deprotonation of the pyrrole nitrogen. The elemental analysis, Table 2.1, agreed with the calculated values showing that **C1** and **C2** are bis(pyrrolide-imine) complexes while **C3** is a tris(pyrrolide-imine) complex. These results are further supported by the ESI-MS where a singly charged species for **C1** was observed at *m/z* 335, for **C2** at *m/z* 330 and that of **C3** at *m/z* 465. For Co(II) complexes of the pyrrole-imine ligands to be synthesized, isolated and characterized, bulky groups such as *tert*-butyl should be used as substituent of the imine group providing efficient stoichiometric control.<sup>26</sup> These complexes are stable at room temperature and can be stored without apparent decomposition.



The molecular structure of **C3** was confirmed by solid state crystal structure, Figure 2.5. The crystal is an orthorhombic system with an octahedral geometry at the metal. The pyrrole-N units are oriented *trans* to each other. The Co-N distances of 1.900(2) Å to 1.960(2) Å are comparable with those of a reported Ni (II) complex<sup>27</sup> but these are much shorter than those of most other pyrrole-imine complexes e.g. Cr (II)<sup>5</sup> which has 2.06 Å and 2.078 Å. The bond angles about the metal are typical of pyrrole-imine complexes reported previously. The bite angles of the pyrrole-imine ligand are 82.94(10), 83.07(10) and 82.17(10)° for N(1)-Co-N(2), N(3)-Co-N(4) and N(5)-Co-N(6), respectively. Crystal structure refinement data is given in Table 2.2 while selected bond lengths and bond angles are listed in Table 2.3.

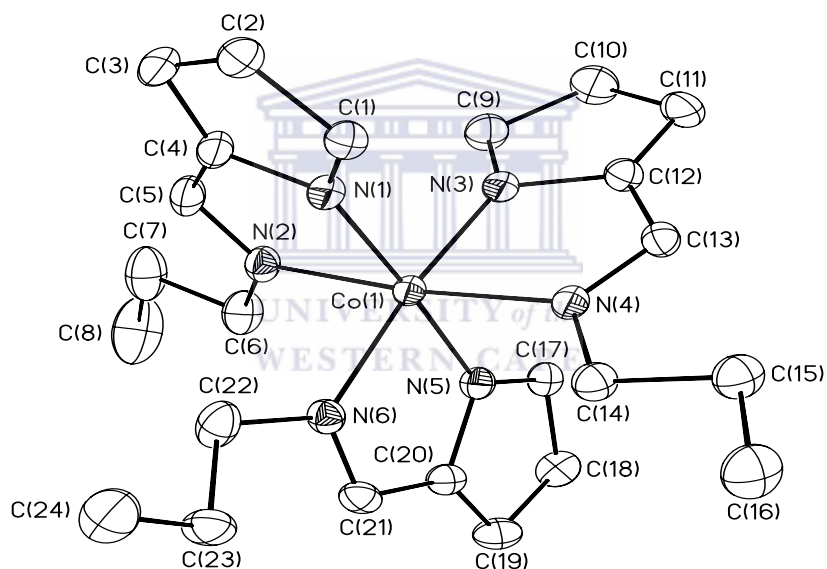


Figure 2.5: Molecular diagram of complex **C3** drawn with 30% probability ellipsoids. Hydrogen atoms are omitted for clarity

Table 2.2: Crystal data and structure refinement for **C3**

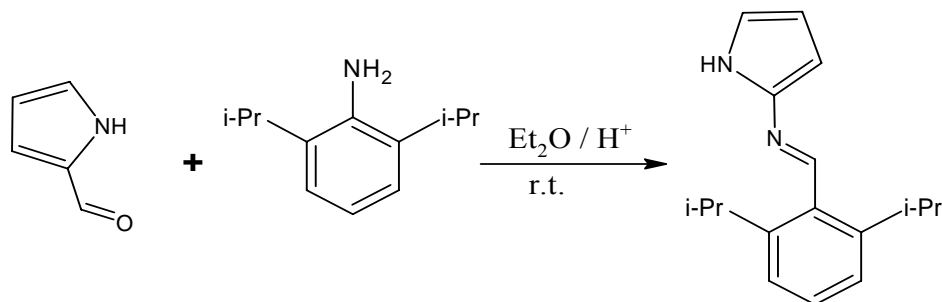
Empirical formula	$C_{24}H_{33}Co N_6$
Formula weight	464.49
Temperature (K)100(2)	Temperature (K)100(2)
Wavelength	0.71073
Crystal system	Orthorhombic
Space group	Pbca
Unit cell dimensions	
$\alpha = 90^\circ$	$a = 15.046(2)\text{\AA}$
$\beta = 90^\circ$	$b = 15.741(2)\text{\AA}$
$\gamma = 90^\circ$	$c = 20.094(3)\text{\AA}$
Volume ( $\text{\AA}^3$ )	4758.9(11)
Z	8
Density (calculated) ( $\text{Mg/m}^3$ )	1.297
Absorption coefficient ( $\text{mm}^{-1}$ )	0.744
F(000)	1968
Crystal size ( $\text{mm}^3$ )	0.51 x 0.43 x 0.30
Theta range for data collection	2.03 to 28.44°
Index ranges	$-20 \leq h \leq 20, -21 \leq k \leq 21, -26 \leq l \leq 26$
Reflections collected	7634
Independent reflections	5971 [R(int) = 0.0420]
Completeness to theta = 28.44°	99.6 %
Absorption correction	Multi-scan with SADABS
Max. and min. transmission	0.8077 and 0.7029
Refinement method	Full-matrix least-squares on $F^2$
Data / restraints / parameters	5971 / 2 / 292
Goodness-of-fit on $F^2$	1.068
Final R indices [ $I > 2\sigma(I)$ ]	R1 = 0.0543, wR2 = 0.1438
R indices (all data)	R1 = 0.0719, wR2 = 0.1618
Largest diff. peak and hole ( $e.\text{\AA}^{-3}$ )	2.046 and -0.425

Table 2.3: Selected bond lengths and angles for **C3**

Bond Lengths [Å]		Bond angles[°]	
Co(1)-N(5)	1.900(2)	N(5)-Co(1)-N(3)	90.38(10)
Co(1)-N(3)	1.906(2)	N(5)-Co(1)-N(1)	177.19(10)
Co(1)-N(1)	1.915(2)	N(3)-Co(1)-N(1)	91.76(10)
Co(1)-N(2)	1.950(2)	N(5)-Co(1)-N(2)	95.16(10)
Co(1)-N(4)	1.953(2)	N(3)-Co(1)-N(2)	92.20(10)
Co(1)-N(6)	1.960(2)	N(1)-Co(1)-N(2)	82.94(11)
N(1)-C(1)	1.333(4)	N(5)-Co(1)-N(4)	89.05(9)
N(1)-C(4)	1.374(4)	N(3)-Co(1)-N(4)	83.07(10)
N(2)-C(5)	1.292(4)	N(1)-Co(1)-N(4)	93.01(10)
N(2)-C(6)	1.470(4)	N(2)-Co(1)-N(4)	173.70(10)
N(3)-C(9)	1.343(4)	N(5)-Co(1)-N(6)	82.17(10)
N(3)-C(12)	1.373(4)	N(3)-Co(1)-N(6)	172.26(10)
N(4)-C(13)	1.290(4)	N(1)-Co(1)-N(6)	95.75(10)
N(4)-C(14)	1.466(4)	N(2)-Co(1)-N(6)	90.56(10)
N(5)-C(17)	1.350(3)	N(4)-Co(1)-N(6)	94.66(9)
N(5)-C(20)	1.365(4)		
N(6)-C(21)	1.287(4)		
N(6)-C(22)	1.472(4)		

### 2.2.2: Synthesis and characterization of the aromatic substituted pyrrole-imine ligand and its Cu(II) and Ni(II) complexes

**L2** ligand was prepared in high yield as a white solid by condensation of pyrrole-2-carboxyaldehyde with one equivalent of 2,6-diisopropylaniline as shown in Scheme 2.4. The ligand showed good solubility in most polar solvents such as dichloromethane, diethyl ether, chloroform, tetrahydrofuran and in aromatic solvents such as toluene. **L2** was characterized by <sup>1</sup>H and <sup>13</sup>C-NMR spectroscopy, microanalysis, FT-IR spectroscopy together with mass spectrometry.



Scheme 2.4: Synthetic route to N-(2,6-diisopropylphenyl)-N-[(1E)-1H-pyrrol-2-ylmethylene]amine, **L2**



Figure 2.6:  $^1\text{H-NMR}$  Spectrum of N-(2,6-diisopropylphenyl)-N-[(1E)-1H-pyrrol-2-ylmethylene]amine, **L2**

The  $^1\text{H-NMR}$  spectrum, Figure 2.6, exhibits a resonance at 8.05 ppm for the imine  $\text{HC}=\text{N}$  proton with a corresponding  $^{13}\text{C-NMR}$  signal of the imine  $\text{HC}=\text{N}$  occurring at 152.72 ppm. The  $^1\text{H-NMR}$  spectrum, Figure 2.6, exhibits a resonance at 8.05 ppm for the imine  $\text{HC}=\text{N}$  proton with a corresponding  $^{13}\text{C-NMR}$  signal of the imine  $\text{HC}=\text{N}$  occurring at 152.72 ppm. Other observed signals in the  $^1\text{H-NMR}$  spectrum are the isopropyl methyls

at 1.2 ppm, the isopropyl CH at 3.1 ppm, while the pyrrole ring protons at between  $\delta$  6.2 - 6.8 ppm and the benzene ring proton at 7.26 ppm. The  $^{13}\text{C}\{^1\text{H}\}$ -NMR spectrum shows signals at 27.90 and 23.56 ppm that can be assigned to the isopropyl  $\text{CH}_3$ , those of the pyrrole ring at 109.89, 116.86, 123.20 and 129.77 ppm while those of the benzene carbons were at 124.32, 124.57, 139.03 and 148.29 ppm.

The peaks observed at 1626, 1586  $\text{cm}^{-1}$  in the FT-IR spectrum are for the (C=N) group. This indicates that condensation of the amine and the aldehyde occurred. The data obtained from microanalysis and ESI-MS all agree with the expected product in composition and molecular weight, Table 2.4.

Table 2.4: Characterization data for **L2**, **C4**, and **C5**

	ESI-MS m/z [M+H] <sup>+</sup>	FT-IR $\nu_{\text{(C=N)}}$ $\text{cm}^{-1}$	Micro analysis, Found (Calc)		
			C	H	N
<b>L2</b>	255	1626, 1586	80.24 (80.27)	8.75 (8.72)	10.80 (11.01)
<b>C4</b>	571	1592, 1574	72.02 (71.61)	7.29 (7.42)	9.99 (9.82)
<b>C5</b>	565	1594, 1578	72.12 (72.22)	7.54 (7.49)	9.51 (9.91)

Complexes of **L2** were prepared as for **C1** whereby the ligand was first deprotonated with NaH. Deprotonation was confirmed in each case by running a  $^1\text{H}$ -NMR spectrum. A significant up field shift of all the signals is observed. After filtration of the excess hydride under nitrogen, two equivalents of the sodium salt of **L2** were reacted with one equivalent of  $\text{Cu}(\text{AOC})_2\cdot\text{H}_2\text{O}$  and  $\text{Ni}(\text{AOC})_2\cdot 4\text{H}_2\text{O}$  for **C4** and **C5** respectively. An attempt to carry out the reaction at elevated temperatures did not improve the yields.

After recrystallization, **C4** and **C5** gave an analytically pure crystalline material of deep green and orange colour respectively. The FT-IR analysis of **C4** showed that the  $\nu_{\text{C=N}}$  shifted from 1626, 1586 to 1592, 1574  $\text{cm}^{-1}$  indicating a change of the imine chemical environment. Elemental analysis and ESI-MS data shown in Table 2.4 agreed with the molecular structure of a 1:2 ratio of Cu:**L2**. Single crystal X-ray analysis of **C4** gave the molecular structure shown in Figure 2.7 supporting the analytical data obtained from the

other techniques. Crystal data and structure refinement parameters are shown in Table 2.5 while selected bond lengths and angles are shown in Table 2.6.

FT-IR spectrum of **C5** also shows a shift of the  $\nu_{\text{C=N}}$  to 1594, 1578  $\text{cm}^{-1}$  from the ligand's 1626, 1586  $\text{cm}^{-1}$ . Elemental analysis as well as the ESI-MS data, Table 2.4, agreed with the molecular composition of a 1:2 ratio of Ni:L2. The solid state structure, Figure 2.8, is obtained from single crystal X-ray analysis. Crystal data and structure refinement parameters are shown in Table 2.5 while selected bond lengths and angles are shown in Table 2.7.

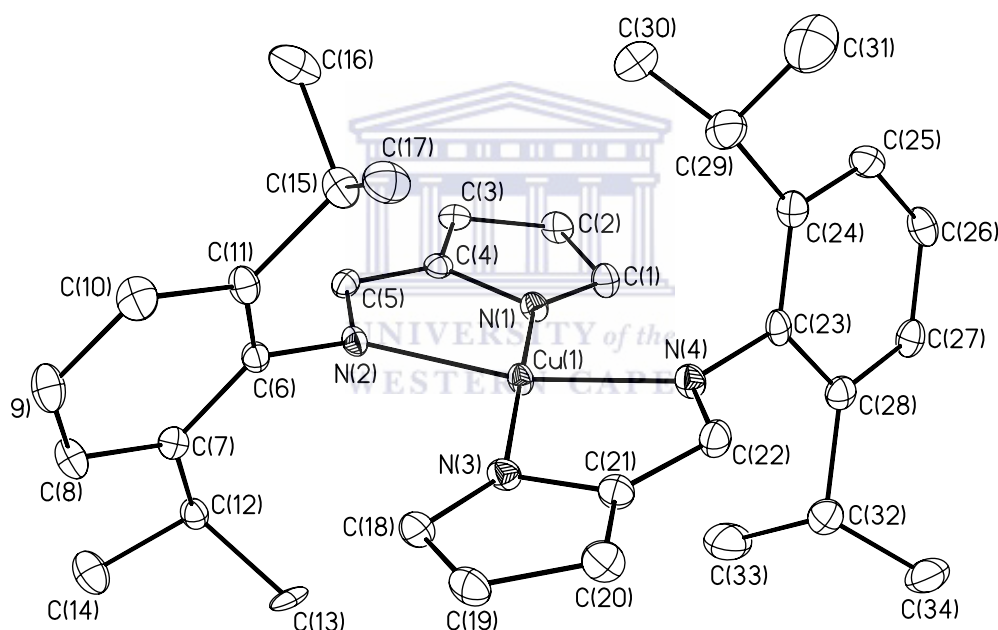


Figure 2.7: Molecular diagram of complex **C4** drawn with 50% probability ellipsoids. Hydrogen atoms are omitted for clarity

The solid state structures of the Cu(II) complex **C4** (Figure 2.7) and Ni(II) complex **C5** (Figure 2.8) are monomeric with a distorted square planar geometry at the metal giving a  $C_2$  symmetry. The pyrrole-N units of the ligands are oriented *trans* to each other. The bite angles are in the range of 82.56(11) to 98.48(10)  $^\circ$  for **C4** and 83.64(7) to 96.75(7)  $^\circ$  for **C5** which is similar to **C3** and those of a reported Cr(II) analogue<sup>5</sup> of 81.8 to 98.4  $^\circ$ .

The imino linkages retain their double bond character [N(2)-C(5) 1.295(4) Å and N(4)-C(22)1.303(4) Å] for **C4** and [N(2)-C(5) 1.305(2) Å and N(4)-C(22)1.302(3) Å] for **C5**. The angles between the imino nitrogen are 166.12(10) ° for N(2)-Cu-N(4) and 169.81(7)° for N(2)-Ni-N(4). This shows a greater distortion as compared to those of Cr(II) which are nearly linear with 179.5 and 179.7 °.

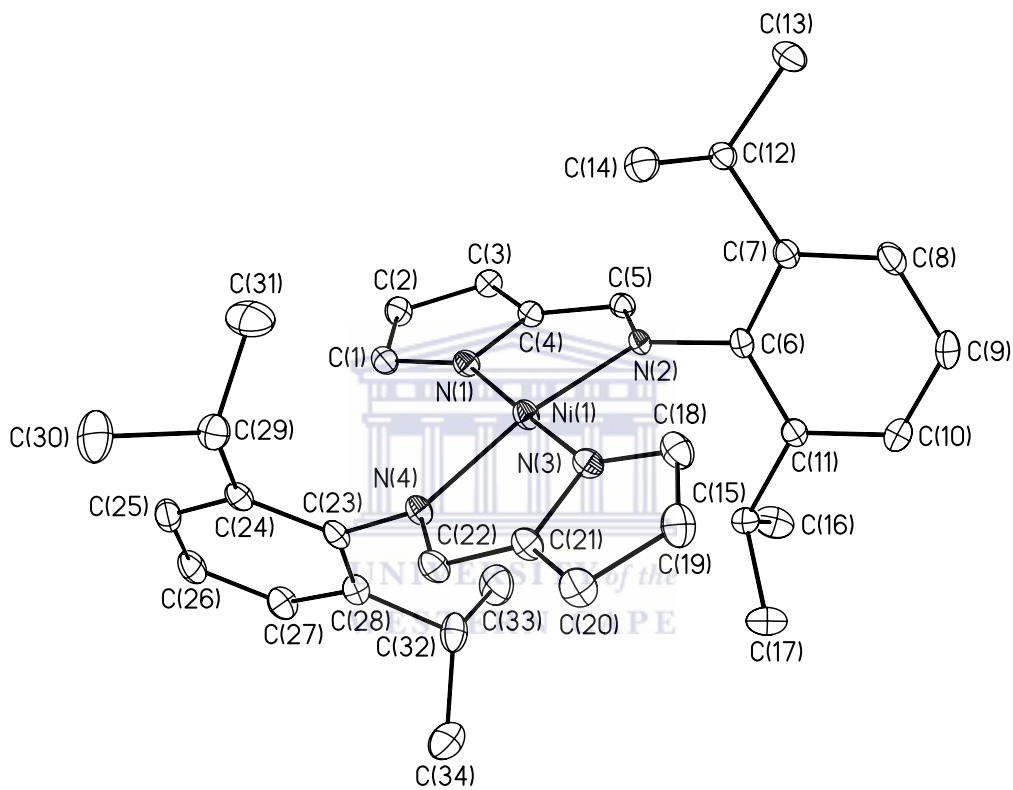


Figure 2.8: Molecular structure of **C5** shown with 50 % probability ellipsoids. All hydrogen atoms are omitted for clarity

Attempts to prepare the cobalt analogue were unsuccessful. When the previously discussed method as used for **C4** and **C5** was employed, the ligand and the cobalt acetate were isolated unreacted. *In situ* deprotonation of the ligand in the presence of  $\text{Co}(\text{AOc})_2 \cdot 4\text{H}_2\text{O}$  as in **C2** did not yield the expected product either. A further attempt to prepare the target molecule using anhydrous  $\text{CoCl}_2$  as the metal source was also futile.

Table 2.5: Summary of crystal data and structure refinement parameters for **C4** and **C5**

	<b>C4</b>	<b>C5</b>
Empirical formula	C <sub>34</sub> H <sub>42</sub> Cu N <sub>4</sub>	C <sub>34</sub> H <sub>42</sub> Cu N <sub>4</sub>
Formula weight	570.26	565.43
Temperature (K)	100(2)	100(2)
Wavelength (Å)	0.71073	0.71073
Crystal system	Monoclinic	Monoclinic
Space group	P2 <sub>1</sub> /c	P2 <sub>1</sub> /c
Unit cell dimensions		
a (Å) [ $\alpha = 90^\circ$ ]	8.2604(11)	8.2594(7)
b (Å), [ $\beta$ , C <sub>4</sub> , = 96.945(2)°, C <sub>5</sub> = 97.4430(10)°]	32.154(4)	31.963(3)
c (Å), [ $\gamma = 90^\circ$ ]	11.3844(15)	11.3602(9)
Volume Å <sup>3</sup>	3001.6(7)	2973.7(4)
Z	4	4
Density (calculated) Mg/m <sup>3</sup>	1.262	1.263
Absorption coefficient (mm <sup>-1</sup> )	0.756	0.681
F(000)	1212	1208
Crystal size(mm <sup>3</sup> )	0.43 x 0.30 x 0.11	0.42 x 0.38 x 0.26
Theta range for data collection	2.20 to 26.43°	1.27 to 27.52°
Index ranges	-10 ≤ h ≤ 10, -40 ≤ k ≤ 40, -13 ≤ l ≤ 14	-10 ≤ h ≤ 10, 41 ≤ k ≤ 40, -14 ≤ l ≤ 14
Reflections collected	32738	38301
Independent reflections	6159 [R(int) = 0.0475]	6828 [R(int) = 0.0313]
Completeness to theta	26.43° = 99.3 %	27.52° = 99.7%
Absorption correction	Multi-scan with SADABS	Multi-scan with SADABS
Max. and min. transmission	0.9214 and 0.7369	0.8427 and 0.7629
Refinement method	Full-matrix least-squares on F <sup>2</sup>	Full-matrix least-squares on F <sup>2</sup>



Table 2.5: Continued

Data / restraints / parameters	6159 / 0 / 361	6828 / 0 / 360
Twin component ratio	3:1	3:1
Goodness-of-fit on F2	1.167	1.042
Final R indices [ $I > 2\sigma(I)$ ]	R1 = 0.0578, wR2 = 0.1137	R1 = 0.0398, wR2 = 0.1104
R indices (all data)	R1 = 0.0705, wR2 = 0.1176	R1 = 0.0705, wR2 = 0.1176
Largest diff. peak and hole e.Å <sup>-3</sup>	0.459 and -0.760	0.569 and -0.614

Table 2.6: Selected bond lengths [Å] and angles [°] for **C4**

Bond Lengths		Bond angles	
Cu(1)-N(3)	1.953(3)	N(3)-Cu(1)-N(1)	174.67(11)
Cu(1)-N(1)	1.956(2)	N(3)-Cu(1)-N(4)	82.56(11)
Cu(1)-N(4)	2.015(3)	N(1)-Cu(1)-N(4)	98.48(10)
Cu(1)-N(2)	2.029(3)	N(3)-Cu(1)-N(2)	98.00(10)
N(1)-C(1)	1.349(4)	N(1)-Cu(1)-N(2)	82.26(10)
N(1)-C(4)	1.385(4)	N(4)-Cu(1)-N(2)	166.12(10)
N(2)-C(5)	1.295(4)		
N(2)-C(6)	1.428(4)		
N(3)-C(18)	1.349(4)		
N(3)-C(21)	1.383(4)		
N(4)-C(22)	1.303(4)		
N(4)-C(23)	1.429(4)		

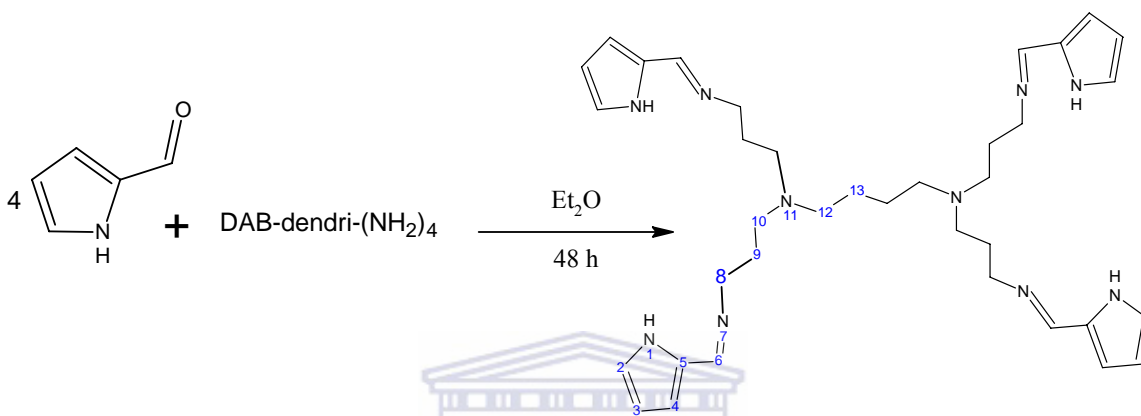
Table 2.7: Selected bond lengths [ $\text{\AA}$ ] and angles [ $^\circ$ ] for **C5**

Bond Lengths		Bond angles	
Ni(1)-N(1)	1.9160(16)	N(1)-Ni(1)-N(3)	176.03(7)
Ni(1)-N(3)	1.9215(17)	N(1)-Ni(1)-N(2)	83.80(7)
Ni(1)-N(2)	1.9302(16)	N(3)-Ni(1)-N(2)	96.52(7)
Ni(1)-N(4)	1.9305(16)	N(1)-Ni(1)-N(4)	96.75(7)
N(1)-C(1)	1.350(2)	N(3)-Ni(1)-N(4)	83.64(7)
N(1)-C(4)	1.384(2)	N(2)-Ni(1)-N(4)	169.81(7)
N(2)-C(5)	1.305(2)		
N(2)-C(6)	1.432(2)		
N(3)-C(18)	1.348(3)		
N(3)-C(21)	1.383(3)		
N(4)-C(22)	1.302(3)		
N(4)-C(23)	1.431(2)		

### 2.2.3: Synthesis and characterization of the dendrimeric pyrrole-imine ligand and its Cu(II), Ni(II) and Co(II) complexes

**L3** was prepared and purified in a similar method as for **L1**. Poly(propylene imine) (DAB-PPI-(NH<sub>2</sub>)<sub>4</sub>) was used in place of propyl amine, Scheme 2.4. A spatula tip of anhydrous MgSO<sub>4</sub> was added to remove water produced as by-product. The functionalized dendrimeric ligand **L3** was isolated as an orange oil in 56 % yield. **L3** was fully characterized by a number of methods. The <sup>1</sup>H-NMR spectrum, Figure 2.9, showed clear evidence of the condensation. The CH<sub>2</sub> signal adjacent to the imino group is observed to move down field from the signal of the CH<sub>2</sub> next to NH<sub>2</sub> of the starting dendrimeric amine as well as a signal due to a proton of the N=CH group emerges at  $\delta$  8.03 ppm. The dendrimer core protons are observed at 1.4 ppm for the internal CH<sub>2</sub> while that at 2.4 ppm can be assigned to CH<sub>2</sub> groups adjacent to nitrogen in the dendrimer and the propyl chain. The other proton signals for the propyl group are observed at 1.7 for the CH<sub>2</sub> in the middle while that at 3.6 ppm is for the CH<sub>2</sub> next to the imine system. The pyrrole ring protons were observed between 6.9-6.2 ppm. The <sup>13</sup>C{<sup>1</sup>H}-NMR spectrum shows signal at 152.1 ppm for the N=CH, 109.5 and pyrrole

ring carbon signals at 114.3, 121.9 and 130.1 ppm. The dendrimeric framework CH<sub>2</sub> carbons are observed between 25.0, 28.3, 51.4, 53.8, 58.8 ppm for carbons 13, 9, 12, 10 and 8 respectively, numbering in Scheme 2.4. FT-IR spectroscopy showed the expected functionalities; a  $\nu_{\text{C}=\text{N}}$  stretching band at 1638 cm<sup>-1</sup>,  $\nu_{\text{N-H}}$  at 3152 cm<sup>-1</sup> and the  $\nu_{\text{C-H}}$  stretching frequencies at 2972-2884 cm<sup>-1</sup>.



Scheme 2.5: Synthetic route to dendrimeric ligand, DAB-PPI-(N=CH(C<sub>4</sub>H<sub>3</sub>NH)<sub>4</sub>), **L3**

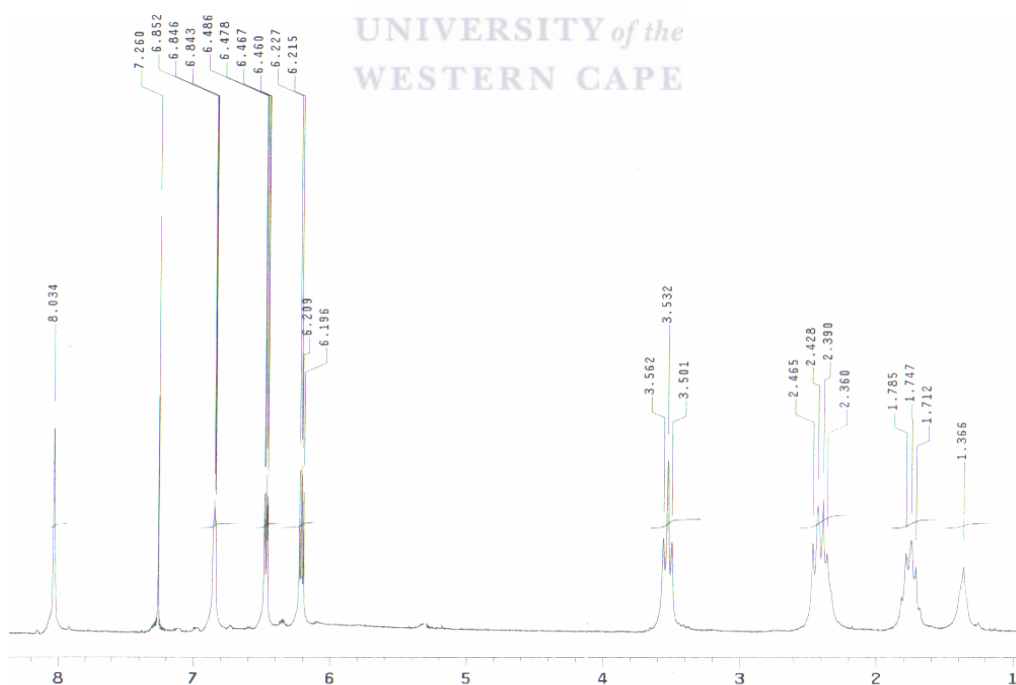


Figure 2.9: <sup>1</sup>H-NMR Spectrum of DAB-PPI-(N=CH(C<sub>4</sub>H<sub>3</sub>NH)<sub>4</sub>), **L3**

The ESI-MS mass spectrum, Figure 2.10, showed a molecular ion peak at  $m/z$  779. This corresponds to the calculated molecular weight of 625 with four potassium ions associated with each of the pyrrole groups on the periphery of the dendrimeric ligand. The data obtained from elemental analysis agrees with the calculated molecular weight and 0.5  $\text{CH}_2\text{Cl}_2$  associated with it as shown in Table 2.8.

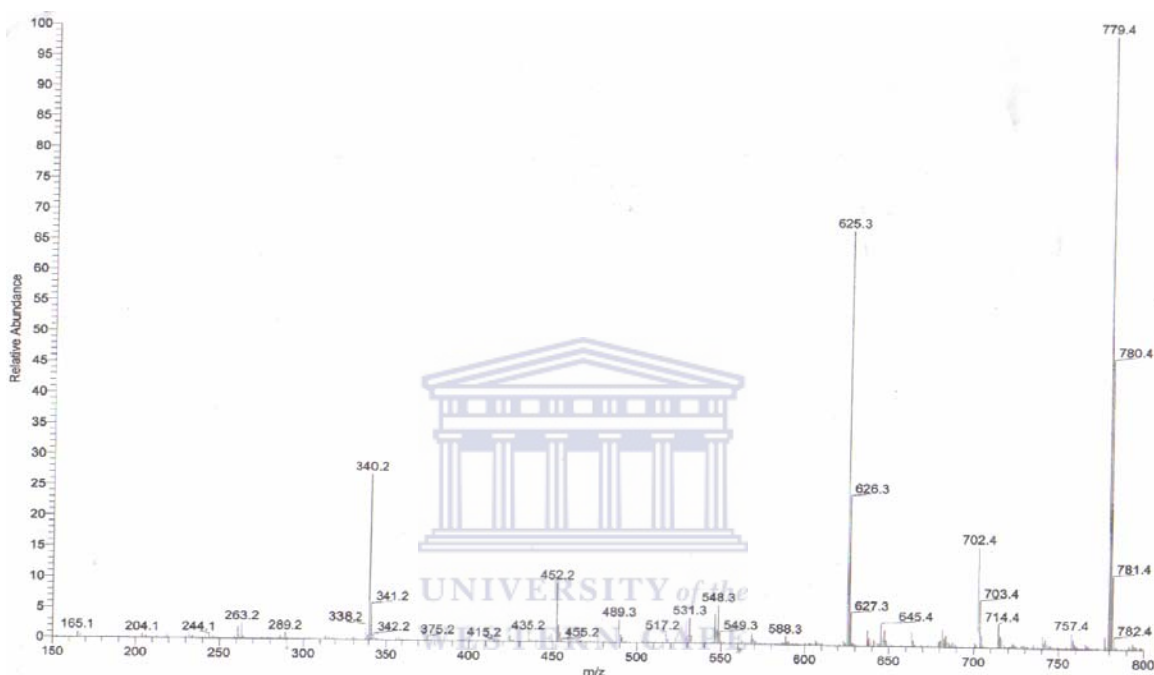


Figure 2.10: ESI-MS spectrum of DAB-PPI-( $\text{N}=\text{CH}(\text{C}_4\text{H}_3\text{NH})_4$ ), **L3**

The Cu(II) complex, **C6**, of this dendritic ligand was prepared via the deprotonation method as discussed for **C1** while the Ni(II), **C7**, and Co(II), **C8**, were prepared as for **C2** and **C3** respectively. **C6** was isolated as a green amorphous solid after precipitation with hexane from  $\text{CH}_2\text{Cl}_2$  in 62 % yield. **C7** and **C8** were also precipitated with hexane as amorphous brown solids from  $\text{CH}_2\text{Cl}_2$  in 70 % and 63 % yields respectively. The FT-IR spectra showed a significant shift of the  $\nu_{\text{C}=\text{N}}$  band ligand from  $1638\text{ cm}^{-1}$  to  $1586\text{ cm}^{-1}$ ,  $1600\text{ cm}^{-1}$ , and  $1596\text{ cm}^{-1}$  for **C6**, **C7** and **C8** respectively. The composition of the complexes was established by mass spectrometry and elemental analysis. The elemental analysis showed that the three dendritic complexes are bimetallic systems. **C7** has 0.25 mol of  $\text{CH}_2\text{Cl}_2$  associated with it. The ESI-MS spectra showed doubly charged species of

these complexes at  $m/z$  375, 369 and 370 for **C6**, **C7** and **C8** respectively. These results are summarized in Table 2.8. These complexes are stable at room temperature and can be stored without apparent decomposition.

Table 2.8: Characterization data for **L3**, **C6**, **C7** and **C8**

	FT-IR $\nu_{(C=N)}\text{cm}^{-1}$	ESI-MS $m/z$	Micro analysis, Found (Calculated)		
			C	H	N
<b>L3</b> <sup>a</sup>	1638	624 <sup>c</sup>	65.02 (65.69)	7.84 (8.01)	19.80 (20.99)
<b>C6</b>	1596	375 <sup>d</sup>	57.82 (57.83)	6.57 (6.47)	17.33 (18.73)
<b>C7</b> <sup>b</sup>	1600	369 <sup>d</sup>	57.22 (57.33)	6.35 (6.44)	17.15 (18.44)
<b>C8</b>	1586	370 <sup>d</sup>	59.16 (58.53)	6.72(6.55)	18.64 (18.96)

<sup>a</sup> microanalysis include 0.5 CH<sub>2</sub>Cl<sub>2</sub>

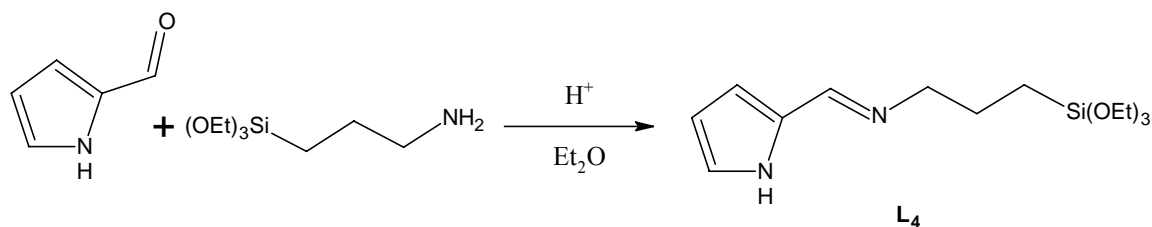
<sup>b</sup> microanalysis include 0.25 CH<sub>2</sub>Cl<sub>2</sub>

<sup>c</sup> represents  $m/z$  for single charged ion

<sup>d</sup> represents  $m/z$  for double charged ion

#### 2.2.4: Synthesis and characterization of the 3-aminopropyltriethoxysilane functionalized pyrrole-imine ligand and its Cu(II) and Ni(II) complexes

Ligand **L4** was prepared by reacting pyrrole-2-carboxyaldehyde with the 3-aminopropyltriethoxysilane, Scheme 2.5, in the ratio of 1:1. A catalytic amount of glacial acetic acid and anhydrous MgSO<sub>4</sub> (*ca.* 0.5 g) to absorb the water formed as by-product were added. Analytically pure orange oil was obtained in high yield of 85 % upon filtration and solvent evaporation. Precaution should be taken to prevent presence of water in the reaction to avoid hydrolysis of the triethoxysilane functionality. In the presence of water a brown paste insoluble in most organic solvents is obtained. This is assumed to be a self-condensation product formed as a result of partial hydrolysis of the ethoxysilane starting materials. **L4** showed good solubility in most solvents such as dichloromethane, diethyl ether, chloroform, ethanol, tetrahydrofuran as well as aromatic solvents such as toluene. Slow evaporation of CH<sub>3</sub>Cl from the ligand solution gave an insoluble orange paste. This implies that **L4** is not stable in solution at room temperature. The product was characterized by <sup>1</sup>H, <sup>13</sup>C-NMR and FT-IR spectroscopy, mass spectrometry and microanalysis.



Scheme 2.6: Synthetic route to triethoxysilane functionalized pyrrole-imine ligand, **L4**

The  $^1H$ -NMR spectrum obtained in  $CDCl_3$  showed signals of the ethoxy  $CH_2$  at 3.8 ppm and that of the  $CH_3$  at 1.2 ppm. Their respective carbon signals in the  $^{13}C$ -NMR spectrum were observed at 58.4 and 18.3 ppm. The  $CH_2$  appears more downfield because of the oxygen attached to the silicon. The  $^1H$ -NMR signal of the  $CH_2$  bonded to imine was observed at 3.5 ppm, the central  $CH_2$  proton peak at 1.7 ppm and that at 0.7 ppm is for the  $CH_2$  bonded to the silicon. The  $^{13}C$  signals of these groups were observed at 63.3, 24.5 and 8.0 respectively. The pyrrole ring protons signals were observed at 6.2, 6.5, and 6.9 ppm. Those of the carbons were observed at 109.6, 114.1, 121.7, 130.1 ppm. The most characteristic signal is that of the pyrrole  $N=CH$  proton observed at 8.04 ppm and  $N=CH$  carbon that appeared at 151.66 ppm. The  $NH$  proton signal of the pyrrole was not observed in this spectrum.

UNIVERSITY of the  
WESTERN CAPE

In the FT-IR spectrum, the band at  $3152\text{ cm}^{-1}$  is for the  $\nu_{N-H}$  of the pyrrole ring while that at  $1640\text{ cm}^{-1}$  for the  $\nu_{C=N}$ . Peaks at  $2972\text{-}2884\text{ cm}^{-1}$  are for the  $\nu_{C-H}$  units of the aromatic and aliphatic groups and those at  $1102\text{-}1080\text{ cm}^{-1}$  is for the  $\nu_{Si-O}$  of the triethoxysilane functionality.<sup>25</sup>

The ESI-MS spectrum, Figure 2.11, shows a molecular ion peak at 299 m/z which correlates with the calculated molecular weight of **L4**. The spectrum also shows very little fragmentation indicating that the molecule is relatively stable under the conditions employed.

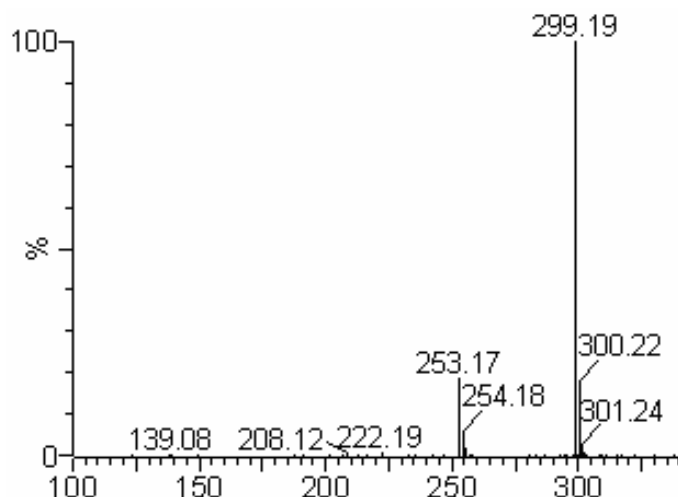


Figure 2.11: ESI-MS spectrum of **L4**

The copper complex, **C9**, was prepared from  $\text{Cu}(\text{OAc})_2 \cdot \text{H}_2\text{O}$ . The ligand was deprotonated with NaH as discussed for **C1** and then the appropriate amount of the metal acetate added. The  $\text{Cu}(\text{OAc})_2 \cdot \text{H}_2\text{O}$  dissolved giving a blue solution that gradually changed to deep green. The product was obtained in 57 % yield as a green amorphous solid. The nickel complex, **C10**, was prepared in a similar method as the Cu analogue. However,  $\text{Ni}(\text{AOC})_2 \cdot 4\text{H}_2\text{O}$  was used as the metal salt. An orange amorphous solid was obtained in 51% yield. As with the ligand, the complexes were prepared and also worked up in distilled and dried solvents.

The complexes **C9** and **C10** were characterized by FT-IR spectroscopy, mass spectrometry and microanalysis and the data is shown in Table 2.9. The FT-IR spectra showed a significant shift of the  $\nu_{\text{C}=\text{N}}$  band from  $1640 \text{ cm}^{-1}$  in the ligand to  $1592$  and  $1584 \text{ cm}^{-1}$  for **C9** and **C10** respectively. When **C9** was left on the bench in a closed vial for 28 days, some of the compound became insoluble in  $\text{CH}_2\text{Cl}_2$ . These complexes could have undergone self-condensation or hydrolysis as shown in Figure 2.12. This suggests the complexes are not very stable at room temperature. The complexes were subsequently stored in the glove box immediately after preparation. The elemental analysis of **C9** in Table 2.9 supported this observation. The Ni analogue, **C10**, also undergoes hydrolysis

but one of the ethoxy groups is still present. The complexes were stored in the glove box thereafter. This may imply that the process is gradual.

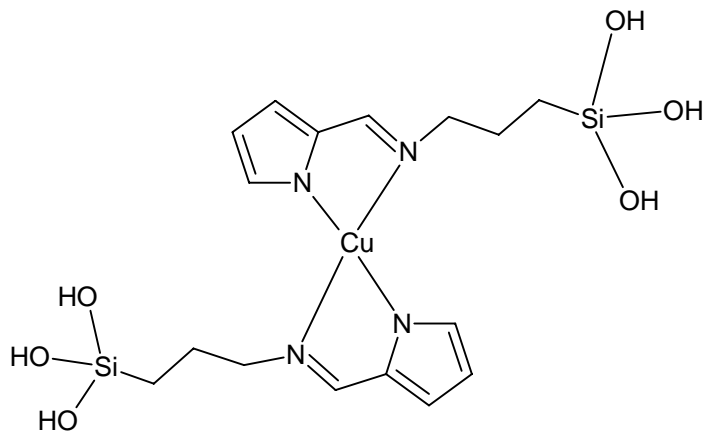


Figure 2.12: Condensation and hydrolysis of **C9**

These complexes were sent for ESI-MS analysis immediately after preparation. The ESI-MS spectra showed doubly charged species of these complexes at  $m/z$  302 and 300 for **C9** and **C10** respectively. However these complexes were observed to have undergone partial hydrolysis as two ethoxy groups had been lost for each of the complexes. The results are summarized in Table 2.9.

Attempts to prepare the cobalt analogue were not successful. When the above mentioned method as in **C9** and **C10** was used a khaki green solid was obtained. This solid was insoluble in all common solvents. This includes  $\text{CH}_2\text{Cl}_2$ ,  $\text{CH}_3\text{Cl}$ , EtOH, MeOH, THF, hexane and others. There was evidence of complexation due to the shift of the  $\nu_{\text{C=N}}$  band of the ligand from 1640 to 1588  $\text{cm}^{-1}$  in the FT-IR spectrum, recorded as KBr pellet. However a broad band *ca.* 3100  $\text{cm}^{-1}$  was observed. This can be attributed to the presence of OH groups. Thus the conclusion was made that the ethoxy groups had been hydrolyzed. With the ethoxy groups hydrolyzed, it would not be possible to anchor this complex onto the inorganic support MCM-41. A further attempt to use anhydrous  $\text{CoCl}_2$  as the metal source was also unsuccessful.



Table 2.9: Characterization data for **L4**, **C9** and **C10**

	FT-IR $\nu_{(C=N)}\text{cm}^{-1}$	m/z	Micro analysis, Found (Calc)		
			C	H	N
<b>L4</b>	1640	299 <sup>a</sup>	56.43(56.34)	8.56(8.78)	9.10(8.78)
<b>C9</b>	1592	302 <sup>b</sup>	41.13(41.50)	4.39(5.01)	11.27(12.10)
<b>C10</b>	1584	300 <sup>b</sup>	44.25(43.85)	4.88(5.47)	11.70(11.69)

<sup>a</sup> represents m/z for single charged ion

<sup>b</sup> represents m/z for double charged ion

### 2.2.5: Synthesis of MCM-41, immobilization and characterization of the Cu(II) and Ni(II) complexes

Mesoporous silica designated as MCM-41 was obtained by the hydrolysis of tetraethyl orthosilicate, TEOS, in the presence of a templating agent cetyltrimethylammonium bromide;  $\text{CH}_3(\text{CH}_2)_{15}\text{N}(\text{CH}_3)_3\text{Br}$ , CTAB. Calcination at 550 °C was done to remove the surfactant. The temperature was increased gradually so that the structure of the MCM-41 does not collapse.<sup>23</sup>

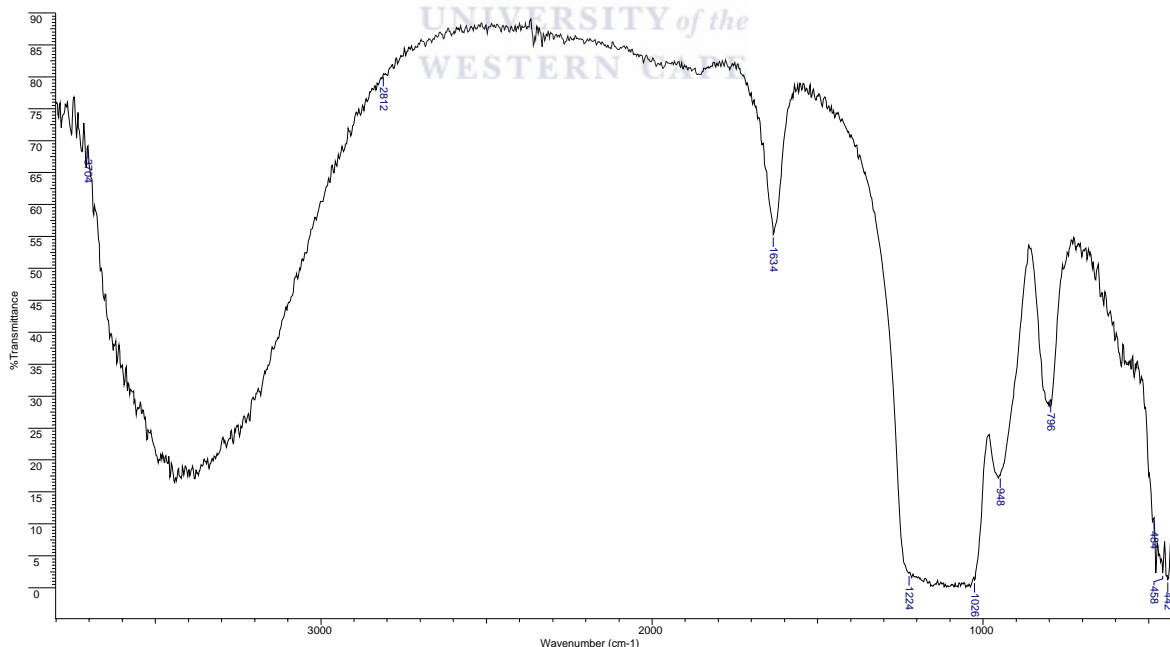


Figure 2.13: FT-IR spectrum of MCM-41

The white material obtained was characterized by FT-IR spectroscopy, XRD and BET surface area analytical method. The FT-IR spectrum, Figure 2.13, of the synthesized MCM-41 show characteristic vibrational bands at 1224-1028, 796, and 480  $\text{cm}^{-1}$  which correspond to the stretching, bending and out of plane deformation vibrations of Si-O-Si bonds. The broad absorption band at 3700-2800  $\text{cm}^{-1}$  can be assigned to the OH groups on the surface and the Si-OH at 1634  $\text{cm}^{-1}$ . The values compare favourably to those reported by Luts *et al.*<sup>28</sup> and Jiang *et al.*<sup>29</sup> for the Si-O-Si and OH groups respectively.

The powder XRD pattern of the synthesized MCM-41, Figure 2.14, exhibit strong peaks at 2.5, 4.3 and 5.0  $^{\circ}$  corresponding to (100), (110) and (200) respectively. These peaks are consistent with the values reported by Cai *et al.*<sup>23</sup> of 2.26, 3.89 and 4.50  $^{\circ}$ . These three low-angle reflections were, ( $d_{100}$ ,  $d_{110}$ ,  $d_{200}$ ), characteristic of a well-ordered hexagonal pore arrangement and the d-spacing values were calculated as 35.31, 41.06 and 52.97  $\text{\AA}$ . Singh *et al.*<sup>30</sup> reported a  $d_{100}$ , spacing value of 35  $\text{\AA}$ .

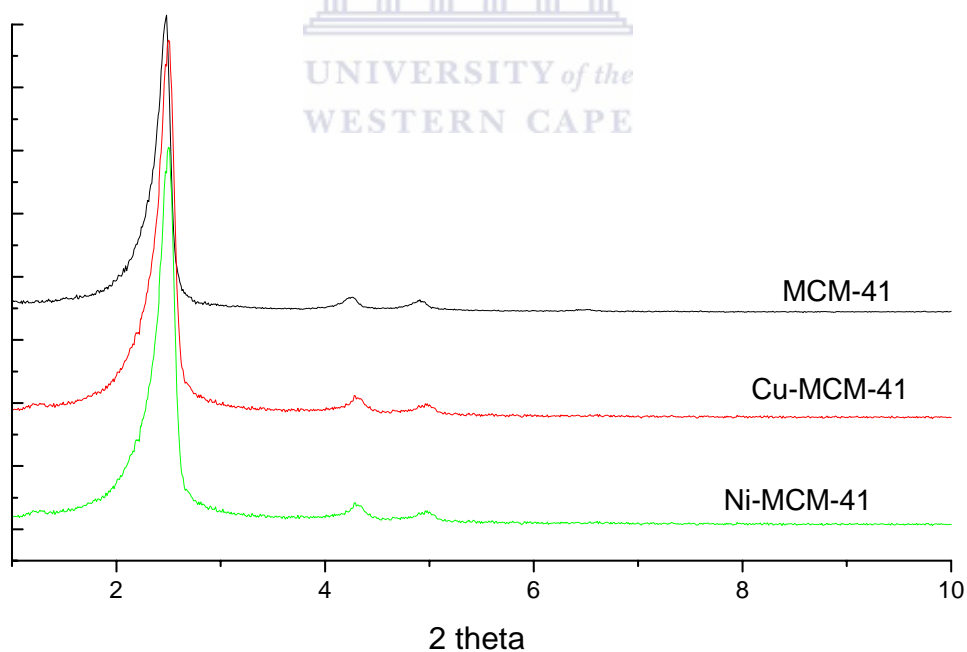


Figure 2.14: The Powder XRD patterns of calcined MCM-41, **Cu-MCM-41** and **Ni-MCM-41**

The copper–Schiff base complex on MCM-41 (**Cu-MCM-41**) and the nickel-Schiff base complex on MCM-41 (**Ni-MCM-41**) materials were prepared by anchoring **C9** and **C10** respectively onto MCM-41. These materials were analyzed and characterized by FT-IR spectroscopy, AAS, XRD and BET surface area analytical methods. The FT-IR spectra of the parent MCM-41, **Cu-MCM-41** and **Ni-MCM-41** samples were similar. All the properties of the synthesized MCM-41 were retained. The  $\nu_{C=N}$  and  $\nu_{C-H}$  bands of the complexes were not observed because they were masked by the Si-OH band and OH bands respectively.

The powder XRD patterns for the **Cu-MCM-41** and **Ni-MCM-41** are also shown in Figure 2.14. The position of  $d_{100}$  reflection remains virtually unchanged post immobilization of the complexes. **Cu-MCM-41**  $d_{100}$ ,  $d_{200}$ ,  $d_{300}$  values are 36.78, 44.14 and 57.57 Å respectively while those of the Ni analogue are 37.24, 44.27 and 57.67 Å. This suggests that the hexagonal pore arrangement of MCM-41 remains intact.

Table 2.10: Characterization data for MCM-41, **Cu-MCM-41** and **Ni-MCM-41**

	Metal loading %	$S_{BET}$ ( $m^2 g^{-1}$ )	$V_{(pore)}$ ( $cm^3 g^{-1}$ )	average pore diameter (Å)
MCM-41		1229.8	1.0	33.78
<b>Cu-MCM-41</b>	0.74	1019.0	0.80	31.59
<b>Ni-MCM-41</b>	0.46	1086.7	0.86	31.69

The amount of metal supported was observed to vary depending on the time taken between the complex preparation and immobilization onto MCM-41. When the **C9** was immobilized immediately after its preparation, it was observed that up to 0.74 % Cu was supported as opposed to only 0.43 % when the complex was left standing on the bench for 28 days. For the Ni(II) analogue, it was observed that up to 0.46 % was anchored after immobilization immediately after preparation and as low as 0.12 % after 28 days. This further supports the earlier observation of stability of these complexes at room temperature. The hydrolysis of the ethoxy groups minimizes the loading onto MCM-41.

The specific surface area, pore size and the pore volume, Table 2.10, of all samples were analyzed by nitrogen adsorption-desorption techniques. The BET surface area, pore diameter and pore volume of the synthesized MCM-41 sample were  $1229 \text{ m}^2\text{g}^{-1}$ ,  $33.78 \text{ \AA}$  and  $1.0 \text{ cm}^3\text{g}^{-1}$ , respectively, typical values of MCM-41 samples prepared under basic conditions by Cai *et al.*<sup>23</sup> but lower than  $1451 \text{ m}^2\text{g}^{-1}$  reported by Clercq *et al.*<sup>31</sup>. A decrease in surface area, pore diameter and pore volume was observed on immobilization of the metal complexes onto the synthesized MCM-41. This indicates the immobilization of Schiff base complex not only occurs on the surface but also within the pores of inorganic MCM-41. It was also observed that the **Ni-MCM-41** sample exhibits larger surface area, pore size and volume values as compared to the **Cu-MCM-41**. This may be explained that since there is higher copper loading than nickel, there is more blocking of the pore in the **Cu-MCM-41** material than the **Ni-MCM-41**.

Nitrogen adsorption isotherms for the parent MCM-41, **Cu-MCM-41** and **Ni-MCM-41** samples (Figure 2.15) showed a loop between 0.2 and 0.3 P/P<sub>0</sub>. This is a typical shape for mesoporous materials.

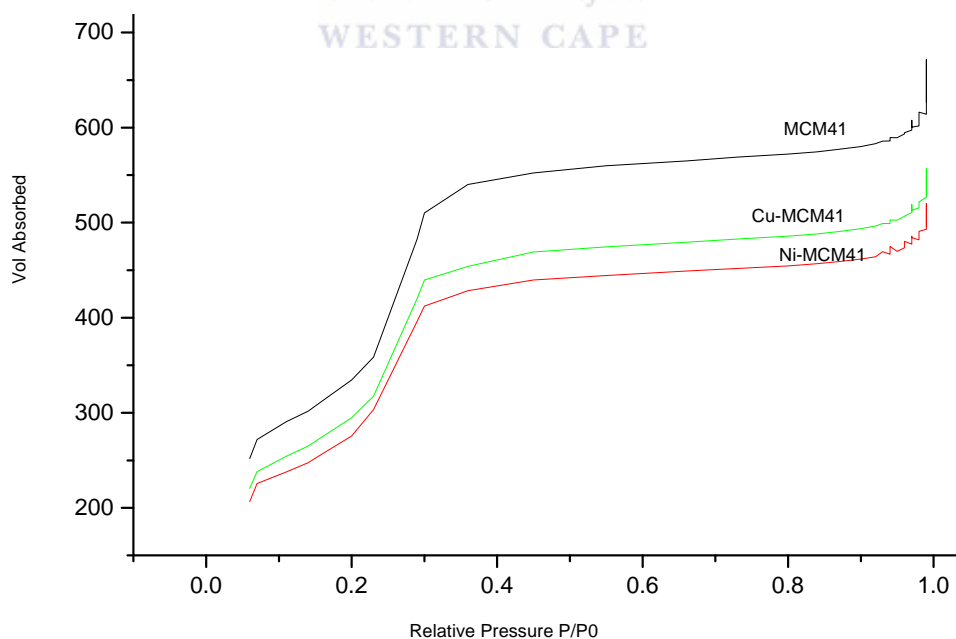


Figure 2.15: Nitrogen adsorption isotherm of MCM-41, **Cu-MCM-41** and **Ni-MCM-41**

A further attempt was made to prepare cobalt-Schiff base MCM-41 (**Co-MCM-41**). An alternative approach reported in literature was employed.<sup>30</sup> The ligand was first immobilized onto MCM-41 and complexation done thereafter. The material obtained after immobilization of the ligand onto the MCM-41 (**L4-MCM-41**) was characterized by FT-IR spectroscopy and XRD. The FT-IR spectrum showed the expected characteristic peaks of the Schiff-base MCM-41 material, a broad OH band in the region 3000- 3650  $\text{cm}^{-1}$ , Si-O-Si frame work at 1254-1008  $\text{cm}^{-1}$  and C-H band at 2978  $\text{cm}^{-1}$  are observed. The **L4-MCM-41** was then treated with NaH to deprotonate the pyrrole nitrogen. Upon deprotonation with NaH the above mentioned bands were retained in the FT-IR spectrum. However, the intensity of the OH band decreases. Then the resulting material was treated with anhydrous  $\text{CoCl}_2$ . The yellow-green material obtained was characterized by FT-IR spectroscopy, AAS, and XRD. The FT-IR spectrum showed all the observed bands as with the NaH treated **L4-MCM-41** material. The amount of Co present was determined to be 4.06 % from the metal analysis. This was much higher than what has been reported in literature using the same approach but with salicylaldiminate ligands. It is also higher than what we obtained with the systems of Cu and Ni we prepared. Maybe  $\text{Co}^{2+}$  did not only react with the immobilized ligand but also with the other OH groups of the surface of the MCM-41. This may also be supported by the reduced intensity of OH band in the FT-IR spectrum.

The powder XRD pattern showed that after complexation the crystallinity of the MCM-41 was lost, Figure 2.16. It was suspected that this resulted from the treatment with the NaH. The following test was carried out to confirm. The parent MCM-41 material was treated with NaH under similar conditions to those of the ligand deprotonation step. When powder XRD was run, the crystallinity had been lost. It was concluded that the use of NaH led to the collapse of the MCM-41 structure. Figure 2.17 shows the comparison of the XRD pattern of the **L4-MCM-41** and that of the NaH treated MCM-41 (**Na-MCM-41**).

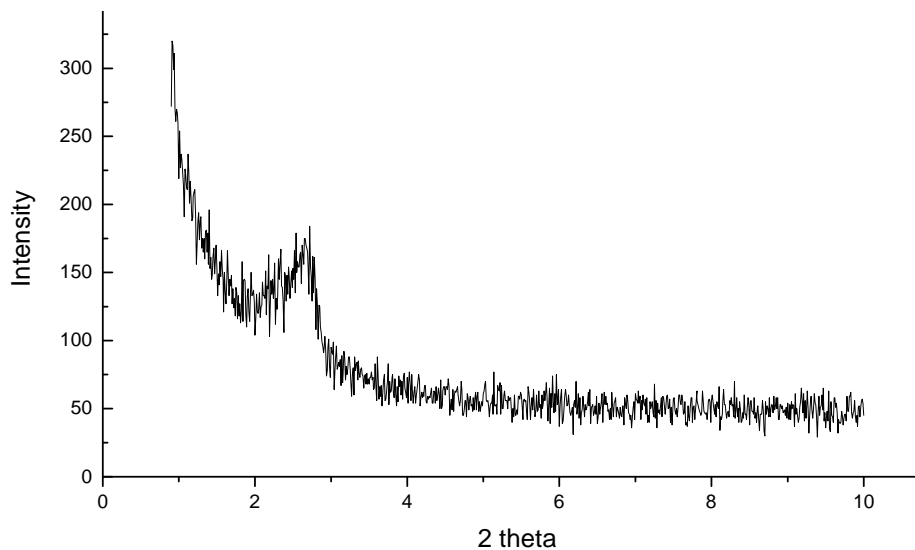


Figure 2.16: The Powder XRD patterns of **Co-MCM-41**

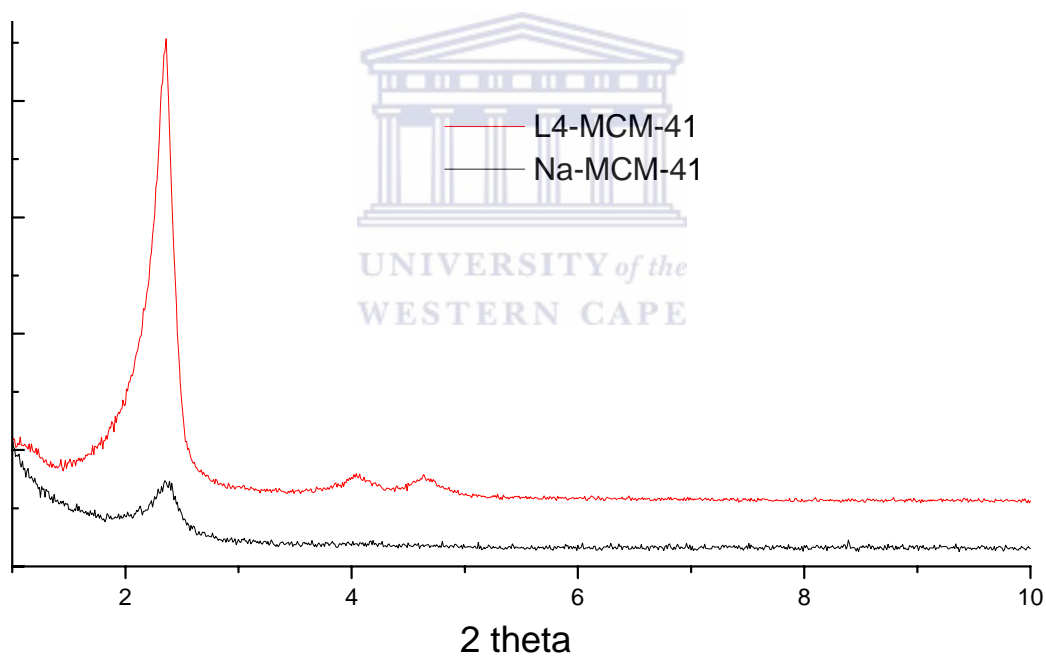


Figure 2.17: The Powder XRD patterns of **L4-MCM-41** and **Na-MCM-41**

## 2.3: Experimental

### 2.3.1: Materials and instrumentation

Ligands and metal complexes were synthesized using standard Schlenk techniques under nitrogen using a dual vacuum/nitrogen line. All solvents used were of analytical grade and were dried and distilled prior to use. Tetrahydrofuran (THF), hexane and diethyl ether were dried and distilled from sodium/benzophenone, methanol from magnesium turnings/iodine and dichloromethane over phosphorous pentoxide. Pyrrole-2-carboxyaldehyde, propylamine, 2,6-diisopropylaniline, 3-aminopropyltriethoxysilane, tetraethylorthosilicate (TEOS) and cetyltrimethylammonium bromide (CTAB) were purchased from Sigma-Aldrich Ltd. Poly(propylene imine) DAB-PPI-(NH<sub>2</sub>)<sub>4</sub> was purchased from Symo-Chem and aqueous ammonia (NH<sub>4</sub>OH) was obtained from Merck. All starting materials were used without further purification.

The NMR spectra were recorded on a Varian Gemini 200 spectrometer (<sup>1</sup>H at 200 MHz, <sup>13</sup>C at 50.3 MHz) at room temperature using tetramethylsilane as an internal standard. The chemical shifts are reported in δ (ppm) and referenced to CDCl<sub>3</sub> the NMR solvent. Infrared spectra were recorded on a Perkin Elmer Paragon 1000PC FT-IR spectrophotometer as KBr pellets for the solids or between NaCl plates for the oils. GC-MS analysis was performed using a Finnigan-Matt GCQ-Gas Chromatograph equipped with an electron ionization source at 70 eV and a 30 m HP-MS capillary column with a stationary phase based 5% phenyl-methylpolysiloxane. ESI-MS data was obtained on a Waters API Q-TOF Ultima spectrometer calibrated with NaF at the University of Stellenbosch. Microanalyses were performed at the University of Cape Town micro analytical Laboratory. The X-ray crystal evaluation and data collected were performed on a Bruker CCD-1000 diffractometer with Mo K<sub>α</sub> (λ = 0.71073 Å) radiation and a diffractometer to crystal distance of 4.9 cm. Powder X-ray diffraction patterns were recorded on a Bruker-AXS diffractometer using a Cu- K<sub>α</sub> radiation (λ = 1.5409 Å) and a graphite monochromator at Ithemba Laboratory, Somerset West, South Africa. The samples were scanned in the 2θ range of 2 to 10 ° with step size of 0.01 at a count time of 1 s per point. Analysis for metal content was performed on a Philips- Du- 9100 atomic

absorption spectrophotometer using air/acetylene fuel with the appropriate lamp. The BET surfaces area analysis was done using a Tristar 3000 micromeritics Surface Area and Porosity Analyzer at the Chemical Engineering Department of the University of Cape Town. Prior to measurements, the samples were degassed at 90 °C for 1 h and ramped to 165 °C over 1 h at a pressure of 70 bar. The analysis bath was kept at 77 °C.

### ***2.3.2: Molecular structure determination using single crystal X-ray analysis***

#### *Data collection*

**C3** is used as an example for the data X-ray analysis. A red crystal with approximate dimensions 0.51 x 0.43 x 0.30 mm<sup>3</sup> was selected under oil under ambient conditions and attached to the tip of a nylon loop. The crystal was mounted in a stream of cold nitrogen at 100(2) K and centered in the X-ray beam by using a video camera. The crystal evaluation and data collection was performed on a Bruker CCD-1000 diffractometer with Mo K<sub>α</sub> ( $\lambda = 0.71073 \text{ \AA}$ ) radiation and the diffractometer to crystal distance of 4.9 cm. The initial cell constants were obtained from three series of  $\omega$  scans at different starting angles. Each series consisted of 20 frames collected at intervals of 0.3° in a 6° range about  $\omega$  with the exposure time of 10 seconds per frame. A total of 244 reflections were obtained. The reflections were successfully indexed by an automated indexing routine built in the SMART program. The final cell constants were calculated from a set of 6968 strong reflections from the actual data collection.

The data was collected by using the hemisphere data collection routine. The reciprocal space was surveyed to the extent of a full sphere to a resolution of 0.80 Å. A total of 76343 data were harvested by collecting three sets of frames with 0.36° scans in  $\omega$  with an exposure time 20 sec per frame and one set of frames with 0.45° scans in  $\omega$  with an exposure time 20 sec per frame. These highly redundant datasets were corrected for Lorentz and polarization effects. The absorption correction was based on fitting a function to the empirical transmission surface as sampled by multiple equivalent measurements.<sup>32</sup>



*Structure Solution and Refinement*

The systematic absences in the diffraction data were uniquely consistent for the space group *Pbca* that yielded chemically reasonable and computationally stable results of refinement. A successful solution by the direct methods provided most non-hydrogen atoms from the *E*-map. The remaining non-hydrogen atoms were located in an alternating series of least-squares cycles and difference Fourier maps. All non-hydrogen atoms were refined with anisotropic displacement coefficients. All hydrogen atoms were included in the structure factor calculation at idealized positions and were allowed to ride on the neighboring atoms with relative isotropic displacement coefficients. Carbon C23 and its hydrogen atoms and the hydrogen atoms on C22 and C24 are disordered over two positions in a 0.559(10):0.441 ratios. The final least-squares refinement of 292 parameters against 5971 data resulted in residuals *R* (based on  $F^2$  for  $I \geq 2\sigma$ ) and  $wR$  (based on  $F^2$  for all data) of 0.0543 and 0.1618, respectively. The residual peak of 2.046  $e \text{ \AA}^{-3}$  near the cobalt atom is considered noise.

**2.3.3: Ligand synthesis****2.3.3.1: Synthesis of (Propyl-(1-*H* pyrrol-2-ylmethylene) imine; **L1****

A yellow solution of pyrrole-2-carboxylaldehyde (1 g, 10.53 mmol) in dry diethyl ether (20 mL), had propyl amine (0.86 mL, 10.53 mmol) syringed into it. Few drops of glacial acetic acid were added as a catalyst. The solution was stirred at room temperature for 6 h. The solvent was then removed from the reaction solution by rotary evaporation giving an orange oil. The product was purified by dissolving it in  $\text{CH}_2\text{Cl}_2$  (25 mL) and washed with water (5 x 25 mL). The organic layer was collected, dried over anhydrous  $\text{MgSO}_4$  and filtered by gravity. Removal of  $\text{CH}_2\text{Cl}_2$  yielded an orange oil. Yield 0.80 g, 56 %.  $^1\text{H-NMR}$  ( $\text{CDCl}_3$ ) (Fig. 2.4)  $\delta$  (in ppm) 0.93 (t, 3H,  $\text{CH}_3$ ,  $^3J_{\text{HH}} = 7.0$  Hz), 1.66 (q, 2H,  $\text{CH}_3\text{CH}_2$ ,  $^4J_{\text{HH}} = 7.0$  Hz), 3.46 (t, 2H,  $\text{NCH}_2$ ,  $^3J_{\text{HH}} = 7.0$  Hz), 6.24 (t, 1H,  $\text{C}_4\text{H}_3\text{NH}$ ,  $^3J_{\text{HH}} = 2.8$  Hz); 6.51 (d, 1H,  $\text{C}_4\text{H}_3\text{NH}$ ,  $^2J_{\text{HH}} = 2.8$  Hz); 6.91 (s, br, 1H,  $\text{C}_4\text{H}_3\text{NH}$ ) and 8.03 (s, 1H,  $\text{HC=N}$ ).  $^{13}\text{C-NMR}$  ( $\text{CDCl}_3$ )  $\delta$  (in ppm) 11.7; 24.3; 62.7, (aliphatic  $\text{CH}_3$  and  $\text{CH}_2$ ), 109.5; 113.7; 121.4, (pyrrole CH), 151.4 (imine CH), FT-IR ( $\text{cm}^{-1}$ , neat between NaCl plates)  $\nu_{\text{C=N}} = 1640$  and GC-MS  $m/z$   $[\text{M+H}]^+$  137 calculated for  $\text{C}_8\text{H}_{12}\text{N}_2$ . Microanalysis

calculated for  $C_8H_{12}N_2+0.25 H_2O$ ; C, 68.29; H, 8.95; N, 19.91. Found C, 68.11; H, 8.48; N, 19.31.

### 2.3.3.2: Synthesis of *N*-(2,6-diisopropylphenyl)-*N*-[1-*H*-pyrrol-2-ylmethylene]amine **L2**

To a stirring yellow solution of pyrrole-2-carboxylaldehyde (3.0 g, 31.55 mmol) in dry diethyl ether (30 mL) 2,6-diisopropylaniline (5.6 g, 31.55 mmol) was added. After addition of a few drops of formic acid, as a catalyst, the solution was stirred at r. t. for 24 h. After the reaction time, diethyl ether was removed by rotary evaporation giving a cream white solid that was recrystallized from  $CH_3OH$  by slow evaporation giving **L2** as white crystals. This method was adapted from reported procedures with slight modification<sup>5, 21</sup>. Yield 6.8 g, 85 %. Melting point 142.3- 143.1 °C,  $^1H$ -NMR  $CDCl_3$  (Fig. 2.6)  $\delta$ : 1.2 (d, 12H, *i*-Pr- $CH_3$ ,  $^2J_{HH} = 8.4$  Hz), 3.1 (m, 2H, *i*-Pr-C-H,  $^3J_{HH} = 7.0$  Hz), 6.2 (s, br, 1H,  $C_4H_3NH$ ), 6.4 (s, br, 1H,  $C_4H_3NH$ ), 6.8 (s, br, 1H,  $C_4H_3NH$ ), 7.3 (m, 3H, Ph-H), 8.05 (s, 1H, H-6 (HC=N)).  $^{13}C$ -NMR ( $CDCl_3$ )  $\{^1H\}$   $\delta$  (in ppm), 23.56, 27.90, (*i*-Pr  $CH_3$ ), 109.89, 116.87, 123.20, 124.32, 124.57, 129.77, 139.03, 148.30, (pyrrole and aromatic CH) and 152.71 (imine CH), FT-IR ( $cm^{-1}$  KBr pellet)  $\nu_{C=N} = 1626$ . ESI-MS  $m/z$   $[M+H]^+$  255 calculated for  $C_{17}H_{22}N_2$ . Microanalysis calculated; C, 80.27; H, 8.72; N, 11.01. Found C, 80.24; H, 8.75; N, 10.80.

### 2.3.3.3: Synthesis of a first-generation Poly (propylene imine) pyrrole-imine ligand; **L3**

Into a Schlenk tube containing dry diethyl ether (20 mL) and anhydrous  $MgSO_4$  (*ca* 2 g) pyrrole-2-carboxylaldehyde (0.48 g, 5.05 mmol) was added yielding an orange yellow mixture. Then the DAB-PPI-( $NH_2$ )<sub>4</sub> (0.4 g, 1.26 mmol) dissolved in dry diethyl ether (5 mL) was added in drop-wise over 2 minutes. A catalytic amount of glacial acetic acid was added and the mixture stirred at r. t. for 2 days. The  $Et_2O$  was then removed from the reaction mixture giving an orange oil. The oil was then dissolved in  $CH_2Cl_2$  (25 mL), filtered and the filtrate washed with water (5 x 25 mL). The organic layer was collected, dried over anhydrous  $MgSO_4$  and filtered by gravity. Removal of  $CH_2Cl_2$  yielded an orange oil. This method was adapted from literature with slight modification<sup>17</sup>. Yield 0.32 g, 41 %.  $^1H$ -NMR ( $CDCl_3$ ) (Fig. 2.9)  $\delta$  (in ppm) (see Scheme 2.4 for numbering), 1.36 (s, br, 4H, H-13), 1.74 (t, 8H, H-9,  $^3J_{HH} = 7.0$  Hz), 2.42 (t, br, 12H, H-12 & 10,  $^3J_{HH}$

= 7.2 Hz), 3.53 (t, 8H, H-8,  $^3J_{\text{HH}} = 6.2$  Hz); 6.22 (t, 8H, H-3,  $^3J_{\text{HH}} = 2.4$  Hz), 6.46 (d, 4H, H-4,  $^2J_{\text{HH}} = 2.2$  Hz); 6.8 (s, 4H, H-2); 8.03 (s, 4H, H-6).  $^{13}\text{C}$ -NMR ( $\text{CDCl}_3$ )  $\{\text{}^1\text{H}\}$   $\delta$  (in ppm), 25.0, 28.3, 51.4, 53.8, 58.8, (dendrimer framework  $\text{CH}_2$ ) 109.5, 114.3, 121.9, 130.1, (pyrrole CH) and 152.1 (imine CH), FT-IR ( $\text{cm}^{-1}$  neat between NaCl plates);  $\nu_{\text{C=N}} = 1636$ . ESI-MS (Fig. 2.10)  $m/z$   $[\text{M}+\text{H}]^+$  625 calculated for  $\text{C}_{36}\text{H}_{52}\text{N}_{10}$ . Microanalysis calculated for  $\text{C}_{36}\text{H}_{52}\text{N}_{10}$  and 0.5  $\text{CH}_2\text{Cl}_2$ ; C, 65.69, H, 8.01, N, 20.90. Found C, 65.02; H, 7.84, N, 19.80.

#### 2.3.3.4: Synthesis of triethoxy silane functionalized pyrrole-imine ligand; **L4**

To a solution of pyrrole -2- carboxaldehyde (1.02 g, 10.68 mmol) in freshly dried diethyl ether (20 mL) was added 3-aminopropyltriethoxysilane (2.4 g, 10.68 mmol). 3 drops of formic acid and two-spatula tips of anhydrous  $\text{MgSO}_4$  were added to the clear solution obtained. The mixture was stirred for 24 h at r. t. during which it acquired an orange colour. Solvent removal gave an orange paste that was dissolved in  $\text{CH}_2\text{Cl}_2$  and filtered.  $\text{CH}_2\text{Cl}_2$  removal from the filtrate yielded an orange oil. Yield 2.72 g, 85 %.  $^1\text{H}$ -NMR ( $\text{CDCl}_3$ ):  $\delta$  0.65 (t, 2H, Si- $\text{CH}_2$ ,  $^3J_{\text{HH}} = 8.4$  Hz); 1.22 (t, 9H, Si-O $\text{CH}_2\text{CH}_3$ ,  $^3J_{\text{HH}} = 7.0$  Hz); 1.72 (t, 2H, N $\text{CH}_2$ ,  $J_{\text{HH}} = 7.0$  Hz); 3.52 (t, 2H, N $\text{CH}_2\text{CH}_2$ ,  $^3J_{\text{HH}} = 7.0$  Hz); 3.83 (q, 6H, Si-O $\text{CH}_2$ ,  $J_{\text{HH}} = 7.0$  Hz); 6.23 (t, 1H,  $\text{C}_4\text{H}_3\text{NH}$ ,  $J_{\text{HH}} = 2.6$  Hz), 6.46 (t, 1H,  $\text{C}_4\text{H}_3\text{NH}$ ,  $J_{\text{HH}} = 2.6$  Hz), 6.90 (s, 1H,  $\text{C}_4\text{H}_3\text{NH}$ ), 8.04 (s, 1H,  $\underline{\text{H}}\text{C}=\text{N}$ ).  $^{13}\text{C}\{\text{}^1\text{H}\}$ -NMR ( $\text{CDCl}_3$ ):  $\delta$  (ppm) 0.99, 8.02, 18.27, 24.47, 58.36, 63.25, (aliphatic  $\text{CH}_2$  and  $\text{CH}_3$ ) 109.61, 114.14, 121.67, 130.10, (pyrrole CH) and 151.66 (imine CH). FT-IR ( $\text{cm}^{-1}$ , neat film between NaCl plates):  $\nu_{\text{C=N}} = 1640$ ,  $\nu_{\text{N-H}} = 3152$  and  $\nu_{\text{Si-O}} = 1102\text{-}1080$ . ESI-MS (Fig. 2.12)  $m/z$   $[\text{M}+\text{H}]^+$  299 calculated for  $\text{C}_{14}\text{H}_{22}\text{N}_2\text{O}_3\text{Si}$ . Microanalysis calculated; C, 56.34; H, 8.78; N, 9.39. Found C, 56.43; H, 8.56; N, 9.10.

#### 2.3.4: Synthesis of complexes

##### 2.3.4.1: Preparation of $[(\text{C}_3\text{H}_7\text{N}=\text{CH})\text{C}_4\text{H}_3\text{N}]_2\text{Cu}$ ; **C1**

**C1** was prepared using a reported method with slight modifications.<sup>5</sup> To a mixture of NaH (0.022 g, 0.92 mmol) and dry THF (15 mL) in a Schlenk tube a solution of **L1** (0.118 g, 0.87 mmol) in THF (5 mL) was added via a syringe giving a pink colour.

Immediate evolution of a gas was observed. The mixture was stirred for 6 h at r. t. and it gradually obtained a red-brown colour. After 6 h the solution was filtered under nitrogen into another Schlenk tube and  $\text{Cu}(\text{OAc})_2 \cdot \text{H}_2\text{O}$  (0.088 g, 0.43 mmol) added. The resulting mixture was then stirred at room temperature for 48 h. The solution gradually acquired a deep green colour. Removal of the solvent in vacuo gave a deep green solid. The solid was then dissolved in  $\text{CH}_2\text{Cl}_2$  and vacuum filtered. A deep green residue was obtained and dried under vacuum. Recrystallization was performed in a mixture of  $\text{CH}_2\text{Cl}_2/\text{EtOH}$  (1:2) at  $-4^\circ\text{C}$ . Yield 0.09 g, 65 %. Melting point  $123\text{-}124^\circ\text{C}$ , FT-IR ( $\text{cm}^{-1}$ , KBr pellet):  $\nu_{\text{C}=\text{N}} = 1590$ . ESI-MS  $m/z$   $[\text{M}+\text{H}]^+$  335 calculated for  $\text{C}_{16}\text{H}_{22}\text{N}_4\text{Cu}$ . Microanalysis calculated; C, 57.55; H, 6.69; N, 16.78 and Found C, 57.00; H, 6.76; N, 17.08.

#### 2.3.4.2: Preparation of $[(\text{C}_3\text{H}_7\text{N}=\text{CH})\text{C}_4\text{H}_3\text{N}]_2\text{Ni}$ ; **C2**

A mixture of NaOH (0.1 g, 2.206 mmol), **L1** (0.3 g, 2.206 mmol) and  $\text{Ni}(\text{OAc})_2 \cdot 4\text{H}_2\text{O}$  (0.28 g, 1.103 mmol) in dry  $\text{CH}_3\text{OH}$  (20 mL) was refluxed for 4 h at  $68^\circ\text{C}$ . After 4 h the mixture was filtered and the solvent removed in vacuo giving a black solid. This solid was then dissolved in  $\text{CH}_2\text{Cl}_2$ , filtered again and concentrated to 10 mL. Hexane (30 mL) was then added precipitating out a deep green almost black solid. Yield 0.21 g, 63 %. Melting Point  $174\text{-}176^\circ\text{C}$ , FT-IR ( $\text{cm}^{-1}$ , KBr pellet):  $\nu_{\text{C}=\text{N}} = 1590$ . ESI-MS  $m/z$   $[\text{M}+\text{H}]^+$  330 calculated for  $\text{C}_{16}\text{H}_{22}\text{N}_4\text{Ni}$ . Microanalysis calculated for  $\text{C}_{16}\text{H}_{22}\text{N}_4\text{Ni} + 0.5 \text{H}_2\text{O}$ ; C, 56.84; H, 6.86; N, 16.57; Found C, 56.29; H, 6.39; N, 13.89.

#### 2.3.4.3: Preparation of $[(\text{C}_3\text{H}_7\text{N}=\text{CH})\text{C}_4\text{H}_3\text{N}]_3\text{Co}$ ; **C3**

The Co(III), **C3**, analogue was prepared in a similar method as used for **C2** at a 1:2:2 ratio of  $\text{Co}(\text{AOC})_2 \cdot \text{H}_2\text{O}:\text{NaOH}:\text{L1}$ . The product was obtained as a deep red crystalline material. Crystals for X-ray analysis were grown at  $-4^\circ\text{C}$  in a mixture of  $\text{CH}_2\text{Cl}_2$  and EtOH at a (1:2) ratio. Yield 0.19 g, 57 %. Melting Point  $191\text{-}192^\circ\text{C}$ , FT-IR ( $\text{cm}^{-1}$ , KBr pellet)  $\nu_{\text{C}=\text{N}} = 1586$ . ESI-MS  $m/z$   $[\text{M}+\text{H}]^+$  465 calculated for  $\text{C}_{24}\text{H}_{33}\text{N}_6\text{Co}$ . Microanalysis calculated for  $\text{C}_{24}\text{H}_{33}\text{N}_6\text{Co} + \text{H}_2\text{O}$ ; C, 59.74; H, 7.31; N, 17.42; Found C, 59.91; H, 7.11; N, 16.59.

*2.3.4.4: Preparation of [(2,6-i-Pr<sub>2</sub>C<sub>6</sub>H<sub>3</sub>)N=CH(C<sub>4</sub>H<sub>3</sub>N-2)]<sub>2</sub>Cu; C4*

**C4** was prepared in a similar method as used for **C1** at a ratio of 1:2:2 for Cu(OAc)<sub>2</sub>.H<sub>2</sub>O:NaH:**L2**. The product was obtained as a deep green crystalline material. Crystals for X-ray analysis were grown in a similar method as for **C3**. Yield 0.49 g 87 %. Melting point 170-171<sup>o</sup> C, FT-IR (cm<sup>-1</sup>)  $\nu_{C=N}$  = 1592, 1574. ESI-MS m/z [M+H]<sup>+</sup> 571 calculated for C<sub>16</sub>H<sub>22</sub>N<sub>4</sub>Cu. Microanalysis calculated; C, 71.61; H, 7.42; N, 9.82, Found C, 72.12; H, 7.29 N, 9.99.

*2.3.4.5: Preparation of [(2,6-i-Pr<sub>2</sub>C<sub>6</sub>H<sub>3</sub>)N=CH(C<sub>4</sub>H<sub>3</sub>N-2)]<sub>2</sub>Ni; C5*

**C5** was prepared in a similar method as used for **C1** at a ratio of 1:2:2 for Ni(OAc)<sub>2</sub>.4H<sub>2</sub>O:NaH:**L2**. The product was obtained as an orange crystalline material. Solid state structure determination crystals for X-ray analysis were grown in a similar method as used for **C3**. Yield 0.44 g, 81 %. Melting point 185-187<sup>o</sup> C, FT-IR (cm<sup>-1</sup>)  $\nu_{C=N}$  = 1594, 1586. ESI-MS m/z [M+H]<sup>+</sup> 565 calculated for C<sub>16</sub>H<sub>22</sub>N<sub>4</sub>Ni. Microanalysis calculated; C, 72.22; H, 7.92; N, 9.91, Found C, 72.12; H, 7.54 N, 9.51.

*2.3.4.6: Preparation of Dendrimeric Cu(II) complex; C6*

**C6** was prepared in a similar method as employed for **C1** at a ratio of 1:2:4 for **L3**:Cu(OAc)<sub>2</sub>.H<sub>2</sub>O:NaH. The product was obtained as a green amorphous solid after recrystallization from CH<sub>2</sub>Cl<sub>2</sub> with hexane. Yield 0.20 g, 62 %, FT-IR (cm<sup>-1</sup>)  $\nu_{C=N}$  = 1584. ESI m/z [M+2H]<sup>+</sup> 375 calculated for C<sub>36</sub>H<sub>48</sub>N<sub>10</sub>Cu<sub>2</sub>. Microanalysis calculated; C, 57.83; H, 6.47, N, 18.73, Found C, 57.82; H, 6.57; N, 17.33.

*2.3.4.7: Preparation of Dendrimeric Ni(II) complex; C7*

The dendrimeric Ni(II) analogue, **C7**, was prepared in a similar method as employed for **C2** at the ratio of 1:2:4 for **L3**:Ni(OAc)<sub>2</sub>.4H<sub>2</sub>O:NaOH. The product was precipitated out of CH<sub>2</sub>Cl<sub>2</sub> with hexane and obtained as a brown amorphous solid. Yield 0.29 g, 70 %. FT-IR (cm<sup>-1</sup>)  $\nu_{C=N}$  = 1584. ESI-MS m/z [M+2H]<sup>+</sup> 369 calculated for C<sub>36</sub> H<sub>48</sub> N<sub>10</sub>Ni<sub>2</sub> Microanalysis calculated for C<sub>36</sub> H<sub>48</sub> N<sub>10</sub>Ni<sub>2</sub> + 0.25 H<sub>2</sub>O; C, 57.33; H, 6.44; N, 18.44; Found C, 57.22; H, 6.35; N, 17.15

#### 2.3.4.8: Preparation of Dendrimeric Co(II) complex; **C8**

The dendrimeric Co(II) analogue, **C8**, was prepared in a similar method as employed for **C2** at the ratios 1:2:4 for **L3**:Co(OAc)<sub>2</sub>.4H<sub>2</sub>O:NaOH and recrystallized as in **C7**. The product was obtained as a brown amorphous solid. Yield 0.26 g, 63 %. FT-IR (cm<sup>-1</sup>)  $\nu_{C=N} = 1584$ . ESI-MS m/z [M+2H]<sup>+</sup> 370 calculated for C<sub>36</sub>H<sub>48</sub>N<sub>10</sub>Co<sub>2</sub>. Microanalysis calculated for C<sub>36</sub>H<sub>48</sub>N<sub>10</sub>Co<sub>2</sub>; C, 58.53; H, 6.55; N, 18.96; Found C, 59.16; H, 6.72; N, 18.64.

#### 2.3.4.9: Preparation of [(EtO)<sub>3</sub>SiC<sub>3</sub>H<sub>6</sub>N=CH)C<sub>4</sub>H<sub>3</sub>N]<sub>2</sub>Cu; **C9**

**C9** was prepared in a similar method as used for **C1** at the same ratio of 1:2:2 for Cu(OAc)<sub>2</sub>.H<sub>2</sub>O:NaH:**L4**. The product was obtained as a green amorphous solid after recrystallization from CH<sub>2</sub>Cl<sub>2</sub> with hexane. Yield 0.78 g, 76 %, FT-IR cm<sup>-1</sup>  $\nu_{C=N} = 1592$  and  $\nu_{Si-O} = 1112-1080$  cm<sup>-1</sup>, ESI-MS m/z [M+2H]<sup>+</sup> 302 calculated for C<sub>24</sub>H<sub>42</sub>N<sub>4</sub>CuO<sub>6</sub>Si<sub>2</sub>. Microanalysis calculated C<sub>24</sub>H<sub>42</sub>N<sub>4</sub>CuO<sub>6</sub>Si<sub>2</sub>; C, 41.50; H, 5.01; N, 12.10; Found C, 41.13; H, 4.94; N, 9.01.

#### 2.3.4.10: Preparation of (EtO)<sub>3</sub>SiC<sub>3</sub>H<sub>6</sub>N=CH)C<sub>4</sub>H<sub>3</sub>N]<sub>2</sub>Ni; **C10**

**C10** was prepared and recrystallized in a similar method as used for **C9** at the same ratio of 1:2:2 for Ni(OAc)<sub>2</sub>.4H<sub>2</sub>O:NaH:**L4**. The product was obtained as an orange amorphous solid. Yield 0.48 g, 77 %. Melting point, FT-IR (cm<sup>-1</sup>)  $\nu_{C=N} = 1592$  and  $\nu_{Si-O} = 1156-1038$ . Microanalysis calculated for C<sub>24</sub>H<sub>42</sub>N<sub>4</sub>NiO<sub>6</sub>Si<sub>2</sub>; C, 44.46; H, 5.60, N, 11.52; Found C, 44.25; H, 4.88; N, 11.69. ESI-MS m/z [M+2H]<sup>+</sup> 300 calculated for C<sub>24</sub>H<sub>42</sub>N<sub>4</sub>NiO<sub>6</sub>Si<sub>2</sub>

#### 2.3.5: Synthesis of mesoporous MCM-41

MCM-41 was prepared using a reported procedure.<sup>22</sup> 25 % NH<sub>3</sub> Solution (205 mL) was mixed with distilled water (270 mL), pH = 12.56, and heated with stirring to 60 °C. A surfactant cetyltrimethylammonium bromide; (CH<sub>3</sub>(CH<sub>2</sub>)<sub>15</sub>N(CH<sub>3</sub>)<sub>3</sub>Br) 2.0 g was added to the solution. When the solution became homogeneous, tetraethyl orthosilicate (TEOS) 10 mL was introduced giving rise to a white slurry. After 2 h of heating and stirring, the resulting product was filtered and washed with 1000 mL distilled water. The white powder obtained was then dried at room temperature overnight followed by calcination at

550 °C for 4 h. The temperature was increased gradually from 100° C at 20 °/10 min. Yield 2.6 g. FT-IR ( $\text{cm}^{-1}$  KBr pellet) (Fig. 2.13)  $\nu_{\text{Si-O-Si}} = 1224\text{-}1028$ ,  $\nu_{\text{Si-OH}} = 1634 \text{ cm}^{-1}$  and  $\nu_{\text{OH}} = 3700\text{-}2800 \text{ cm}^{-1}$ . BET surface area  $1229 \text{ m}^2\text{g}^{-1}$ , pore size  $31.59 \text{ \AA}$  and pore volume of  $0.86 \text{ cm}^3\text{g}^{-1}$ . The XRD results show three well resolved peaks are observed  $d_{100}$ ,  $d_{110}$ , and  $d_{200}$  with values of  $35.31 \text{ \AA}$ ,  $41.06 \text{ \AA}$  and  $52.92 \text{ \AA}$  respectively.

### 2.3.6: Immobilization of the metal complexes

#### 2.3.6.1: Immobilization of $(\text{EtO})_3\text{SiC}_3\text{H}_6\text{N}=\text{CH})\text{C}_4\text{H}_3\text{N}]_2\text{Cu}$ onto MCM-41

Immobilization onto MCM-41 was performed using reported methods with slight modification.<sup>25,28</sup> A 100 mL round bottomed flask was charged with 1.0 g MCM-41 material, 0.1 g **C9** and dry toluene, 20 mL. The mixture obtained was refluxed for 4 h after which the resulting lightly greenish solid was collected by simple filtration and washed with  $\text{CH}_2\text{Cl}_2$  extensively until the filtrate was colourless to remove unsupported complex. The light green solid was then dried in vacuum overnight, 12 h, with heating at 100 °C.

Analysis for copper was performed using AAS in an air/acetylene fuel. Samples (ca. 0.05 g) was digested using 15 mL 2N  $\text{H}_2\text{SO}_4$  in a beaker. The mixture was then heated to almost dryness. After cooling  $\text{H}_2\text{O}$ , 10 mL, was added and filtered into a 50 mL volumetric flask. The filtrate was then topped up to 50 mL. An amount of copper was then determined by AAS against standard solutions of 10, 8, 6, 4 and 2 ppm. Yield 0.92 g, 83.6 %. FT-IR ( $\text{cm}^{-1}$ )  $\nu_{\text{Si-O-Si}} = 1238\text{-}1036 \text{ cm}^{-1}$ ,  $\nu_{\text{Si-OH}} = 3600\text{-}3200 \text{ cm}^{-1}$  and  $\nu_{\text{Si-OH}} = 1634 \text{ cm}^{-1}$ . The XRD results show three well resolved peaks are observed  $d_{100}$ ,  $d_{110}$ , and  $d_{200}$  with values of  $36.78$ ,  $44.14$  and  $57.57 \text{ \AA}$  respectively. BET surface area of  $1019.0 \text{ m}^2\text{g}^{-1}$ , pore volume  $0.8 \text{ cm}^3\text{g}^{-1}$  and pore diameter of  $31.59 \text{ \AA}$  were obtained. The copper analysis showed up to 0.74 % and as low as 0.43 % was immobilized.

#### 2.3.6.2: Immobilization of $(\text{EtO})_3\text{SiC}_3\text{H}_6\text{N}=\text{CH})\text{C}_4\text{H}_3\text{N}]_2\text{Ni}$ onto MCM-41

**C10** was immobilized onto MCM-41 in a similar method as employed for **C9**. Yield 0.94 g, 85.45 %. The FT-IR ( $\text{cm}^{-1}$ )  $\nu_{(\text{Si-O-Si})} = 1238\text{-}1036 \text{ cm}^{-1}$ ,  $\nu_{(\text{OH})} = 3600\text{-}3200 \text{ cm}^{-1}$  and  $\nu_{(\text{Si-OH})} = 1634 \text{ cm}^{-1}$ . The XRD results show three well resolved peaks are observed

$d_{100}$ ,  $d_{110}$ , and  $d_{200}$  with values of 37.24 Å, 44.27 Å and 57.67 Å respectively. BET surface area of 1086 m<sup>2</sup>g<sup>-1</sup>, pore volume 0.86 cm<sup>3</sup>g<sup>-1</sup> and pore diameter of 31.60 Å were obtained. The nickel AAS analysis showed up to 0.46 % and as low as 0.12 %.

#### **2.4: Conclusion**

Mononuclear, dendrimeric and immobilized Cu(II), Ni(II) and Co(II) complexes of monofunctional and multifunctional pyrrole-imine ligands have been successfully prepared and obtained in moderate yields. These compounds were characterized by a combination of techniques. FT-IR spectroscopy, microanalysis and mass spectrometry confirmed the molecular formulae of the complexes. <sup>1</sup>H-NMR and <sup>13</sup>C-NMR spectroscopy was also used to characterize the ligands. X-ray analysis of **C3**, **C4** and **C5** confirmed that the ligands are bidentate.

The triethoxysilane functionalized complexes of copper and nickel were successfully immobilized onto MCM-41.



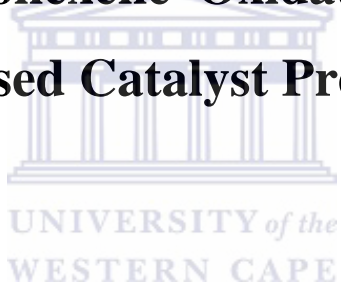


**2.5: References**

1. L-C. Liang, C-W. Yang, M. Y. Chiang, C-H. Hung, P-Y. Lee, *J. Organomet. Chem.*, **679** (2003) 135.
2. S. D. Drouin, H. M. Foucault, G. P. A. Yap, D. E. Fogg, *Can. J. Chem.*, **83** (2005) 748.
3. Y. Yoshida, J. Saito, M. Mitani, Y. Takagi, S. Matsui, S-I. Ishii, T. Nakano, N. Kashiwa, T. Fujita, *J. Chem. Soc., Chem. Commun.*, (2002) 1298.
4. Y. Yoshida, S. Matsui, T. Fujita *J. Organomet. Chem.*, **690** (2005) 4382.
5. V. C. Gibson, C. Newton, C. Redshaw, G. A. Solan, A. J. P. White, D. J. Williams, *J. Chem. Soc., Dalton Trans.*, (2002) 4017.
6. M. Kimura, T. Shiba, T. Muto, K. Hanabusa, H. Shirai, *J. Chem. Soc., Chem. Commun.*, (2000) 11.
7. B. Donnio, J. Barberá, R. Giménez, D. Guillon, M. Marcos, J. L. Serrano, *Macromolecules*, **35** (2002), 370.
8. A. W. Bosman, H. M. Janssen, E. W. Meijer, *Chem. Rev.*, **99** (1999) 1665.
9. T. R. Krishna, N. Jayaraman, *Tetrahedron*, **60** (2004) 10325.
10. J. C. Hummelen, J. L. van Dongen, E. W. Meijer, *Chem. Eur. J.*, **3** (1997) 1489.
11. R. Meijboom, J. R. Moss, A. T. Hutton, T-A. Makaluza, S. F. Mapolie, F. Waggie, M. R. Domingo, *J. Organomet. Chem.*, **689** (2004) 1876.
12. R. van Heerbeek, P. C. J. Kamer, P. W. N. M. V. Leeuwen, J. N. H. Reek, *Chem. Rev.*, **102** (2002) 3717.
13. G. J. M. Koper, M. H. P. van Genderen, C. E. Roman, M. W. P. L. Baars, M. Borkovec, *J. Am. Chem. Soc.*, **119** (1997) 6512.
14. R. Velarde-Ortiz, G. Larsen, *Chem. Mater.*, **14** (2002) 858.
15. R. Meijboom, M. J. Overett, J. R. Moss, *J. Organomet. Chem.*, **689** (2004) 987.
16. G. R. Newkome, E. He, C. N. Moorefield, *Chem. Rev.*, **99** (1999) 1689.
17. G. Smith, R. Chen, S. F. Mapolie, *J. Organomet. Chem.*, **673** (2003) 111.
18. R. Marx, H-W. Moulines, F. Wagner, T. Astruc, D. Hexaki. *Angew. Chem.: Int. Ed. Engl.*, **35** (1996) 1701.
19. I. Cuadrado, M. Morán, C. M. Casado, B. Alonso, F. Lobete, B. García, M. Ibisate, J. Losada, *Organometallics*, **15** (1996) 5278.

20. C. O. Noble, R. L. McCarley, *Organic Letters*, **1** (1999) 1021.
21. J. S. Beck, J. C. Vartuli, W. U. Roth, M. E. Leonowicz, C. T. Kresge, K. D. Schmitt, C. T-W. Chu, D. H. Olson, E. W. Sheppard, S. B. McCullen, J. B. Higgins, J. L. Schlenker, *J. Am. Chem. Soc.*, **114** (27) (1992) 10834.
22. B. Marler, U. Oberhagemann, S. Vortmann, H. Gies, *Micropor. Mater.*, **6** (1996) 375.
23. Q. Cai, W-Y. Lin, F-S. Xiao, W-Q. Pang, X-H. Chen, B-S. Zou, *Micropor. Mesopor. Mater.*, **32** (1999) 1.
24. C. W. Jones, M. W. McKittrick, J. V. Nguyen, K. Yu, *Top. Catal.*, **34** (2005) 67.
25. Helmut Günzeler and Hans-Ulrich Gremlich, *An Introduction to IR Spectroscopy*, Translated by Mary-Joan Blümich, 2002, WILEY-VCH Verlag GmbH, 69469 Weinheim (Federal Republic of Germany) pages 176-246.
26. A. Chakravorty, R. H. Holm, *Inorg. Chem.* **3** (1964) 1521.
27. Y-S. Li, Y-R. Li, X-F. Li, *J. Organomet. Chem.*, **667** (2003) 185.
28. T. Luts, W. Suprun, D. Hofmann, O. Klepel, H. Papp, *J. Mol. Catal. A: Chem.*, **261** (2007) 16.
29. S. Jiang, Y. Kong, J. Wang, X. Ren, Q. Yan, *J. Porous Mater.*, **13** (2006) 341.
30. U. G. Singh, R. T. Williamsa, K. R. Hallamb, G. C. Allen , *J. Solid State Chem.*, **178** (2005) 3405.
31. B. De Clercq, F. Lefebvre, F. Verpoort, *Appl. Catal.*, **247** (2003) 345.
32. Bruker-AXS. (2000-2003) SADABS V.2.05, SAINT V.6.22, SHELXTL V.6.10 & SMART 5.622 Software Reference Manuals. Bruker-AXS, Madison, Wisconsin, USA.

## **Chapter 3 : Cyclohexene Oxidation Mediated by Pyrrole–imine based Catalyst Precursors**



### 3.1: Introduction

The catalytic oxyfunctionalization of hydrocarbons using peroxides as oxidant has been extensively studied in the past. Such oxyfunctionalization products are important intermediates in many industrial processes and the use of peroxides results in more environmental-friendly processes as discussed in Chapter 1.<sup>1</sup> Although dioxygen (O<sub>2</sub>) is the ideal source of oxygen in biomimetic oxygenation of organic substrates, the successful development of catalysts requires alternative oxidants e. g. hydrogen peroxide, organic peroxides or iodobenzene.<sup>2-4</sup>

Various epoxides are among the most widely used intermediates in organic synthesis as well as in the production of pharmaceuticals acting as precursors to more complex molecules. The search for new and efficient homogeneous and heterogeneous catalysts based on transition metal complexes for olefin epoxidation has been the subject of much research efforts. Many catalytic oxidation methods have been developed but selective epoxidation of alkenes using heterogeneous catalysts and clean oxidants under mild conditions is still a challenge.<sup>5</sup>

One of the major contributions to waste in chemical processes is the difficulty in separating the products and catalysts from reaction mixtures. In cases where solvent extraction is used, the catalyst often gets destroyed thus elimination of this step is highly desirable. As outlined in chapter 1, immobilizing transition-metal complexes on microporous or mesoporous matrices by various means has been employed for catalysts used in oxidation reactions. These materials have potential applications in industry.

Schiff base complexes have been the most extensively studied as homogeneous catalysts for oxidation reactions. Several papers concerning the incorporation of transition metal salen complexes onto the surface of MCM-41 and its utilization in the liquid-phase oxidation of olefins have been published.<sup>6,7</sup>

The imino-pyrrolato complexes on the other hand have not been explored previously for the oxidation of olefins. Among existing catalysts, the closest relatives are

salicylaldiminato Schiff base derivatives which form six-membered rather than five-membered chelate rings as is the case with the imino-pyrrolato complexes.<sup>8</sup>

In this chapter we report the results of the epoxidation of cyclohexene using hydrogen peroxide as oxidant in the presence of molecular oxygen with the pyrrole-imine complexes synthesized in Chapter 2. These include the mononuclear complexes with a n-propyl substituent at the imino nitrogen, Cu(II), **C1**, Ni(II), **C2**, and Co(III), **C3**, and the 2,6-diisopropylphenyl substituents (Cu(II), **C4**, and Ni(II),**C5**). The dendrimeric complexes of Cu(II), **C6**, Ni(II), **C7**, and Co(II), **C8** and the MCM-41 supported catalysts **Cu-MCM-41** and **Ni-MCM-41** were also evaluated in this study.

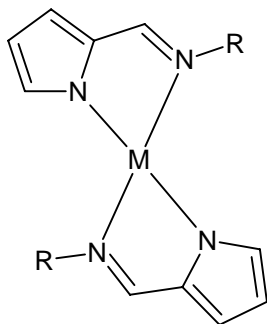
We investigated the changes in activity and selectivity when the aliphatic propyl chain at the imine nitrogen in **C1** and **C2** is substituted with an aromatic group such as diisopropylphenyl (**C4** and **C5**). We also compared the efficiency of the heterogenized homogeneous catalysts. Finally we contrasted dendrimer and silica supported catalysts. In order to determine the optimum reaction conditions we investigated several parameters such as metal concentration, oxidant concentration and substrate concentration.

## **3.2: Results and discussion**

### ***3.2.1: Oxidation of cyclohexene***

The liquid phase epoxidation reactions of cyclohexene by H<sub>2</sub>O<sub>2</sub> were done using pyrrolyaldiminato complexes of copper, cobalt and nickel in their homogeneous and heterogeneous states. The catalysts employed are shown in Figure 3.1 – 3.3.

- i. Mononuclear complexes of copper (**C1** and **C4**), nickel (**C2** and **C5**) and cobalt **C3**,



**C1:** R = *n*-propyl, M = Cu

**C2:** R = *n*-propyl, M = Ni

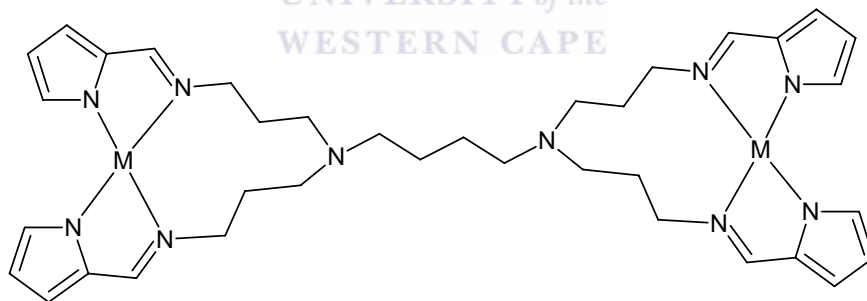
**C3:** R = *n*-propyl, M = Co

**C4:** R = 2,6-diisopropylphenyl, M = Cu

**C5:** R = 2,6-diisopropylphenyl, M = Ni

Figure 3.1: Mononuclear pyrrolylaldiminato complexes

- ii. Dendrimeric complexes of copper (**C6**), nickel (**C7**), and cobalt (**C8**)



**C6:** M = Cu

**C7:** M = Ni

**C8:** M = Co

Figure 3.2: Dendrimeric pyrrolylaldiminato complexes

- iii. MCM-41 supported copper and nickel catalysts **Cu-MCM-41** and **Ni-MCM-41**.

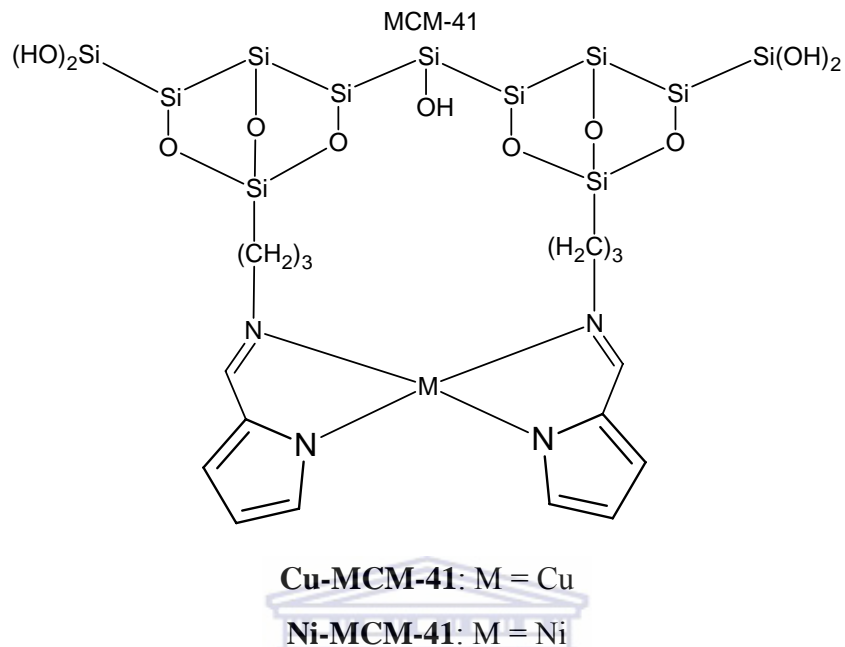
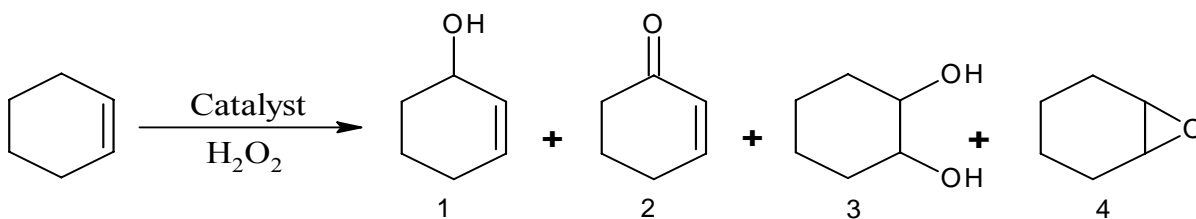


Figure 3.3: MCM-41 immobilized pyrrolylaldiminato complexes

In the base-line reaction, a cyclohexene to metal ratio of 400:1 and 1:1 ratio of cyclohexene to  $\text{H}_2\text{O}_2$  were employed. The catalytic runs were carried out in such a way as to ensure that the metal concentration in the reaction mixture was constant irrespective of the catalyst system used. Acetonitrile was used to top up the reaction mixture to a total volume of 5 mL. Since high selectivity to cyclohexene oxide is desired, optimization of reaction conditions to favour epoxidation was also investigated. The identification of products was done using GC analysis and the quantification was done using the internal standard technique.

Under the conditions used, all the catalyst precursors were found to be active in the oxidation of cyclohexene however not necessarily in the epoxidation. When the cyclohexene oxidation was attempted in hydrogen peroxide alone without the metal complexes, no oxidation occurred. The possible oxidation products shown in Scheme 3.1 are 2-cyclohexen-1-ol (1), 2-cyclohexen-1-one (2), 1,2-cyclohexane-diol (3), and 7-oxabicyclo[4,1,0]heptane (cyclohexene-oxide) (4).<sup>11</sup>



Scheme 3.1: Cyclohexene oxidation products

The presence of 2-cyclohexen-1-ol and 2-cyclohexen-1-one as the major products shows the inclination of these catalytic systems to activate the C-H bond over the attack on the C=C bond which produces the epoxide and subsequently the 1,2-cyclohexane-diol. The 1,2-cyclohexene-diol results from the ring opening of the epoxide. The conditions used herein promote the allylic oxidation pathway and the epoxidation is minimized. Karandikar *et al.*<sup>10</sup> also observed the C-H bond activation in the oxidation of cyclohexene. The allylic hydrogen was found to be more reactive than the C=C double bond towards the *t*-butyl peroxy radical when using salen complexes of copper and cobalt immobilized on MCM-41. As Nam and co-workers pointed out, another possible explanation for the formation of the allylic products could depend on the nature of the active species generated from the *t*-BuOOH or  $\text{H}_2\text{O}_2$  during the cyclohexene oxidation. The allylic products are formed from cleavage of the species of O-O bond of the peroxide while the epoxidation reactions occur by direct reaction of the olefin with a coordinated  $\text{HOO}\cdot$  radical.<sup>9</sup>

The copper and cobalt mononuclear complexes were more active than the dendrimeric and the immobilized systems. In the case of the nickel system the dendrimeric analogue was the most active.

### 3.2.2: Catalytic oxidation of cyclohexene using mononuclear catalysts

#### 3.2.2.1: Activity

The three mononuclear catalysts of copper, nickel and cobalt, **C1** - **C3**, entries 1 – 18, Table 3.1 were found to be active in the oxidation of cyclohexene under different conditions. The base-line conditions employed for the oxidation of cyclohexene were



metal concentration of  $6.0 \times 10^{-3} \text{ molL}^{-1}$ , cyclohexene concentration of  $2.4 \text{ molL}^{-1}$  and  $[\text{H}_2\text{O}_2]$  of  $2.4 \text{ molL}^{-1}$ . At these base-line conditions TOF values of 16.6, 10.5 and 11.9 were obtained for mononuclear Cu (**C1**), Ni (**C2**) and Co (**C3**) catalysts respectively shown in Table 3.1 entries 1, 7 and 13. At the base-line conditions, the Cu catalyst was observed to be more active than the other two analogues. However previously Salavati and co-workers<sup>12</sup> had reported that Co was more active than Cu and Ni while using N-N'-bis( $\alpha$ -methylsalicylidene)-2,2-dimethylpropane-1,3-diamine as ligand. They used a slightly higher metal concentration of  $7.9 \times 10^{-3} \text{ molL}^{-1}$ . The difference in the order of activity for the different metals of our catalytic systems compared to that reported by Salavati may be due to the nature of the ligand around the metal cation.<sup>12</sup>

*i. The effects of metal concentration*

In the study of the effects of catalyst concentration, different ratios of catalyst to substrate were employed. In these experiments substrate concentration was maintained at a constant level while the catalyst amounts fluctuated. Varying the amount of catalyst affected not just the activity but also the product distribution. Table 3.1 entries 2, 8, and 14 show the activities of the mononuclear catalyst of  $\text{Cu}^{2+}$ ,  $\text{Ni}^{2+}$  and  $\text{Co}^{2+}$ , respectively with increased metal concentration. At elevated levels of catalysts, these three systems showed a reduction in activity. This may be as a result of aggregation of the metal leading to deactivation of the catalysts.

Reducing the catalyst concentration to  $3.0 \times 10^{-3} \text{ molL}^{-1}$  resulted in increased activity. This is evident from the TOF values. The nickel system gave the highest TOF value of 30.9, cobalt gave 25.1 while copper gave 22.2. Recently Mukherjee *et al.*<sup>11</sup> reported a salicylaldiminato copper complex capable of oxidizing cyclohexene with aqueous hydrogen peroxide as the oxidant at even lower catalyst concentration than that of our experiments. This salicylaldiminato based catalyst gave a TOF of 12 when a  $1.0 \times 10^{-3} \text{ molL}^{-1} [\text{Cu}^{2+}]$  was employed. This activity is much lower than that of our pyrrolylaldiminato copper complex that gave a TOF value of 22.1. However, the metal concentration of our experiments was  $3.0 \times 10^{-3} \text{ molL}^{-1}$ , three times higher than what Mukherjee and his co-workers used. The increase in activity for our catalysts at the

lower metal concentration as compared to that of the base-line reaction could be because of minimized aggregation of the metal.

*ii. The effects of oxidant concentration*

The effect of the oxidant concentration was studied. The concentration of  $\text{H}_2\text{O}_2$  was changed but that of the metal and cyclohexene were maintained at those of the base-line reaction. A decline in activity for the three catalysts was observed when the  $[\text{H}_2\text{O}_2]$  was reduced from 2.4 to 1.2 to  $\text{molL}^{-1}$ . Increasing the hydrogen peroxide concentration to 4.8  $\text{molL}^{-1}$  did not improve the TOF values either. The optimal ratio of substrate to catalyst was observed as 1:1. It can be concluded that the oxidation efficiency with respect to activity is dependent on the cyclohexene concentration.

*iii. The effects of substrate concentration*

The substrate concentration was reduced to 1.2  $\text{molL}^{-1}$  while keeping the other conditions unchanged. A substrate: oxidant ratio was also maintained at 1:1. Changing the concentration of the substrate impacts differently on the catalytic systems. The three catalysts showed substantially lower activities at the reduced substrate concentration. The activities reduced by more than half for the copper catalyst unlike that of nickel and cobalt whose activities showed a smaller reduction.

In addition to the three mononuclear catalysts discussed above, two other mononuclear catalysts of Cu and Ni (**C4** and **C5**) were evaluated. In these complexes the propyl substituent at the imino nitrogen is replaced by a 2,6-diisopropylphenyl group. These two catalysts were evaluated under similar conditions to those of the other mononuclear catalysts. The results are shown in Table 3.1 entries 19 – 30. The catalysts were also found to be active in the oxidation of cyclohexene. However, these two catalysts were found to be less active than the aliphatic substituted systems. The reduction in activity could be due to the increased steric hindrance around the metal centre caused by the bulkier substituents. This would reduce substrate access to the active site of the catalysts.

In the base-line experiment, the Cu system **C4** gave TOF value of 11.8 while the Ni **C5** gave a value of 10.5. Changing the amount of catalysts once again alters the behaviour of the catalysts. On increasing catalyst concentration, the two catalysts showed a great reduction in activity as evident from the TOF values. The reduction in activity could be as a result of dimerization or aggregation of the metal centers as the concentration of the metal increases. On the other hand decreasing the concentration of the catalyst from  $6 \times 10^{-3}$  to  $3 \times 10^{-3} \text{ molL}^{-1}$  resulted in increased catalytic activity. The Ni catalyst, **C5**, showed the greatest increase in activity by a factor of 3. This dramatic increase was also observed in the case of the propyl substituted analogue, **C2**.

Changing the oxidant amounts did not improve activity either. Thus the best oxidation rate occurs when a ratio of 1:1 is used for oxidant: substrate. The catalysts oxidation efficiencies depended on the cyclohexene and not the  $\text{H}_2\text{O}_2$  concentration.

Reducing the substrate amount does not improve the activity either. The TOF values decrease from those of the base-line reaction as was the case with the aliphatic mononuclear systems.

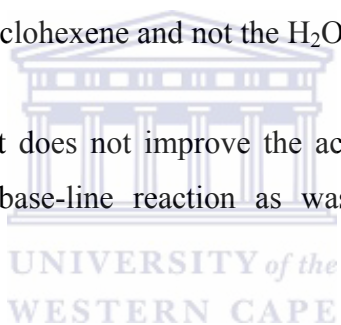


Table 3.1: Cyclohexene oxidation catalyzed by mononuclear complexes in  $\text{CH}_3\text{CN}^a$

Complex	Entry	Conversion (%)	TOF <sup>g</sup>	Selectivity (%)		
				CH-oxide	2-CH-1-ol	2-CH-1-one
<b>C1</b>	1	99.4	16.6	24.6		75.3
	2 <sup>b</sup>	94.4	7.9		53.9	46.1
	3 <sup>c</sup>	66.2	22.1		40.0	60.0
	4 <sup>d</sup>	71.1	11.9	6.2	37.7	56.2
	5 <sup>e</sup>	73.8	12.3		38.6	61.4
	6 <sup>f</sup>	92.2	7.7			100
<b>C2</b>	7	63.1	10.5	50.0		50.0
	8 <sup>b</sup>	50.7	4.2	44.6		55.4
	9 <sup>c</sup>	92.6	30.9	33.3		66.7

Table 3.1: Continued

<b>C2</b>	10 <sup>d</sup>	48.4	8.1		100	
	11 <sup>e</sup>	47.4	7.9	29.2	70.8	
	12 <sup>f</sup>	66.1	5.5			
<b>C3</b>	13	71.3	11.9	trace	42.9	57.1
	14 <sup>b</sup>	63.7	5.3		40.7	59.3
	15 <sup>c</sup>	75.2	25.1		48.0	52.0
	16 <sup>d</sup>	68.9	11.5	17.7	33.3	49.1
	17 <sup>e</sup>	67.8	11.3		20.31	69.6
	18 <sup>f</sup>	82.8	6.9		42.1	57.9
<b>C4</b>	19	70.8	11.8	5.2	34.4	60.4
	20 <sup>b</sup>	66.7	5.6		19.89	80.1
	21 <sup>c</sup>	37.4	12.5		46.1	53.9
	22 <sup>d</sup>	60.8	10.1	4.5	42.1	53.4
	23 <sup>e</sup>	64.1	10.7		26.1	38.4
	24 <sup>f</sup>	64.5	5.4			100
<b>C5</b>	25	61.0	10.5	50.0		50.0
	26 <sup>b</sup>	55.5	4.6	40.0		60.0
	27 <sup>c</sup>	91.9	30.6	36.8		63.2
	28 <sup>d</sup>	44.2	7.4			100
	29 <sup>e</sup>	41.3	8.6			100
	30 <sup>f</sup>	52.7	4.4			

<sup>a</sup> [metal] =  $6.0 \times 10^{-3}$  molL<sup>-1</sup>; [H<sub>2</sub>O<sub>2</sub>] = 2.4. molL<sup>-1</sup>; [cyclohexene] = 2.4. molL<sup>-1</sup>; duration = 24 h; total volume 5 mL

<sup>b</sup> [metal] =  $1.2 \times 10^{-2}$  molL<sup>-1</sup>

<sup>c</sup> [metal] =  $3.0 \times 10^{-3}$  molL<sup>-1</sup>

<sup>d</sup> [H<sub>2</sub>O<sub>2</sub>] = 1.2 molL<sup>-1</sup>

<sup>e</sup> [H<sub>2</sub>O<sub>2</sub>] = 4.8 molL<sup>-1</sup>

<sup>f</sup> [cyclohexene] = 1.2 molL<sup>-1</sup>

<sup>g</sup> TOF = moles cyclohexene consumed/moles metal/hour

## 3.2.2.2: The Product distribution

The concentration of the catalyst seems to play a vital role in the type of product obtained. The nickel system has the highest selectivity for the cyclohexene oxide. Another distinct observation is that nickel gave no 2-cyclohexen-1-ol. This means that the nickel catalyst further oxidized all the 2-cyclohexen-1-ol to 2-cyclohexen-1-one.

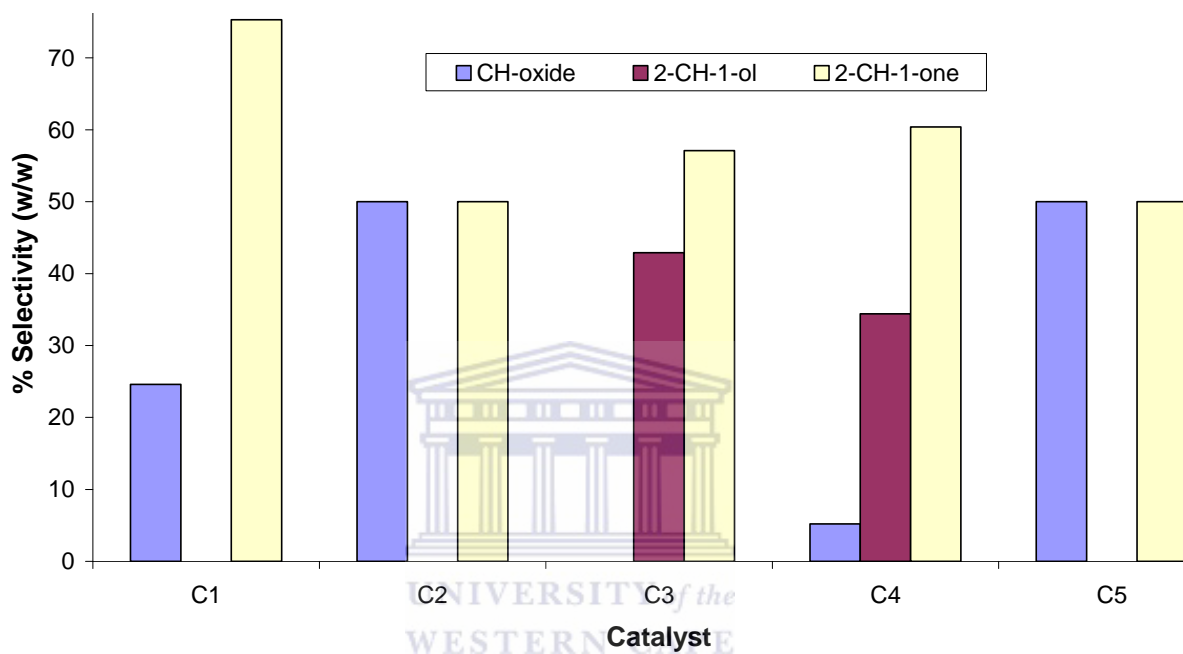


Figure 3.4: Product distribution of the mononuclear pyrrolylaldiminato catalysts,  $[M^{2+}] = 6.0 \times 10^{-3} \text{ molL}^{-1}$ ; M:  $\text{H}_2\text{O}_2$ : cyclohexene = 1:400:400.

Cyclohexene oxide was obtained for all the catalysts except for **C3**, Figure 3.4. The metal concentration for these experiments was  $6.0 \times 10^{-3} \text{ molL}^{-1}$ . At this metal concentration, the two nickel catalysts gave the highest selectivity for cyclohexene oxide. The copper and cobalt catalysts produced 2-cyclohexen-1-one as the major product. However, the copper catalysts produced some oxide as a minor product. Increasing the metal concentration to  $1.2 \times 10^{-2} \text{ molL}^{-1}$  improved the selectivity for 2-cyclohexen-1-one to as high as 80 % for **C4** from 60 % at the base reaction. Graphical representations of these results are shown in Figure 3.5.

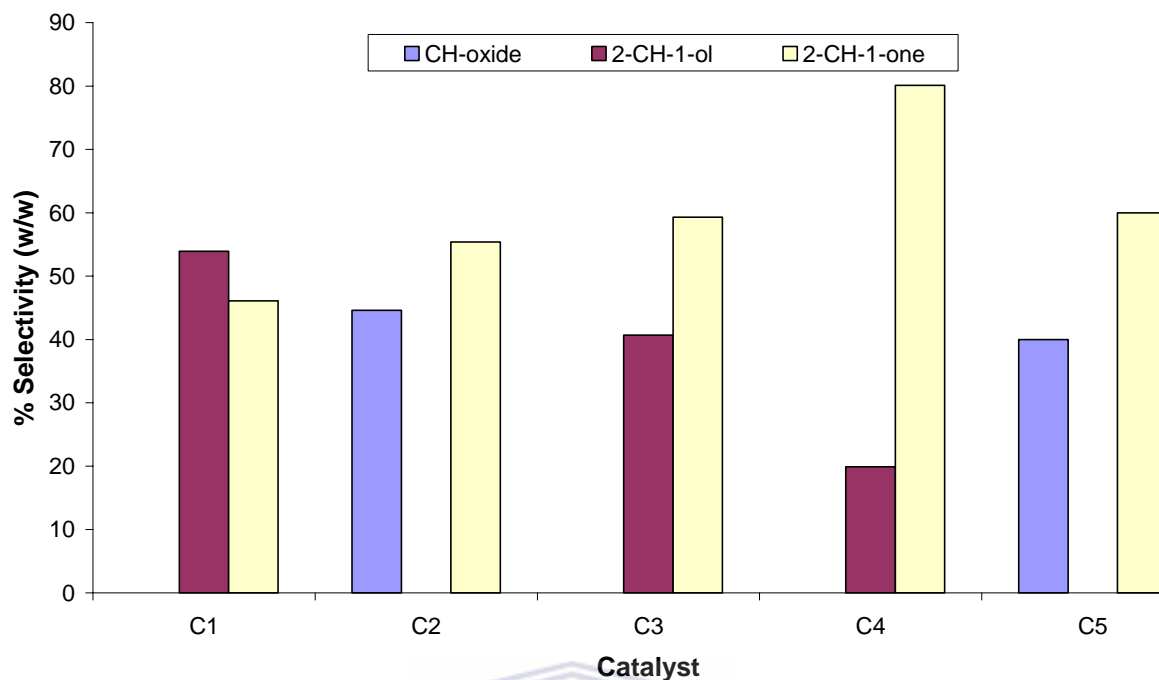


Figure 3.5: Product distribution of the mononuclear pyrrolylaldiminato catalysts,  $[M^{2+}] = 1.2 \times 10^{-2} \text{ molL}^{-1}$ ; M:  $\text{H}_2\text{O}_2$ : cyclohexene = 2:400:400.

At a lower metal concentration of  $3.0 \times 10^{-3} \text{ molL}^{-1}$  again, 2-cyclohexen-1-one was observed as the major product. The nickel catalyst gave a significant amount of the oxide with over 30 % for both catalysts as shown in Figure 3.6. At catalyst concentrations higher or lower than that of the base-line experiment, the catalysts favoured C-H bond attack over the activation of C=C bond. Mukherjee and co-workers reported that when  $1.0 \times 10^{-3} \text{ molL}^{-1}$   $\text{CuHqCl}\cdot\text{H}_2\text{O}$  (Hq = 8-hydroquinoline) with aqueous hydrogen peroxide was used 2-cyclohexen-1-ol and 2-cyclohexen-1-one were obtained as the only products.<sup>11</sup> Their metal concentration was much lower than what we employed in our experiments.

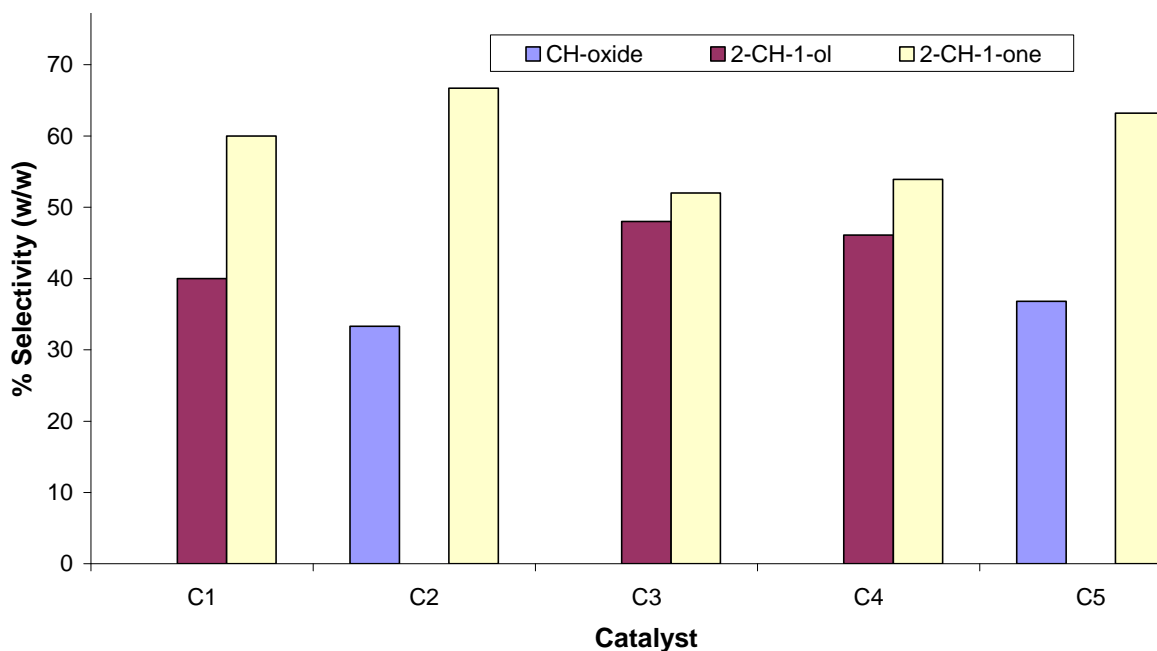


Figure 3.6: Product distribution of the mononuclear pyrrolylaldiminato catalysts,  $[M^{2+}] = 3.0 \times 10^{-3} \text{ molL}^{-1}$ ; M:  $\text{H}_2\text{O}_2$ : cyclohexene = 0.5:400:400.

Changing the oxidant concentration also affected the product distribution. There was an increase in selectivity for 2-cyclohexen-1-one as the  $\text{H}_2\text{O}_2$  concentration was reduced to  $1.2 \text{ molL}^{-1}$ . At this lower concentration of  $\text{H}_2\text{O}_2$ , the nickel catalyst only gave 2-cyclohexene-1-one. **C3** only showed formation of 2-cyclohexen-1-one under this low concentration  $\text{H}_2\text{O}_2$ . The results are summarized in Figure 3.7. At higher concentration of  $\text{H}_2\text{O}_2$  than the base-line reaction, 2-cyclohexen-1-one was again observed as the major product in this case. The  $\text{H}_2\text{O}_2$  concentration was doubled to  $4.8 \text{ molL}^{-1}$  in this case. However, **C3**, **C4** and **C5** gave a considerable amount of 1,2-cyclohexane-diol. The graphical representation of these results is shown in Figure 3.8. The diol is formed from the ring opening hydrolysis of the epoxide. The best ratio for the formation of the cyclohexene-oxide is 1:1, oxidant to substrate for the copper and nickel catalysts while that of cobalt catalysts is 1:2. Mukherjee and co-workers proposed that higher concentration of  $\text{H}_2\text{O}_2$  in the medium helps in the C-H, hydride abstraction thus the formation of 2-cyclohexene-1-one as the major product.<sup>11</sup> Our catalysts also show increased C-H bond attack at high  $\text{H}_2\text{O}_2$  concentration.

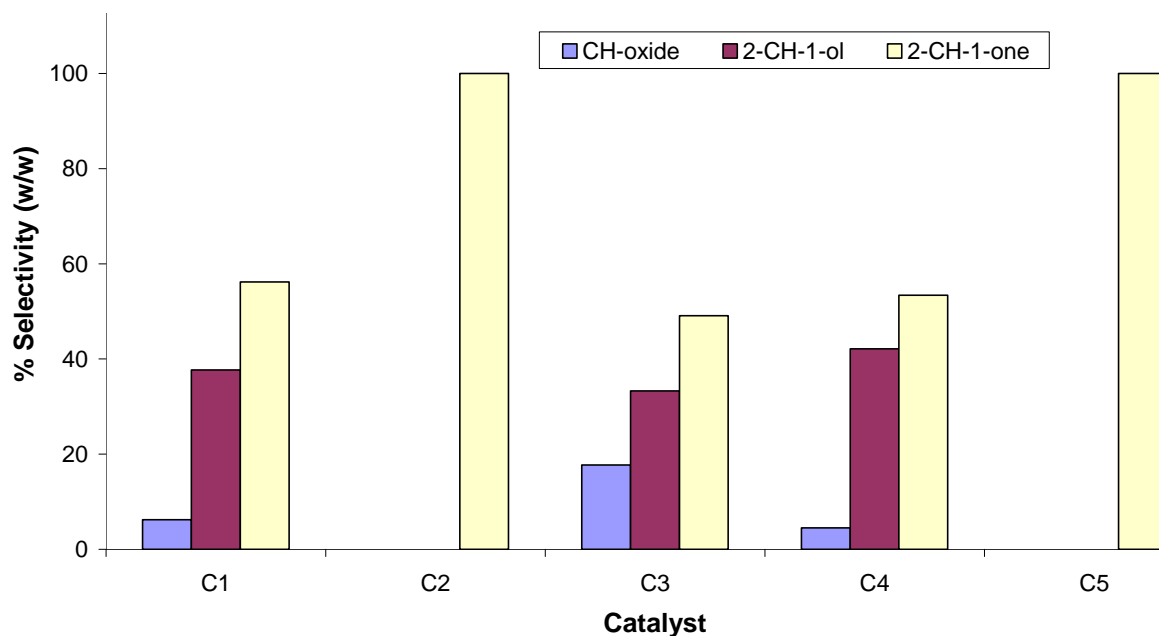


Figure 3.7: Product distribution of the mononuclear pyrrolylaldiminato catalysts,  $[M^{2+}] = 6.0 \times 10^{-3} \text{ molL}^{-1}$ ; M:  $\text{H}_2\text{O}_2$ : cyclohexene = 1:200:400.

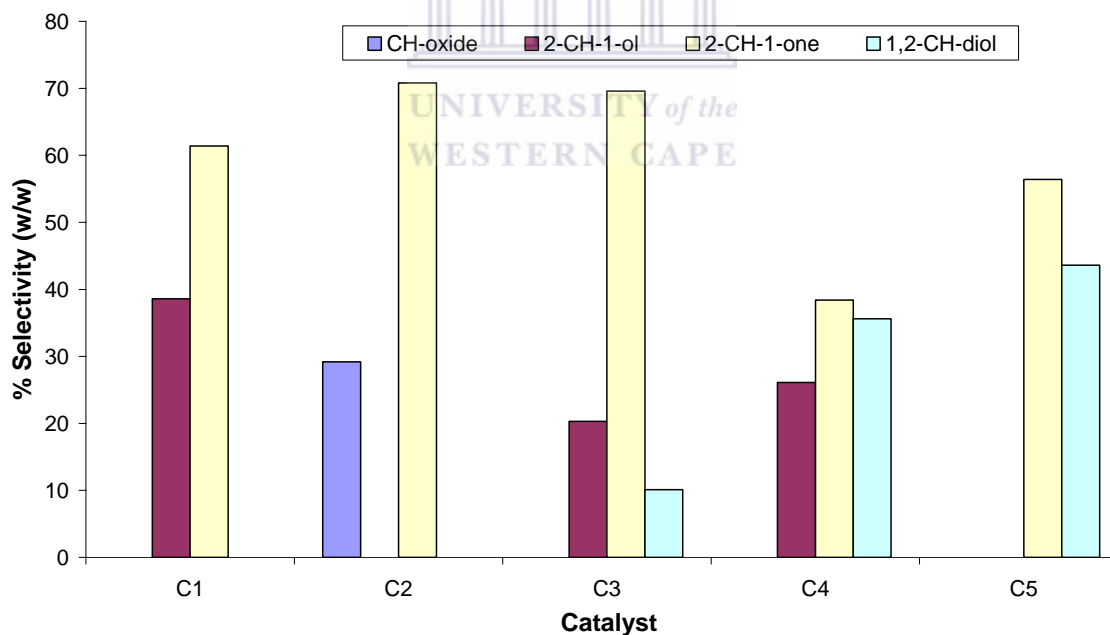


Figure 3.8: Product distribution of the mononuclear pyrrolylaldiminato catalysts,  $[M^{2+}] = 6.0 \times 10^{-3} \text{ molL}^{-1}$ ; M:  $\text{H}_2\text{O}_2$ : cyclohexene = 1:800:400.



Substrate concentration also plays a significant role in the product distribution. The results are shown in Figure 3.9. The copper catalysts, **C1** and **C4**, only produce 2-cyclohexen-1-one. The cobalt catalyst **C3** gave 2-cyclohexene-1-ol and 2-cyclohexen-1-one. However although the nickel catalysts showed consumption of cyclohexene the usual oxidation products as shown in Scheme 3.1 were not observed. The GC trace showed presence of new products that could not be identified and further investigation to identify the nature of these products needs to be carried out.

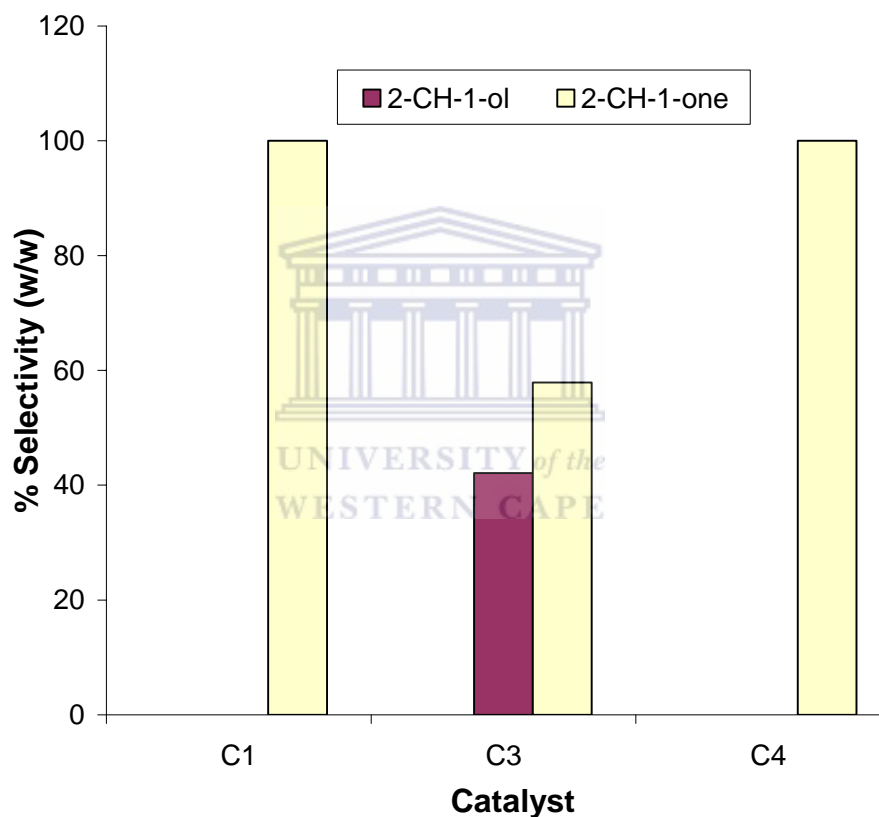


Figure 3.9: Product distribution of the mononuclear pyrrolyaldiminato catalysts,  $[M^{2+}] = 6.0 \times 10^{-3} \text{ molL}^{-1}$ ; M:  $\text{H}_2\text{O}_2$ : cyclohexene = 1:200:200.

### 3.2.3: Catalytic oxidation of cyclohexene using dendrimeric and MCM-41 immobilized catalysts

#### 3.2.3.1: Activity of the dendrimeric catalyst

The dendrimeric catalysts of copper, nickel and cobalt, **C6** – **C8** were also found to be active in the oxidation of cyclohexene under similar conditions as those used for the mononuclear catalysts in 3.2.2. The results are shown in Table 3.2, entries 1 – 18. Again the copper system was found to be more active than the Ni and Co analogues. Under the base-line conditions, TOF values of 14.5, 13 and 10.4 were obtained for **C6**, **C7** and **C8** respectively. Yang *et al.*<sup>13</sup> reported six generations of polyamidoamine-salicylaldehyde functionalized (PAMAMSA)–Mn(II) complexes that were active in cyclohexene oxidation with molecular oxygen as oxidant. Later on Chavan and co-workers<sup>14</sup> reported a PAMAMSA-benzimidazole-functionalized dendrimer of molybdenum as a cyclohexene epoxidation catalyst. They observed that the 1<sup>st</sup> generation catalyst gave a TOF value of 73.5 with tert-BuOOH as oxidant. This activity is far greater than that of our systems although it must be noted that we employed H<sub>2</sub>O<sub>2</sub> as oxidant.

#### i. The effects of metal concentration

Different concentrations of catalyst were employed as with the mononuclear systems. The amount of catalyst was changed as other parameters remained unaltered. Table 3.2 entries 2, 8, and 14 show the activities of the dendrimeric catalysts of Cu<sup>2+</sup>, Ni<sup>2+</sup> and Co<sup>2+</sup> respectively with increased metal concentrations. At this elevated concentration of 1.2 x 10<sup>-2</sup> molL<sup>-1</sup>, these three catalysts showed reduction in activity as evident from the TOF values. **C8** showed the highest reduction by a factor of 4.7. The reduction in activity was attributed to catalyst deactivation possibly by dimerization or aggregation of the metal centers. As the metal concentration was reduced to 3.0 x 10<sup>-3</sup> molL<sup>-1</sup>, there was a dramatic increase in activities for the three dendrimeric catalysts. Such an observation was also reported by Yang and co-workers.<sup>13</sup> They reported that optimal activity for cyclohexene oxide was obtained at 0.5:5 ratio of catalyst: substrate with the 3<sup>rd</sup> generation polyamidoamine-salicylaldehyde functionalized (PAMAMSA)-Mn(II) complex when compared to ratios of 1:5 and 2:5.

Table 3.2: Oxidation of cyclohexene by dendrimeric complexes in CH<sub>3</sub>CN<sup>a</sup>

		Conversion (%)	TOF	Selectivity (%)		
				CH-oxide	2-CH-1-ol	2-CH-1-one
<b>C6</b>	1	87.2	14.5	trace	50.0	50.0
	2 <sup>b</sup>	77.7	6.5		51.7	48.2
	3 <sup>c</sup>	92.7	30.9		45.4	54.7
	4 <sup>d</sup>	81.0	13.5	4.3	41.3	54.4
	5 <sup>e</sup>	90.0	16.7		48.4	51.6
	6 <sup>f</sup>	82.6	6.9		36.2	63.8
<b>C7</b>	7	79.2	13.2	47.0		53.0
	8 <sup>b</sup>	51.1	4.3	40.3		59.7
	9 <sup>c</sup>	81.2	27.1	trace		100
	10 <sup>d</sup>	33.7	5.6			100
	11 <sup>e</sup>	51.3	8.6			100
	12 <sup>f</sup>	77.1	6.4			
<b>C8</b>	13	62.3	10.4	trace	45.5	54.6
	14 <sup>b</sup>	26.1	2.2	31.1		68.9
	15 <sup>c</sup>	56.1	22.0			100
	16 <sup>d</sup>	56.1	9.4			100
	17 <sup>e</sup>	80.3	13.4		31.1	68.9
	18 <sup>f</sup>	85.5	7.1	29.3		70.6

<sup>a</sup> [metal] = 6.0 x 10<sup>-3</sup> molL<sup>-1</sup>; [H<sub>2</sub>O<sub>2</sub>] = 2.4. molL<sup>-1</sup>; [cyclohexene] = 2.4. molL<sup>-1</sup>; duration = 24 h; total volume 5 mL

<sup>b</sup> [metal] = 1.2 x 10<sup>-2</sup> molL<sup>-1</sup>

<sup>c</sup> [metal] = 3.0 x 10<sup>-3</sup> molL<sup>-1</sup>

<sup>d</sup> [H<sub>2</sub>O<sub>2</sub>] = 1.2 molL<sup>-1</sup>

<sup>e</sup> [H<sub>2</sub>O<sub>2</sub>] = 4.8 molL<sup>-1</sup>

<sup>f</sup> [cyclohexene] = 1.2 molL<sup>-1</sup>

<sup>g</sup> TOF = moles cyclohexene consumed/moles metal/hour

*ii. The effects of oxidant concentration*

The effect of the oxidant concentration was studied under similar conditions as those used for the mononuclear catalysts. Reducing the concentration of  $\text{H}_2\text{O}_2$  to  $1.2 \text{ molL}^{-1}$  resulted in reduction in activity for the three dendrimeric catalysts, entries 4, 10 and 16. Under the same conditions, the mononuclear catalyst also showed a reduction in activity. An increase of the oxidant to  $4.8 \text{ molL}^{-1}$  yielded improvement in activity for **C6** and **C8**. However, the nickel catalyst showed reduction in activity, Table 3.2 entry 11.

*iii. The effects of substrate concentration*

This set of experiments was carried out under similar conditions to those used for the mononuclear catalysts. The substrate concentration was reduced to  $1.2 \text{ molL}^{-1}$  while keeping the other conditions unchanged. The substrate: oxidant ratio was also maintained at 1:1. The activity of the three dendrimeric catalysts declined with reduction in substrate concentration. The TOF values of **C6** and **C7** reduced to less than half of that of the base line reaction. The reduction in activity was less pronounced in **C8** with the TOF value falling from 10.4 to 7.1.

*3.2.3.2: Activity of MCM-41 immobilized catalysts*

The MCM-41 supported catalysts showed moderate activities using similar conditions to those employed for the mononuclear catalysts in 3.2.2. The results are shown in Table 3.3 (entries 1 – 12). Our copper catalyst showed similar conversion to that previously reported for silica immobilized  $\text{CuHqCl}\cdot\text{H}_2\text{O}$  ( $\text{Hq} = 8$  – hydroquinoline). Our catalyst gave a 56 % conversion while the latter gave a maximum conversion of 53 %. However in the case of  $\text{CuHqCl}\cdot\text{H}_2\text{O}$  the conversion increased to 76 % when *tert*-BuOOH was used instead of aqueous  $\text{H}_2\text{O}_2$ .<sup>11</sup> Although the conversions were similar, the TOF values varied. Our system gave a TOF value of 9.4 while the reported silica immobilized  $\text{CuHqCl}\cdot\text{H}_2\text{O}$  gave a value of 33. In addition, the catalytic evaluation was at a lower metal concentration ( $7.6 \times 10^{-4} \text{ molL}^{-1}$ ) as compared to that of our catalysts which was  $6 \times 10^{-3} \text{ molL}^{-1}$ . Thus it can be concluded that our system is less active than the system reported by Mukherjee *et al.*<sup>11</sup>. Recently activity of up to 181 was reported when a salicylaldimine copper complex on MCM-41 was used as catalyst in conjunction with

*tert*-BuOOH. A metal concentration of  $3.2 \times 10^{-4} \text{ molL}^{-1}$  was employed in their catalytic evaluations.<sup>5</sup>

*i. The effect of metal concentration*

The MCM-41 supported catalysts were also evaluated at various metal concentrations as was the case with the mononuclear systems. The other parameters remained unchanged as the catalyst amounts were varied. The results are shown in Table 3.3, entries 2 and 3, for the **Cu-MCM-41** and entries 7 and 8 for **Ni-MCM-41**. At an elevated metal concentration ( $1.2 \times 10^{-2} \text{ molL}^{-1}$ ) there is a reduction in activity for these two catalysts. This may be due to deactivation as a result of dimerization of the metal centers as was the case with the homogeneous analogues. It maybe that the supporting the complexes on MCM-41 does not give enough separation between any two metal centers to prevent the dimerization. Lower metal concentrations on the other hand lead to enhancement of the activity for the supported catalysts. At a metal concentration of  $3 \times 10^{-3} \text{ molL}^{-1}$  TOF value increased from 9.4 to 16.5 for **Cu-MCM-41** and from 7.0 to 14.6 for **Ni-MCM-41**. Increase in activity was also observed in the mononuclear catalyst under similar conditions.

*ii. The effects of oxidant concentration*

The effect of the oxidant concentration was studied under similar conditions used for the mononuclear catalysts. Reducing the concentration of  $\text{H}_2\text{O}_2$  to  $1.2 \text{ molL}^{-1}$  resulted in a reduction in activity for both catalysts. Increasing the amounts of oxidant to  $4.8 \text{ molL}^{-1}$  did not improve the conversion however. The mononuclear catalysts also showed reduction in activity when evaluated at the higher and lower concentration of oxidant.

*iii. The effects of substrate concentration*

The TOF values of the MCM-41 immobilized catalyst also declined with a reduction of substrate concentration. This reduction was also observed for the other catalytic systems. The activities reduced from 9.4 to 5.4 for **Cu-MCM-41** and 7.0 to 4.4 for **Ni-MCM-41**. It can thus be concluded that just as with our other catalysts evaluated the substrate

concentration plays a more significant role with respect to activity than the oxidant concentration.

Table 3.3: Oxidation of cyclohexene MCM-41 immobilized complexes in CH<sub>3</sub>CN<sup>a</sup>

Complex		Conversion (%)	TOF <sup>g</sup>	Selectivity (%)		
				CH-oxide	2-CH-1-ol	2-CH-1-one
<b>CuMCM-41</b>	1	56.5	9.4	14.4		85.6
	2 <sup>b</sup>	46.3	3.9		52.7	47.3
	3 <sup>c</sup>	49.4	16.5		21.7	78.3
	4 <sup>d</sup>	37.4	6.2	6.7	35.9	57.4
	5 <sup>e</sup>	36.7	6.1		36.5	63.5
	6 <sup>f</sup>	64.5	5.4			100
<b>NiMCM-41</b>	7	41.7	7.0	44.0		56.0
	8 <sup>b</sup>	27.8	2.3	37.3		62.7
	9 <sup>c</sup>	43.9	14.6	27.5		72.5
	10 <sup>d</sup>	33.4	5.6			100
	11 <sup>e</sup>	23.8	4.0		43.4	56.6
	12 <sup>f</sup>	52.7	4.4			

<sup>a</sup> [metal] = 6.0 x 10<sup>-3</sup> molL<sup>-1</sup>; [H<sub>2</sub>O<sub>2</sub>] = 2.4. molL<sup>-1</sup>; [cyclohexene] = 2.4. molL<sup>-1</sup>; duration = 24 h; total volume 5 mL

<sup>b</sup> [metal] = 1.2 x 10<sup>-2</sup> molL<sup>-1</sup>

<sup>c</sup> [metal] = 3.0 x 10<sup>-3</sup> molL<sup>-1</sup>

<sup>d</sup> [H<sub>2</sub>O<sub>2</sub>] = 1.2 molL<sup>-1</sup>

<sup>e</sup> [H<sub>2</sub>O<sub>2</sub>] = 4.8 molL<sup>-1</sup>

<sup>f</sup> [cyclohexene] = 1.2 molL<sup>-1</sup>

<sup>g</sup> TOF = moles cyclohexene consumed/moles metal/hour

### 3.2.3.3: The Product distribution using supported catalysts

Under all the conditions investigated, the nickel catalysts, both the dendrimeric and silica immobilized, were found to be more selective for the formation of cyclohexene oxide. At a metal concentration of 6 x 10<sup>-3</sup> molL<sup>-1</sup> only **C7** gave the epoxide for the dendrimeric

catalysts with 47 % selectivity. This was the highest selectivity obtained for the epoxide from the dendrimeric catalysts as shown in Figure 3.10.

Under these baseline conditions the **Ni-MCM-41** catalyst also produced epoxide but with lower selectivity as compared to that of the mononuclear and dendrimeric catalysts. However, the **Cu-MCM-41** showed a 13 % selectivity which is also lower than that of the homogeneous catalyst.

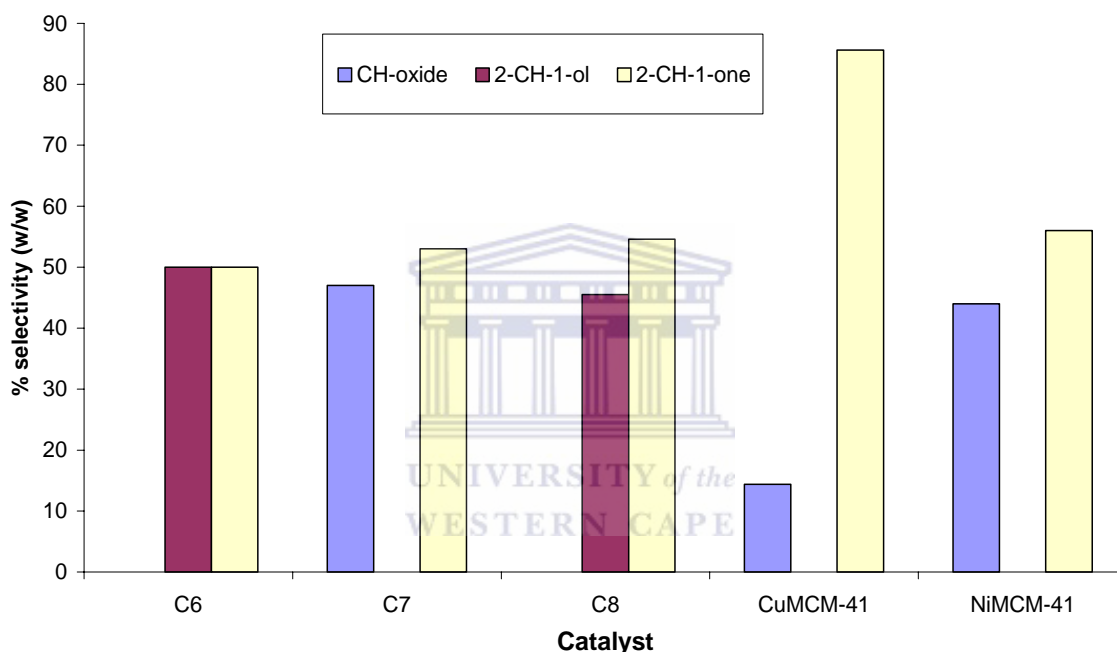


Figure 3.10: Product distribution of the supported pyrrolylaldiminato catalysts,  $[M^{2+}] = 6.0 \times 10^{-3} \text{ molL}^{-1}$ ; M:  $\text{H}_2\text{O}_2$ : cyclohexene = 1:400:400.

As the concentration of the metal was increased to  $1.2 \times 10^{-2} \text{ molL}^{-1}$ , the dendrimeric Ni and **Ni-MCM-41** catalyst shows decreased selectivity for the oxide while **C8** showed a dramatic increase to 31 %, Figure 3.11. However unlike at the base-line conditions, **C6** and **Cu-MCM-41** gave 2-cyclohexen-1-ol as the major product. It can be concluded that further oxidation of the alcohol to the ketone was not favoured under these conditions for the two copper catalysts.

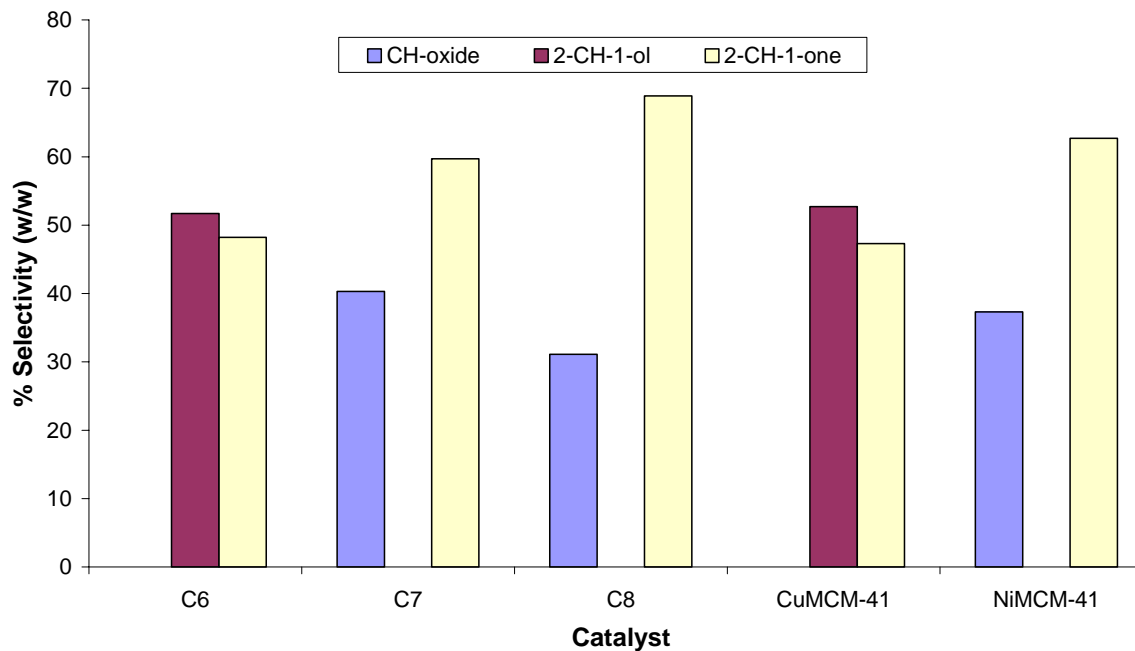


Figure 3.11: Product distribution of the supported pyrrolylaldiminato catalysts,  $[M^{2+}] = 1.2 \times 10^{-2} \text{ molL}^{-1}$ ; M:  $\text{H}_2\text{O}_2$ : cyclohexene = 2:400:400.

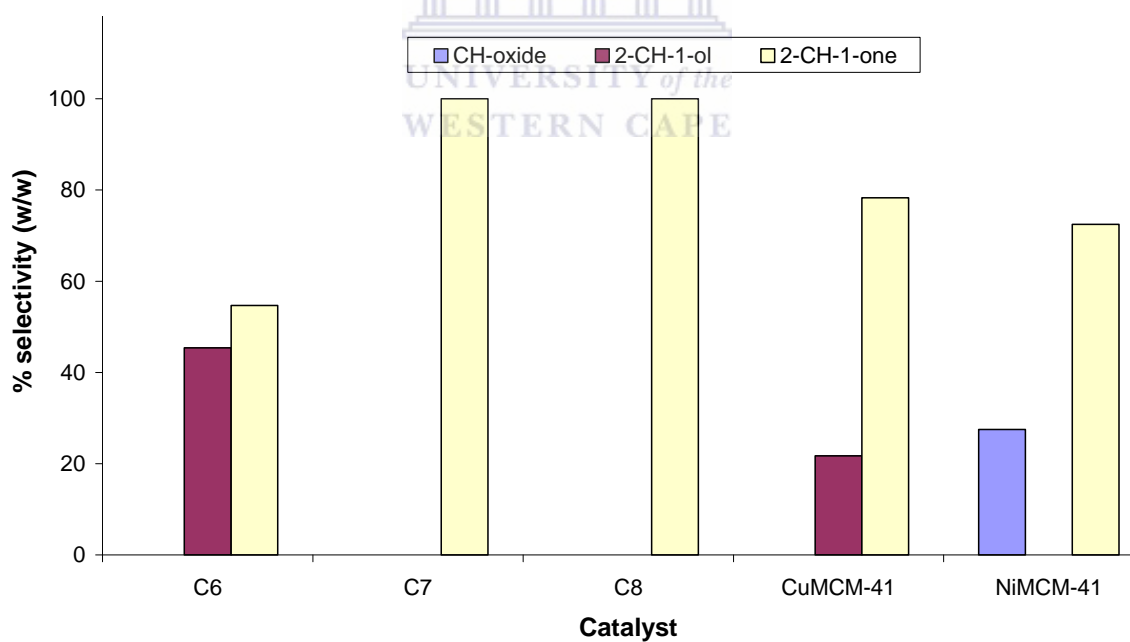


Figure 3.12: Product distribution of the supported pyrrolylaldiminato catalysts,  $[M^{2+}] = 3.0 \times 10^{-3} \text{ molL}^{-1}$ ; M:  $\text{H}_2\text{O}_2$ : cyclohexene = 0.5:400:400.



When the concentration of the metal was reduced to  $3.0 \times 10^{-3} \text{ molL}^{-1}$ , only the allylic products were obtained for the dendrimeric catalysts, Figure 3.12. 2-cyclohexen-1-one was observed as the only product obtained for **C7** and **C8** while **C6** gave 2-cyclohexen-1-one and 2-cyclohexen-1-ol. In the case of MCM-41 supported catalysts, the **Ni-MCM-41** gave cyclohexene oxide at 37 % while **Cu-MCM-41** gave only allylic products.

The concentration of  $\text{H}_2\text{O}_2$  was also an important factor affecting cyclohexene oxide selectivity. At a 1:400:200 ratio of metal: cyclohexene:  $\text{H}_2\text{O}_2$ , 2-cyclohexen-1-ol and 2-cyclohexen-1-one were obtained as the major products. At this low concentration of oxidant the copper catalysts produced some cyclohexene oxide as shown in Figure 3.13.

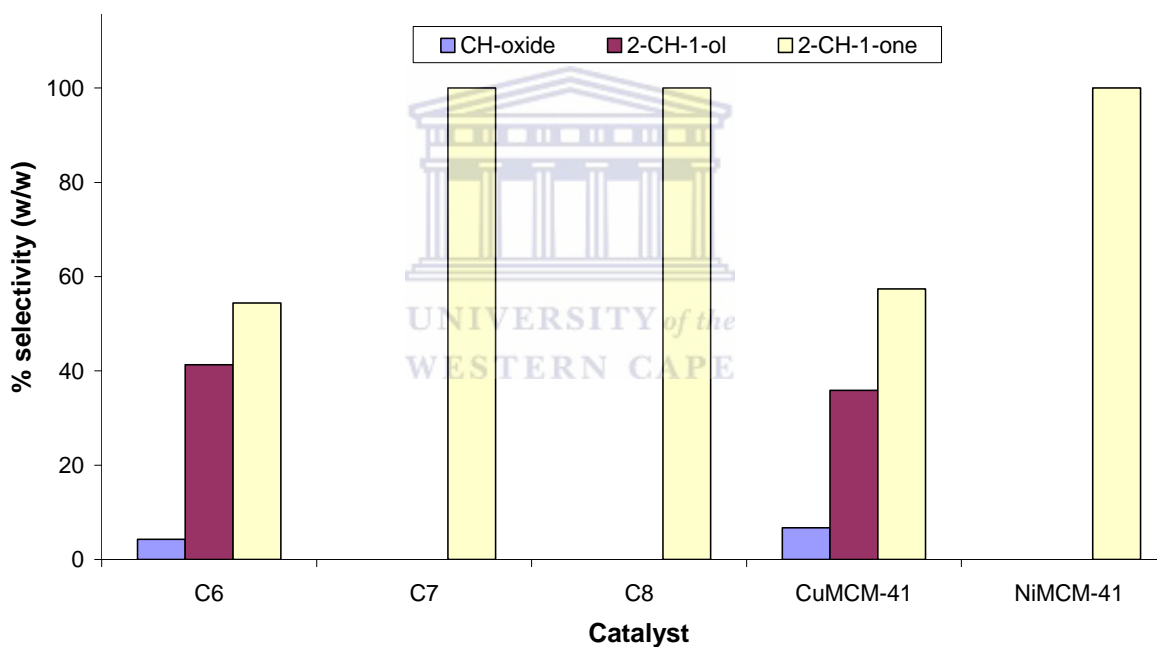


Figure 3.13: Product distribution of the supported pyrrolaluminato catalysts,  $[\text{M}^{2+}] = 6.0 \times 10^{-3} \text{ molL}^{-1}$ ; M:  $\text{H}_2\text{O}_2$ : cyclohexene = 1:400:200.

The use of higher oxidant concentrations did not improve the amount epoxide but rather gave better selectivity for 2-cyclohexen-1-one for all the supported catalysts, Figure 3.14.

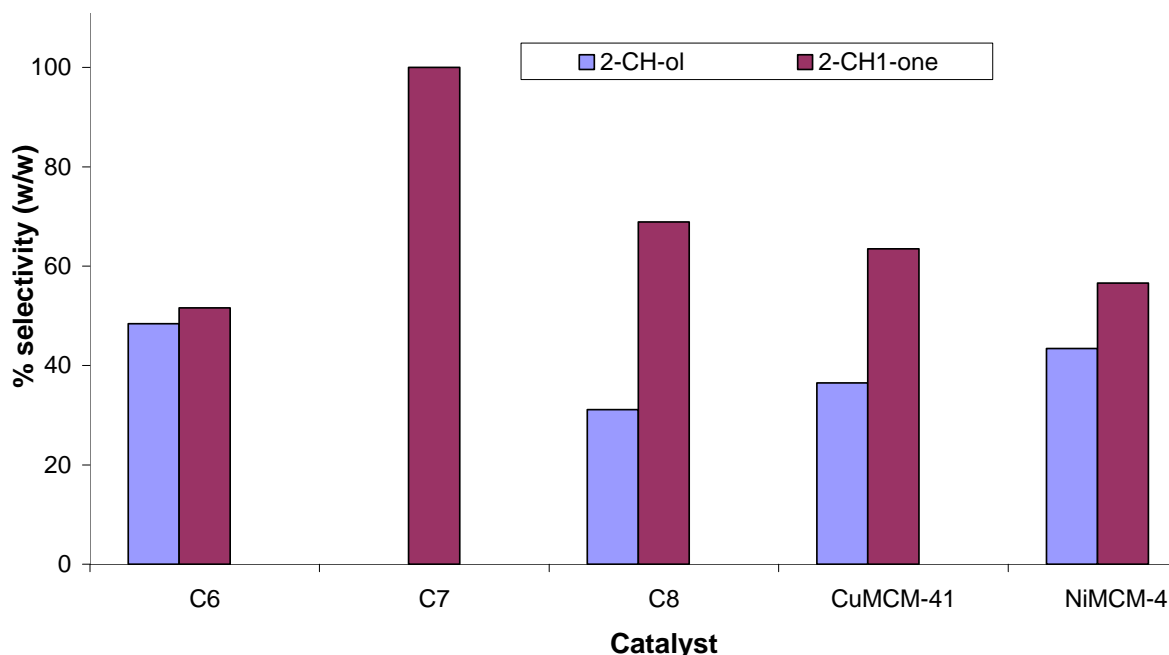


Figure 3.14: Product distribution of the supported pyrrolylaldiminato catalysts,  $[M^{2+}] = 6.0 \times 10^{-3} \text{ molL}^{-1}$ ; M:  $\text{H}_2\text{O}_2$ : cyclohexene = 1:800:400.

A reduction of the substrate concentration improved the 2-cyclohexen-1-one selectivity to 100 % for the **Cu-MCM-41** catalyst, Figure 3.15. At these conditions, again the nickel systems showed conversion but none of the expected products as shown in Scheme 3.1 were identified. A further investigation into the nature of these products is needed to identify them.

Our dendrimeric catalysts behaviour with regard to product distribution differs from some of the reported catalytic systems in the literature. Yang *et al.*<sup>13</sup> reported that in the case where PAMAMSA (1.0)-Mn(II) complexes were used in the oxidation of cyclohexene, cyclohexene oxide, cyclohexen-2-ol, cyclohexen-2-one and 7-oxabicyclo[4,1,0]hepta-2-one, Figure 3.16, were obtained in yields of 5, 22, 30 and 42 % respectively. In these experiments they used  $1.4 \times 10^{-1} \text{ molL}^{-1}$  of Mn. Chavan and co-workers reported selectivity above 80 % for epoxide with a molybdenum-benzimidazole-functionalized dendrimer of PAMAMSA. They also observed that as they increased the Mo concentration, the activity increased and the selectivity for the epoxide also increased.<sup>14</sup>

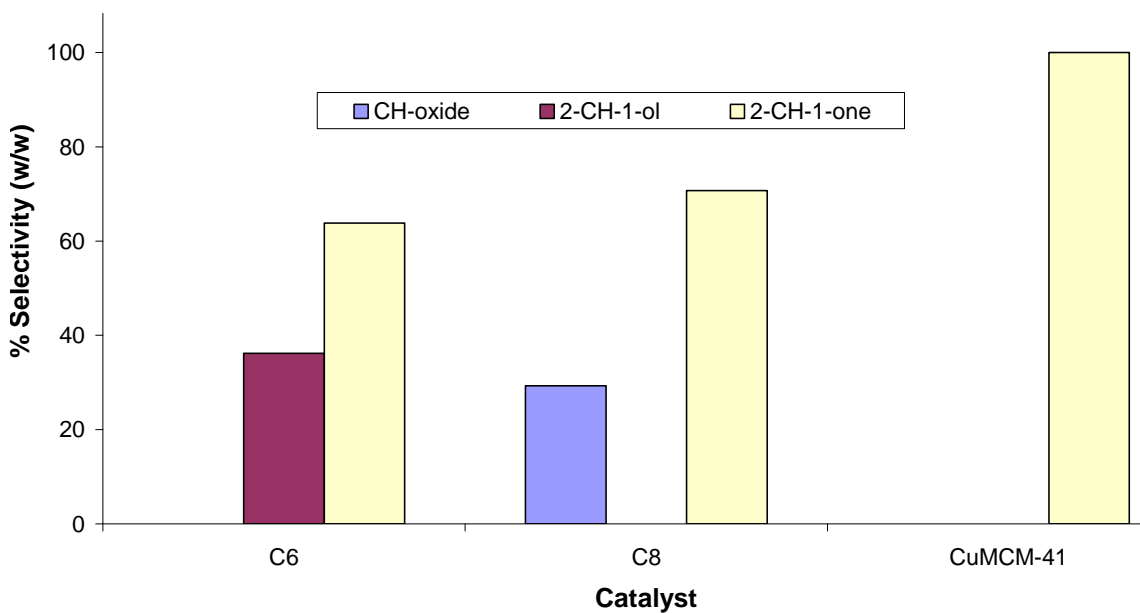


Figure 3.15: Product distribution of the supported pyrrolylaldiminato catalysts,  $[M^{2+}] = 6.0 \times 10^{-3} \text{ molL}^{-1}$ ; M:  $\text{H}_2\text{O}_2$ : cyclohexene = 1:200:200.

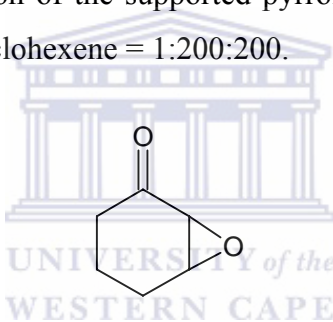


Figure 3.16: 7-oxabicyclo[4.1.0]hepta-2-one

Under all the conditions investigated, the nickel catalyst was found to be more selective for the formation of cyclohexene oxide. Mukherjee *et al.*<sup>11</sup> reported that immobilization of  $\text{CuHqCl}\cdot\text{H}_2\text{O}$  (Hq=8-hydroquinoline) on silica also did not yield epoxide when using aqueous hydrogen peroxide as oxidant. They reported that only allylic products were obtained at a  $6.0 \times 10^{-4} \text{ molL}^{-1}$  copper concentration. However, more recently Jana *et al.*<sup>5</sup> reported remarkable selectivity for cyclohexene oxide when copper salen immobilized on MCM-41 was used in conjunction with *tert*-BuOOH as oxidant. The other major product was 2-cyclohexen-1-ol. This is unlike our system that seems to favour further oxidation of the 2-cyclohexen-1-ol to 2-cyclohexen-1-one. It would thus appear that our catalysts are more efficient in further oxidation of alcohols to ketones.

The **Ni-MCM-41** catalyst only gave epoxide at substrate to H<sub>2</sub>O<sub>2</sub> ratio of 1:1 irrespective of the metal concentration. However when the amounts of cyclohexene was reduced to 1.2 molL<sup>-1</sup>, no epoxide was observed. This could be that the higher levels of H<sub>2</sub>O<sub>2</sub> in the medium helps in, C-H, hydride abstraction thus forming 2-cyclohexene-1-one as the major product as explained earlier. The use of different concentration of oxidant is also quite noticeable producing no cyclohexene oxide at all. Reduced cyclohexene concentration produced none of the expected products. A further investigation into the nature of these products is needed to identify them.

### **3.2.4: Homogeneous versus heterogeneous catalysts**

#### *i. Activity*

The homogeneous catalysts **C1** and **C2** are more active than the immobilized analogues, **Cu-MCM-41** and **Ni-MCM-41**. This is not unexpected, heterogenizing homogeneous catalysts tend to reduced their activity.<sup>15</sup> However Luo and Lin, reported that the homogeneous catalyst, Co(salen)<sub>2</sub>, was not as active as the heterogenized MCM-41-Co(salen)<sub>2</sub> in the oxidation of styrene while using H<sub>2</sub>O<sub>2</sub> as oxidant. The Co(salen)<sub>2</sub> gave low conversion of 41.7 % while the MCM-41-Co(salen)<sub>2</sub> gave 56.5 %. This could be a result of catalyst deactivation in the homogeneous catalyst that is avoided in the MCM-41-Co(salen)<sub>2</sub> due to loading onto the support.<sup>6</sup> In our case, the homogeneous catalyst is stable under the conditions used and no form of deactivation via aggregation of the metal centers seemed to occur.

The copper systems were more active than the nickel analogues, irrespective of whether they were immobilized or not. This was also observed by Salavati-Niasari and Mirsattari.<sup>1</sup> They reported that on comparing the catalytic activities of alumina supported Mn(II), Co(II), Cu(II), and Ni(II) bis(2-hydroxyanil)benzyl complexes for the oxidation of cyclohexene, the activity decreased in the order: [Mn(habenzil)]-Al<sub>2</sub>O<sub>3</sub> > [Co(habenzil)]-Al<sub>2</sub>O<sub>3</sub> > [Cu(habenzil)]-Al<sub>2</sub>O<sub>3</sub> > [Ni(habenzil)]-Al<sub>2</sub>O<sub>3</sub>.

*ii. Product selectivity*

Our copper catalysts, **C1** and **Cu-MCM-41**, are more selective for the allylic products. Immobilization of the homogeneous catalyst does influence the selectivity. In the case of the nickel systems, the homogeneous system, **C2** showed 50 % selectivity for the epoxide and **Ni-MCM-41**, reduces the selectivity for the oxide slightly to 44 %. Jana et al<sup>5</sup> observed that MCM-41-Cu(salen)<sub>2</sub> catalyzed epoxidation of olefins with *tert*-BuOOH to produce the corresponding epoxide with remarkable selectivity. Styrene oxide was obtained at 89 % selectivity at 86 % conversion. Cyclohexene showed better conversion of 94 % but gave a lower selectivity for the oxide. When aqueous H<sub>2</sub>O<sub>2</sub> was used, only 34 % styrene was converted with 6 % epoxide selectivity.

### **3.3: Conclusions**

All the catalysts evaluated are active in the oxidation of cyclohexene. The presence of 2-cyclohexen-1-ol and 2-cyclohexen-1-one as the major products shows the preference of attack of the activated C-H bond over the C=C bond. The conditions used herein promote the allylic oxidation pathway and epoxidation is minimized. The copper catalysts are the most active while the nickel catalysts are most selective for cyclohexene oxide. 2,6-diisopropyl groups on the phenyl substituent of the imino nitrogen provides hindrance on the metal center thus resulting in reduction in activity. There is also a remarkable reduction in activity when the homogeneous catalysts are heterogenized.

### **3.4: Experimental**

#### **3.4.1: Materials and instrumentation**

Cyclohexene, 2-cyclohexen-1-ol, 2-cyclohexen-1-one, cyclohexene oxide and 1,2-cyclohexane-diol were purchased from Sigma-Aldrich Ltd. Acetonitrile was purchased from BDH chemicals Ltd while toluene and H<sub>2</sub>O<sub>2</sub> (30 % wt) were from Merck Chemicals.

Oxidation reactions were carried out on a 12 place Radley's Discovery Technologies parallel reactor equipped with glass reaction vessels. GC analyses were performed on a Varian CP-3800 with a HP PONA column. Calibration was performed using authentic

samples. Conversion and product yields were determined using toluene as internal standard.

#### **3.4.2: Catalytic cyclohexene oxidation**

Cyclohexene oxidation was carried out on a 12 place Radley's Discovery Technologies Heated Carousel Reaction Station fitted with a reflux unit as well as a gas distribution system. The reactions were carried out in 45 mL glass reaction vessels under oxygen atmosphere. In the baseline run, 1.2 mL (12 mmol) cyclohexene, 0.01 g (0.03 mmol of Cu) **C1** and 2.6 mL CH<sub>3</sub>CN were heated to 60 °C. In all runs, the amounts of catalyst were adjusted to have the same amounts of metal in each of the reactions. The oxidation was initiated by addition of 1.2 mL (12 mmol) H<sub>2</sub>O<sub>2</sub> (30 % wt). Once the desired temperature had been obtained, the mixture was refluxed for 24 h. After 24 h, 1 mL of the organic layer was filtered using a syringe filter into a vial and 0.05 mL toluene added as internal standard. GC analysis was performed within 12 h.

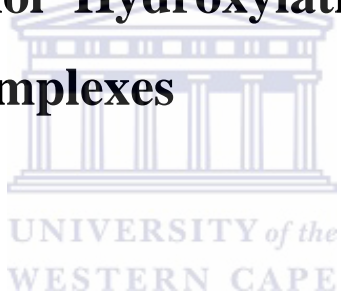
#### **3.5: References**

1. M. Salavati, S. N. Mirsattari, *J. Mol. Cat. A: Chem.*, **268** (2007) 50.
2. T. Luts, W. Suprun, D. Hofmann, O. Klepel, H. Papp, *J. Mol. Cal. A: Chem.*, **261** (2007)16.
3. M. Ghadiri, F. Farzaneh, M. Ghandi, M. Alizadeh, *J. Mol. Cat A: Chem.*, **233** (2005)127.
4. C. N. Kato, S. Negishi, K. Yoshida, K. Hayashi, K. Nomiya, *Appl. Catal. A*, **292** (2005) 97.
5. S. Jana, B. Dutta, R. Bera, S. Koner, *Langmuir*, **23** (2007) 2492.
6. Y. Luo, J. Lin, *Micropor. Mesopor. Mater.*, **86** (2005) 23.
7. M. Salavati-Niasari, M. Hassani-Kabutarkhani, F. Davar, *Catal. Commun.*, **7** (2006) 955.
8. S. D. Drouin, H. M. Foucault, G. P. A. Yap, D. E. Fogg, *Can. J. Chem.*, **83** (2005) 748.
9. W. Nam, R. Ho, J. S. Valentine, *J. Am. Chem. Soc.*, **113** (1991) 7052.

10. P. Karandikar, K.C. Dhanya, S. Deshpande, A.J. Chandwadkar, S. Sivasanker, M. Agashe, *Catal. Commun.*, **5** (2004) 69.
11. S. Mukherjee, S. Samanta, A. Bhaumik, B. Chandra, *Appl. Catal. B*, **68** (2006) 12.
12. M. Salavati-Niasari, P. Salemi, F. Davar, *J. Mol. Cat. A: Chem.*, **238** (2005) 215.
13. Z-W. Yang, Q-X. Kang, H-C. Ma, C-L. Li, Z-Q. Lei, *J. Mol. Cat. A: Chem.*, **213** (2004) 169.
14. S. Chavan, W. Maes, J. Wahlen, P. Jacobs, D. De Vos, W. Dehaem, *Catal. Commun.*, **6** (2005) 241.
15. C. W. Jones, M. W. McKittick, J. V. Nguyen, K. Yu, *Top. Catal.*, **34** (2005) 67.



## **Chapter 4 : Phenol Hydroxylation Catalyzed by Pyrrole-imine Complexes**





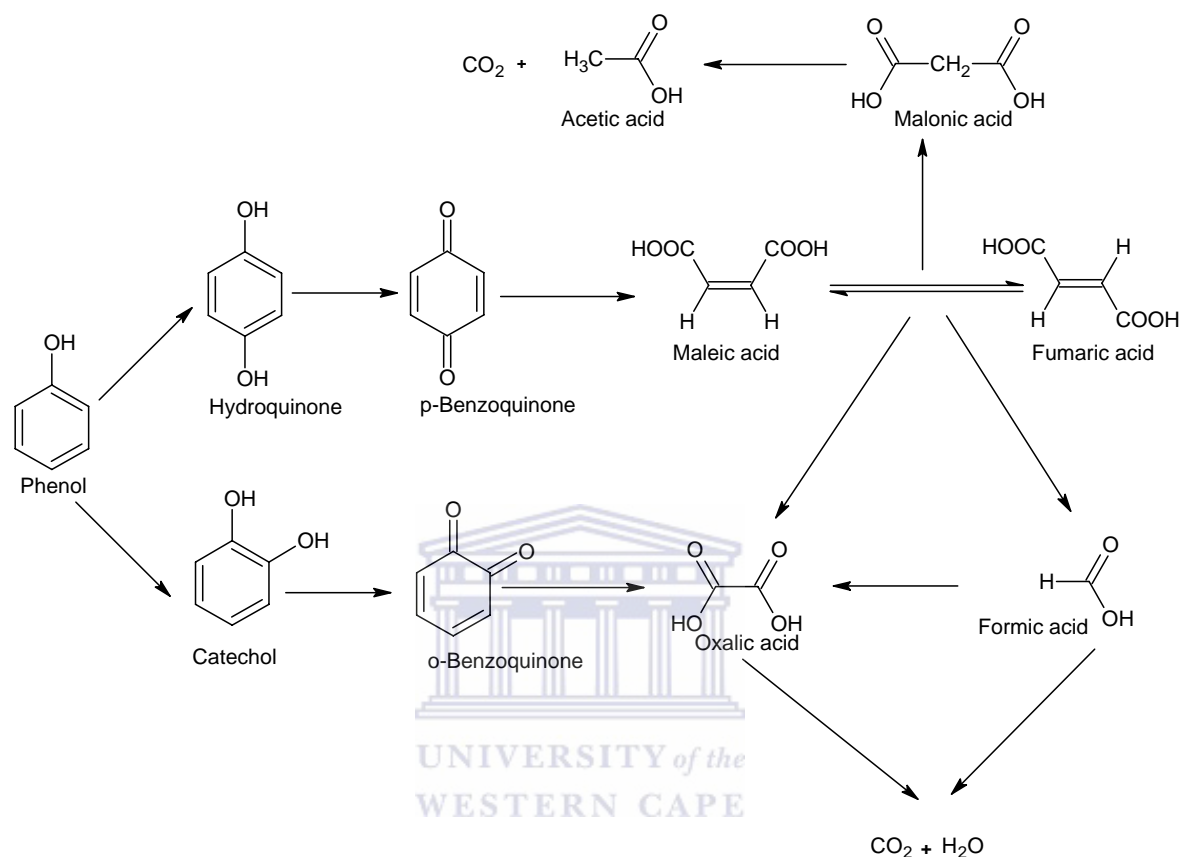
#### 4.1: Introduction

Catalytic wet peroxide oxidation (CWPO) is a well known route for the oxidation of phenol that can be accomplished under mild conditions (130 °C, 0.5 - 1 MPa) with good yields and selectivity of up to 95 % using hydrogen peroxide and a homogeneous source of  $\text{Fe}^{2+}$ .<sup>1-3</sup> Nowadays, aqueous hydrogen peroxide is viewed as one of the most attractive oxidants from both an ecological and economical view point.  $\text{H}_2\text{O}_2$  is a relatively strong oxidant, stable and produces water as a by-product. The CWPO process, being homogeneous, has some main drawbacks such as using it with difficulty in continuous processes, catalyst separation and recovery. These disadvantages increase the cost of the process. Another limitation is the narrow pH range, usually around 3.0, in which this process can efficiently operate. Heterogeneous catalysis can overcome some of these problems and in doing so provides protection of the environment.

Natural peroxidases have also been studied in the oxidation of phenol but the instability and the high cost of natural enzymes have stimulated a search for alternatives that could be used in a catalytic manner. A number of different materials containing copper, iron, molybdenum or zinc precursors supported on (or intercalated in) oxides, clay, polymers and mesoporous silica have been proposed as catalysts but few have shown significant activity or satisfactory product selectivity in aqueous media. Some of these materials also require very complicated syntheses.<sup>4-6</sup> Schiff base complexes containing transition metal ions such as Fe(II), Fe(III), Mn(III), Co(II) and Cu(II) have been used as mimetic peroxidases in the catalytic oxidation of phenol by hydrogen peroxide.<sup>7,8</sup> Supported homogeneous catalysts have also been reported using different types of supports e.g. polymeric coordinated complexes<sup>9</sup> and metal complexes immobilized on inorganic supports or encapsulated in zeolites.<sup>10-13</sup>

Phenol is hydroxylated to catechol (CT) and hydroquinone (HQ) as the primary products. The hydroxylation mechanism is generally accepted to be a free radical mechanism.<sup>14-16</sup> Hydroquinone can be further oxidized to *p*-benzoquinone (*p*-BQ) while catechol yields *o*-benzoquinone (*o*-BQ). At elevated temperatures in the presence of a catalyst and water, these quinones can subsequently be oxidized to carboxylic acids. *p*-BQ can be further

oxidized to short chain acids such as maleic, malonic, fumaric and acetic acid whereas *o*-BQ gives oxalic and formic acid, Scheme 4.1 (adapted from reference 17).



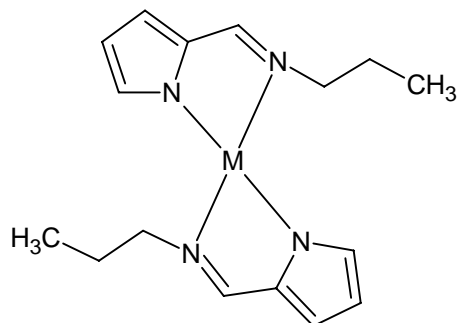
Scheme 4.1: Proposed reaction pathway for phenol oxidation in the aqueous phase

Catechol and hydroquinone are widely used in the production of photographic chemicals, anti-oxidants, polymerization inhibitors, flavouring agents, medicine and pesticides. Catechol is also used as an organic sensitizer in photoelectrochemical cells.<sup>18</sup>

In this chapter we report the preliminary results of the hydroxylation of phenol using hydrogen peroxide as oxidant in the presence of molecular oxygen and employing some of the complexes synthesized in Chapter 2. The complexes employed are the mononuclear complexes of copper, **C1**, and nickel, **C2**, with a propyl group at the imino nitrogen, dendrimeric Cu(II), **C6**, and Ni(II), **C7**, and the MCM-41 supported Cu and Ni,

**Cu-MCM-41** and **Ni-MCM-41** respectively. These catalysts are shown in Figure 4.1-4.3.

- i. Mononuclear complexes of copper (**C1**) and nickel (**C2**).

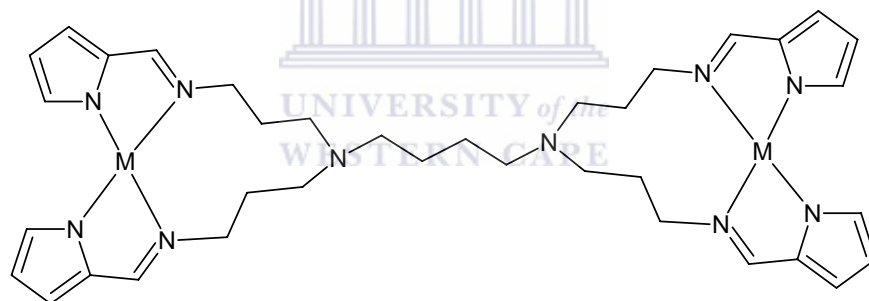


**C1:** M = Cu

**C2:** M = Ni

Figure 4.1: Mononuclear pyrrolylaldiminato complexes

- ii. Dendrimeric complexes of copper (**C6**) and nickel (**C7**),



**C6:** M = Cu

**C7:** M = Ni

Figure 4.4.2: Dendrimeric pyrrolylaldiminato complexes

- iii. MCM-41 supported copper and nickel catalysts **Cu-MCM-41** and **Ni-MCM-41**.

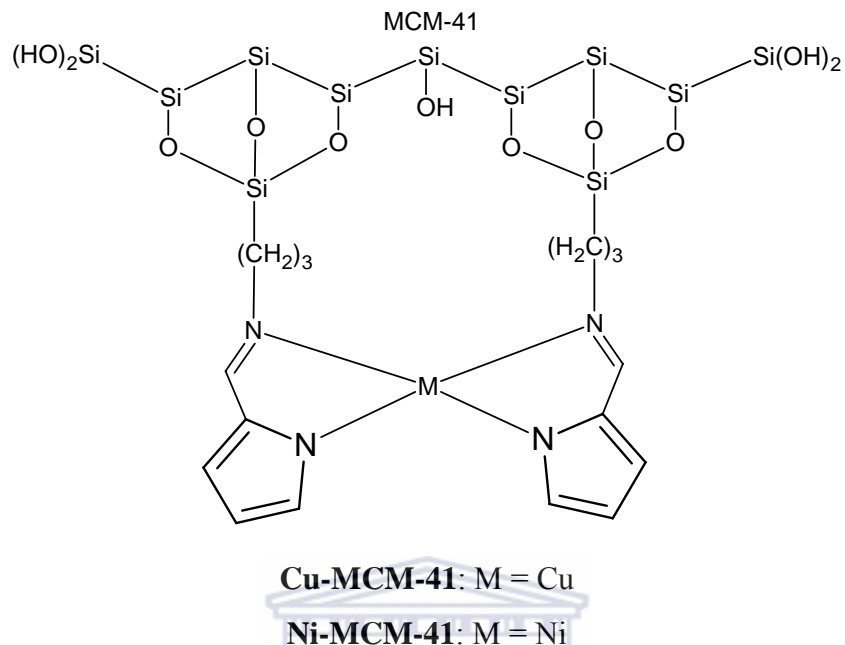


Figure 4.3: MCM-41 immobilized pyrrolylaldiminato complexes

Comparative studies of the homogeneous copper system, **C1**, and that of nickel, **C2**, against their heterogenized analogues, **Cu-MCM-41** and **Ni-MCM-41** were also conducted. We also compared the efficiency of the dendrimer catalysts with that of the mononuclear analogues. In order to determine the optimum reaction conditions we investigated several parameters such as pH and substrate to oxidant ratios.

## 4.2: Results and discussion

### 4.2.1: Hydroxylation of phenol

Hydroxylation of phenol by  $\text{H}_2\text{O}_2$  was investigated using pyrrolylaldiminato complexes of copper and nickel in both homogenous and heterogeneous catalysis. Thus **C1**, **C2**, **C6**, **C7**, **Cu-MCM-41** and **Ni-MCM-41** were employed as catalysts. The metal concentration of  $1.0 \times 10^{-3} \text{ molL}^{-1}$  was also kept constant in all the catalytic runs irrespective of the catalyst used. In all cases a phenol: metal ratio of 100:1 and 1:1 phenol to  $\text{H}_2\text{O}_2$  ratio was maintained unless otherwise stated. The catalysts were evaluated over a pH range of 2 - 6 in order to establish the effect of the acidity of the

reaction medium. A further evaluation at pH 7 and 8 for **C6** and **C7** was done. The results for conversion and product selectivity are shown in Tables 4.1 - 4.3.

It was found that all the catalysts were active for phenol hydroxylation. Under the conditions used, catalyst **C1** was the most active over a wide pH range with the highest conversion of (82 %) being obtained at pH 3. At this pH the other catalysts also showed their highest percentage phenol conversion apart from **Ni-MCM-41** who's highest activity was recorded at pH 4. **C2** is the least active catalyst overall. Figure 4.4 shows a graphic representation of the activities of the six catalysts. The catalysts could be ranked as follows in terms of activity for phenol hydroxylation: **C1**>**CuMCM-41**>**C6**>**NiMCM-41**>**C7**>**C2**. From this it can be seen that copper-based catalysts are generally more active than the nickel analogues.

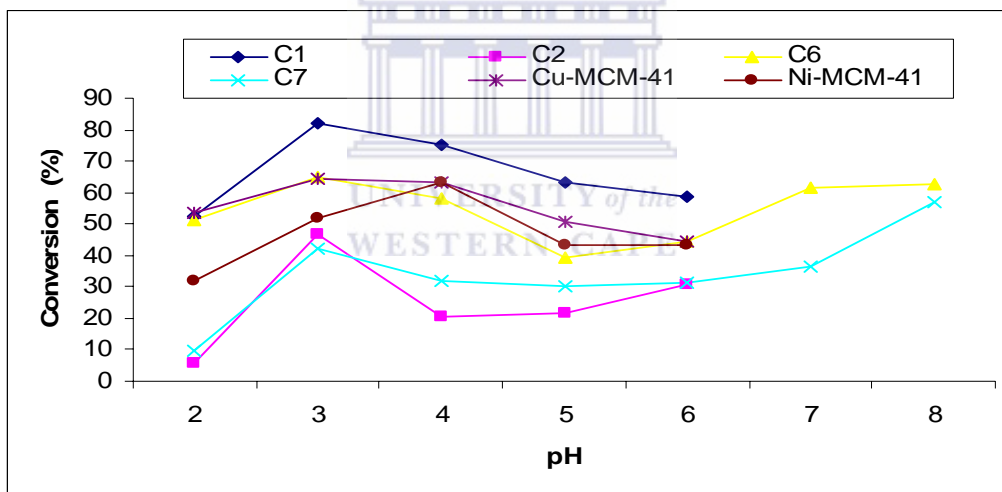
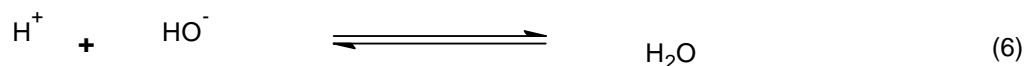
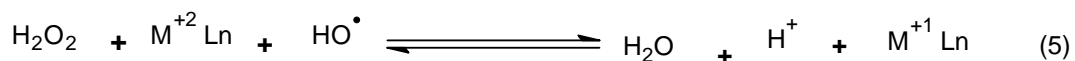
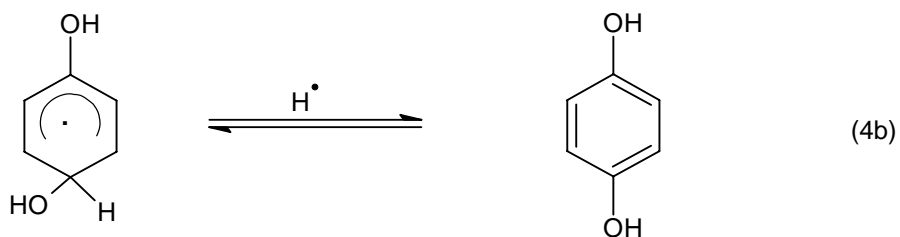
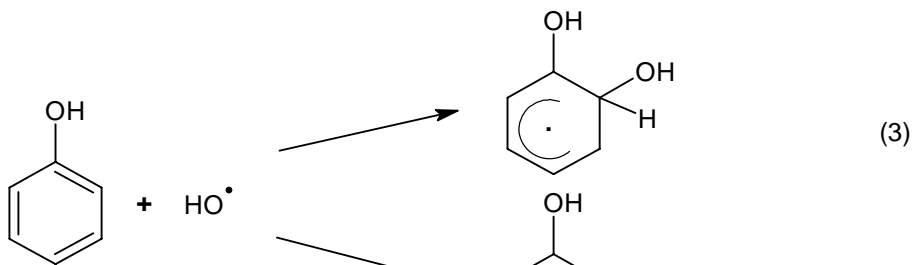
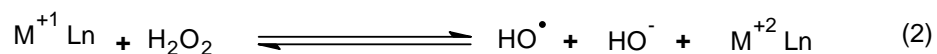
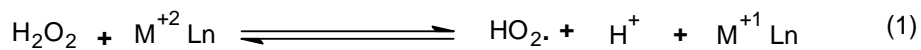


Figure 4.4: Phenol conversion for the catalysts evaluated

The results are in general agreement with what is reported in the literature. These results can be explained in terms of the generally accepted radical reaction mechanism for the hydroxylation of aromatic hydrocarbons<sup>19</sup> Scheme 4.2 shows a step-wise outline of the hydroxylation mechanism by a metal catalyst such as copper. The same mechanism applies for the nickel catalyst. The hydroxyl radical is readily formed by metal mediated decomposition of H<sub>2</sub>O<sub>2</sub> in acidic media. This can be facilitated by the removal of the OH<sup>-</sup> produced in step 2; Scheme 4.2 thus shifting the equilibrium to the right. At pH 2,

all the catalysts showed the least activity. It can be concluded that at relatively low pH the step 1 in Scheme 4.2 was being repressed thus resulting in low conversion.<sup>21</sup>



M = Cu or Ni

Scheme 4.2: Proposed radical mechanism for the hydroxylation of phenol to catechol and hydroquinone

#### ***4.2.2: The effect of pH on phenol conversion using mononuclear catalysts***

The mononuclear homogeneous copper catalysts, **C1**, showed a higher activity than the nickel system over the pH range evaluated, Table 4.1. The highest activity is obtained at pH 3 in both systems. The copper system showed increased activity from pH 2 to 3 followed by a decrease from pH 3 to 6. The nickel analogue also showed a similar trend with activity increasing from pH 2 to 3 and then decreasing from pH 3 to 5. However there was a slight increase in activity at pH 6. It appears that pH 3 is the optimal pH for the metal mediated decomposition of H<sub>2</sub>O<sub>2</sub> to produce the hydroxyl radical. Tatibouët *et al.*<sup>22</sup> reported that the homogeneous and heterogeneous systems of commercially available Greek bentonite (mixture of Al-Fe species) at atomic ratio Al:Fe equal to 9:1 were very sensitive to pH changes. In these systems homogeneous catalysts gave a broad maximum phenol conversion in the pH range of 3 – 3.7. Dramatic reduction in conversion levels from ≈80 % at pH = 3 to less than 5 % at pH = 2.5 and 10 % at pH 4 was observed. In the case of the heterogeneous bentonite system, a sharp maximum at pH value of 3.7 was observed. Our systems also show sensitivity to changes in pH with a similar dramatic reduction in activity at pH 2.

UNIVERSITY of the

The low activity of the nickel system, **C2**, as compared to the copper system, **C1**, could be due to dimerization of the nickel metal centers as well as other forms of aggregation of the metal centers. It could also be due to formation of a stable peroxonickel(II) complex.<sup>13</sup> In case of dimerization the catalyst activity would be destroyed. In the case of the formation of the peroxonickel(II) complex, its stability hinders the transfer of the oxygen to the substrate. Since there is considerable high activity at pH 3, the peroxonickel(II) complex cannot be the reason for this. The optimum pH value for homogeneous Fenton processes is around 3.<sup>2</sup> Thus it can be concluded that our systems do in fact exhibit Fenton-type reactions. The low catalytic activity of **C2** could also be due to higher stability of the nickel active species as opposed to that of the copper in the acidic medium.

In terms of the effect of pH, our catalysts differ from natural enzymes. Xie *et al.*<sup>8</sup> reported that the first order rate constant initially increases, up to a maximum, and then

falls when the pH value of the solution increases from 5.0 to 8.0. The optimum acidity of the enzyme-like system was *ca.* pH 7.0, while the optimum of the natural enzyme, horseradish peroxidase obtained from plants, was *ca.* pH 5.8 in a phosphate buffer.

Table 4.1: Effect of pH on catalytic activity of mononuclear catalysts<sup>a</sup>

Catalyst	Metal	pH	% selectivity (w/w) <sup>b</sup>			% Phenol Conversion	TOF <sup>c</sup>
			CT	HQ	<i>p</i> -BQ		
<b>C1</b>	Cu	2	54.37	44.37	0.69	52.46	8.74
	Cu	3	66.97	32.23	0.80	82.00	13.67
	Cu	4	62.40	37.42	0.18	75.21	12.54
	Cu	5	67.55	32.18	0.27	63.13	10.52
	Cu	6	75.48	24.21	0.31	58.75	9.79
<b>C2</b>	Ni	2	95.04	4.95	-	5.90	0.98
	Ni	3	72.37	27.41	0.22	46.77	7.80
	Ni	4	75.31	24.69	-	20.55	3.43
	Ni	5	93.23	6.62	0.15	21.40	3.57
	Ni	6	99.92	-	0.08	30.79	5.13

<sup>a</sup> 10mL buffer solution, [M] =  $1 \times 10^{-4}$  molL<sup>-1</sup>, Phenol:M = 100:1, 30% H<sub>2</sub>O<sub>2</sub> as oxidant; Phenol:H<sub>2</sub>O<sub>2</sub> = 1:1, 110 °C at 1 atm O<sub>2</sub>

<sup>b</sup> Products, HQ, CT and BQ, distribution is given on a tar free basis

<sup>c</sup> TOF = moles phenol consumed/moles metal/hour

#### 4.2.3: The effect of pH on phenol conversion using dendrimeric catalysts

The dendrimeric catalysts evaluated are bimetallic in nature. The catalytic reactions were done in such a way as to ensure that the metal concentration remained the same as that used for the mononuclear catalyst systems. The results are shown in Table 4.2. Once again the dendrimeric copper catalyst shows higher activity when compared to the nickel. Both catalysts **C6** and **C7** showed an increase in activity when the pH was changed from pH 2 to 3. Beyond pH 3, **C6** showed a gradual reduction in activity until pH 5 thereafter activity increased slightly at pH 6. **C7** catalytic activity remained largely unaffected by



pH values in the range of 4 - 6. The low activity of **C7** at pH 2 could be due to dimerization as was the case for **C2**. The copper catalyst appears to be affected differently by changes in the pH when compared to the nickel systems. The dendrimer catalysts also appear to behave differently than the monomeric catalysts. Thus for example it is observed that activity increased dramatically beyond pH 6.

Table 4.2: Effect of pH on catalytic activity of dendrimeric catalysts<sup>a</sup>

Catalyst	Metal	pH	% selectivity (w/w) <sup>b</sup>			% Phenol Conversion	TOF <sup>c</sup>
			CT	HQ	<i>p</i> -BQ		
<b>C6</b>	Cu	2	55.33	42.23	2.44	51.26	8.54
	Cu	3	73.63	25.15	1.22	64.90	10.82
	Cu	4	83.76	15.96	0.28	58.35	9.73
	Cu	5	52.59	47.24	0.47	39.53	6.59
	Cu	6	63.67	35.81	0.51	44.31	7.39
	Cu	7	74.64	24.41	0.95	61.64	10.27
	Cu	8	61.19	37.90	0.91	62.82	10.47
	<b>C7</b>	Ni	2	96.18	3.82	0	9.75
Ni		3	92.62	6.69	0.69	41.90	6.98
Ni		4	80.00	19.73	0.27	21.37	5.33
Ni		5	89.96	10.04	0	30.27	5.05
Ni		6	99.89	-	0.11	31.53	5.26
Ni		7	85.91	13.74	0.35	36.74	5.05
Ni		8	68.88	30.67	0.45	56.93	9.49

<sup>a</sup> 10mL buffer solution,  $[M] = 1 \times 10^{-4} \text{ molL}^{-1}$ , Phenol:M = 100:1, 30%  $\text{H}_2\text{O}_2$  as oxidant; Phenol: $\text{H}_2\text{O}_2 = 1:1$ , 110 °C at 1 atm  $\text{O}_2$

<sup>b</sup> Products, HQ, CT, and BQ, distribution is given on a tar free basis

<sup>c</sup> TOF = moles phenol consumed/moles metal/hour

It was thought that the nitrogen groups in the dendrimer backbone may be protonated in acidic medium. This would lead to retardation of the catalytic process. In this case as

free  $[H^+]$  is lowered; step 2 (Scheme 4.2) equilibrium of is pushed to the left thus slowing down the formation of the hydroxyl radical. Reactions were thus also performed in neutral and slightly basic reaction media. In both cases an increase in phenol conversion was observed from pH 6 to 8. In a neutral or slightly basic medium, the protonation of internal N atoms of the dendrimer is hampered by the high  $[OH^-]$ . This results in increased oxidation activity.

#### ***4.2.4: The effect of pH on phenol conversion using MCM-41 supported catalysts***

The catalytic reactions using the supported catalysts were done in such a way to ensure that the metal concentration remained the same as for the mononuclear systems. The results are shown in Table 4.3. In the case of the MCM-41 immobilized catalyst, copper is slightly more active than the nickel analogue. As with the mononuclear and the dendrimeric systems, conversion is once again optimal at pH 3. Thereafter a gradual decrease in activity through to pH 6 for the **Cu-MCM-41** is observed. However the nickel system shows a slight difference with optimum conversion being at pH 4. Thus, this means that for the nickel system optimum decomposition of  $H_2O_2$  leading to production of the hydroxyl radical (step 2 of Scheme 4.2) was at pH 4. Mei *et al.*<sup>3</sup> reported that using heterogeneous Fe-exchanged Ti-pillared interlayered montmorillonite (Fe-Ti-PILC) the optimum pH value for the hydroxylation of phenol was also around 4.0. However Ray *et al.*<sup>18</sup> recently reported that salicylaldehyde complexes of copper and nickel immobilized on MCM-41 showed optimum conversion at pH 6.

In summary it was observed that the copper catalyst, **C1**, showed the highest conversion over the pH range evaluated. The dendrimeric and the heterogenized copper catalysts gave lower activity than those of the homogeneous system. However, the nickel catalysts showed the opposite effect. The heterogenized nickel catalyst was the most active while the homogeneous **C2** was the least active. It is thought that in the case of the nickel systems, immobilization of the metal complexes increases catalyst stability by preventing metal agglomeration. The latter often leads to catalyst deactivation.

Table 4.3: Effect of pH on catalytic activity of MCM-41 immobilized catalysts<sup>a</sup>

Catalyst	Metal	pH	% selectivity (w/w) <sup>b</sup>			% Phenol Conversion	TOF <sup>c</sup>
			CT	HQ	<i>p</i> -BQ		
<b>Cu-MCM-41</b>	Cu	2	52.65	44.68	2.68	53.69	8.95
	Cu	3	68.84	30.52	0.64	64.28	10.71
	Cu	4	58.09	41.82	0.10	63.10	10.51
	Cu	5	52.82	47.05	0.13	50.91	8.49
	Cu	6	73.37	26.42	0.20	44.53	7.42
<b>Ni-MCM-41</b>	Ni	2	53.25	44.66	2.10	31.91	5.32
	Ni	3	80.07	19.52	0.41	51.88	8.65
	Ni	4	64.62	35.25	0.13	62.95	10.49
	Ni	5	54.66	44.86	0.48	43.48	7.25
	Ni	6	78.71	20.95	0.32	43.41	7.23

<sup>a</sup> 10mL buffer solution,  $[M] = 1 \times 10^{-4} \text{ molL}^{-1}$ , Phenol:M = 100:1, 30% H<sub>2</sub>O<sub>2</sub> as oxidant; Phenol:H<sub>2</sub>O<sub>2</sub> = 1:1, 110 °C at 1 atm O<sub>2</sub>

<sup>b</sup> Products; HQ, CT and BQ, distribution is given on a tar free basis

<sup>c</sup> TOF = moles phenol consumed/moles metal/hour

#### 4.2.5: The effect of pH on catalyst selectivity

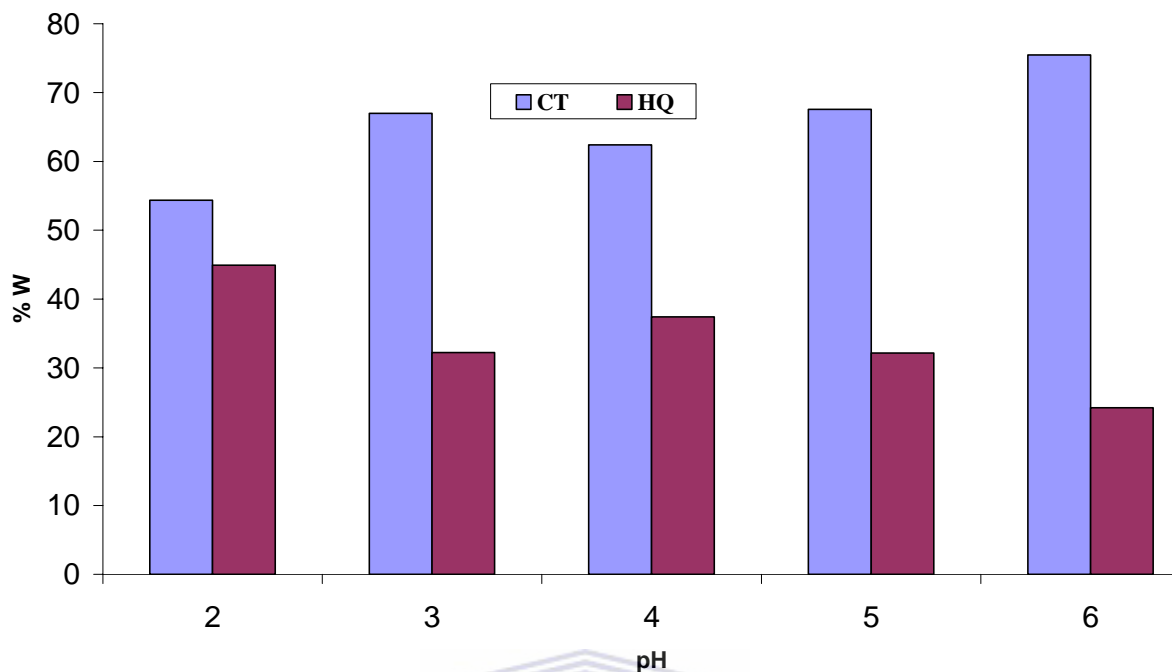
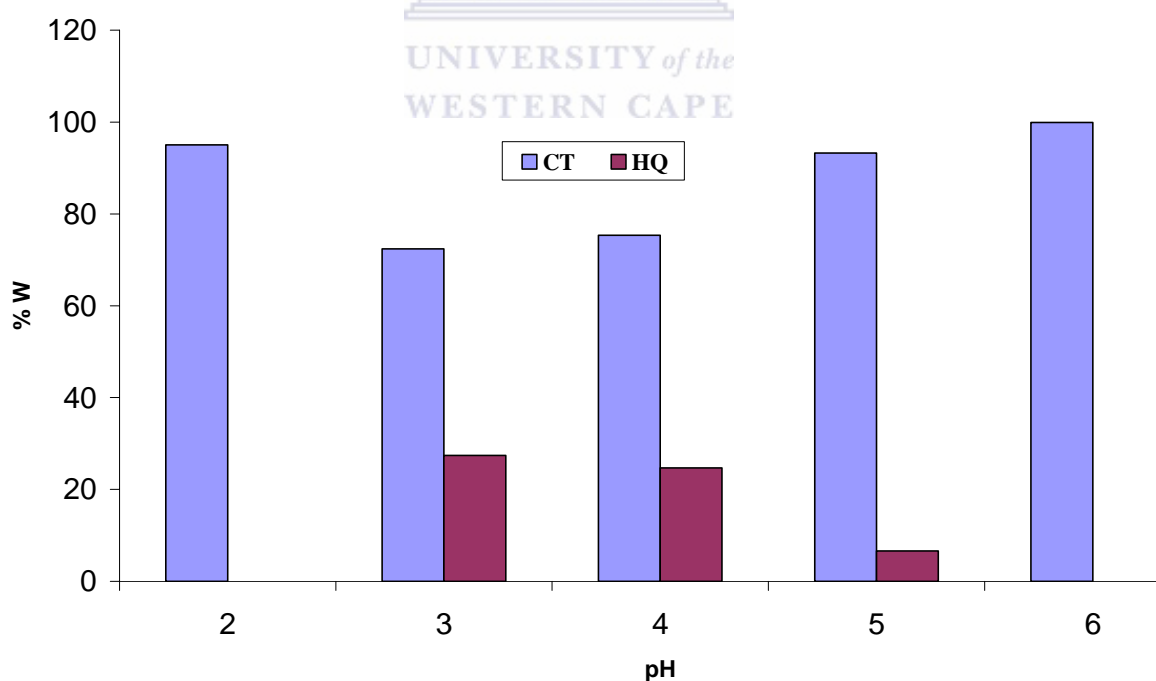
The major products observed from the phenol hydroxylation are catechol and hydroquinone with catechol often formed in larger quantities. The predominance of catechol is not unexpected for copper-mediated hydroxylation occurring *via* a pathway which involves initial weak coordination of both phenol and H<sub>2</sub>O<sub>2</sub> to the active site. The anchoring of the two reactants in close proximity leads predominantly to a *cis* arrangement, which in turn results in ortho-substitution of the phenol.<sup>19</sup> However a considerable amount of *p*-benzoquinone is also observed. This indicates that under our conditions hydroquinone undergoes secondary oxidation but catechol does not. The highest amount of benzoquinone is obtained at lower TOF values.

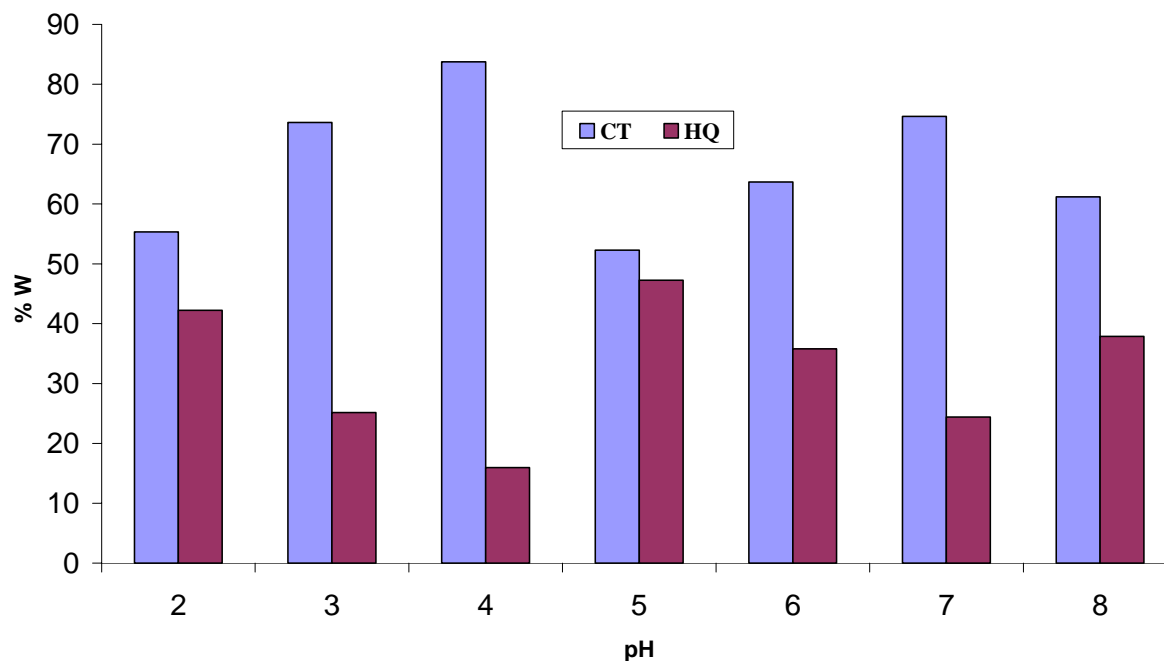
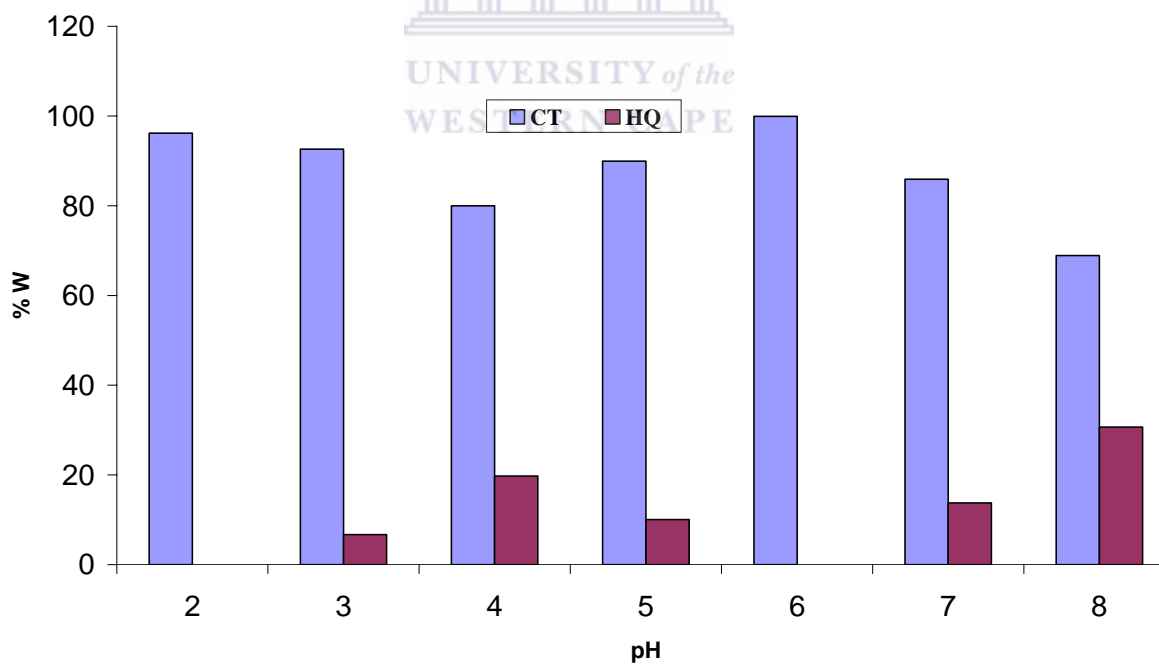
The ratio of catechol to hydroquinone is greatly affected by the pH of the reaction and not as much by the catalyst type, Figures 4.5 – 4.10. Under acidic conditions Santo *et al.*<sup>14</sup> proposed that the primary intermediates HQ and CT can be further oxidized to *p*-BQ and *o*-BQ respectively. The stability of these primary intermediates formed from the substrate and the active species should also change with pH variations. They observed that at pH 3.8 the hydroperoxide radical formed facilitated the formation of HQ and CT. The optimum pH for this radical formation was established to be pH 3.8.

In the case of the mononuclear systems, the CT: HQ ratios vary from *ca* 1:1 at pH 2 to 2:1 at pH 3 - 5. At pH 6 the amount of catechol produced increases giving CT: HQ ratio of 3:1 ratio. In the nickel systems, there is a significant selectivity for catechol. In some cases e.g. pH 2 and 6, no hydroquinone was observed using these nickel catalysts, thus indicating a highly selective system.

The dendrimeric nickel catalyst was more selective for catechol over hydroquinone than the copper analogue. However the two catalysts showed similar trends in selectivity to that found in the mononuclear systems. The only difference in the case of the mononuclear catalysts is that the CT: HQ ratio was more pronounced in the dendrimeric systems. The dendrimeric nickel catalyst, **C7**, gave no hydroquinone at pH 2 and 6 just like in the case of the monomeric **C2**.

For the MCM-41 supported catalysts, the copper system showed similar ratios to those of the unsupported catalyst. However for the **Ni-MCM-41** catalyst there is a dramatic increase in amounts of hydroquinone especially at pH 2 where the ratio is almost 1:1.

Figure 4.5: Catechol and hydroquinone ratio for the mononuclear copper catalyst, **C1**Figure 4.6: Catechol and hydroquinone ratio for the mononuclear nickel catalyst, **C2**

Figure 4.7: Catechol and hydroquinone ratio for the dendrimeric copper catalyst, **C6**Figure 4.8: Catechol and hydroquinone ratio for the dendrimeric nickel catalyst, **C7**

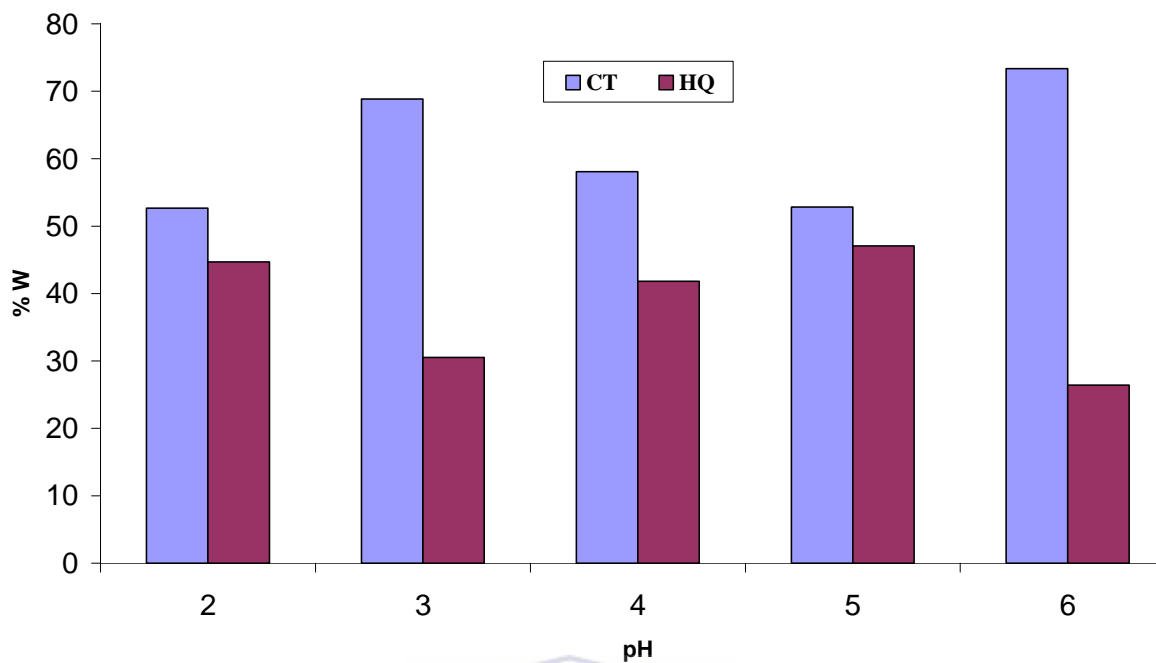


Figure 4.9: Catechol and hydroquinone ratio for the MCM-41 supported copper catalysts, **Cu-MCM-41**

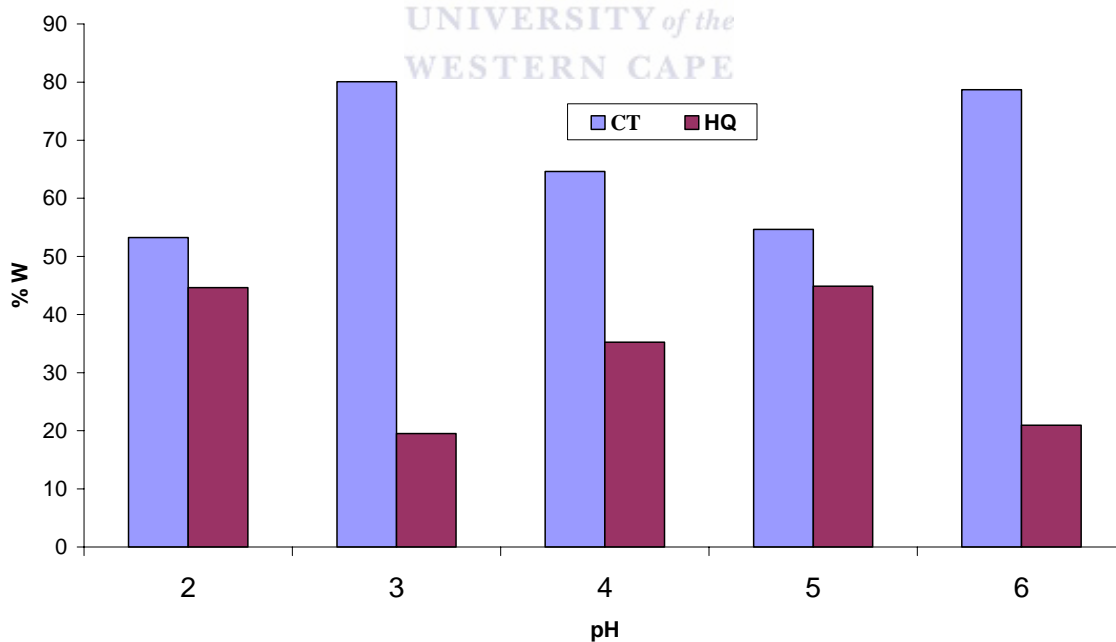


Figure 4.10: Catechol and hydroquinone ratio for the MCM-41 supported nickel catalysts, **Ni-MCM-41**

#### 4.2.6: Effect of the nature of the metal on

##### *i. Phenol conversion*

Copper catalysts were observed to be more active than the nickel catalysts. It is well known that copper has higher efficiency as an oxidation catalyst. When a comparison of the two metals was made for the same ligand system, the copper analogues showed better activity. **C1** is more active than **C2**, **C6** than **C7** and **Cu-MCM-41** than **Ni-MCM-41**. The catalysts also showed similar trend of activity at different pH values of the reaction medium.

##### *ii. Product selectivity*

For all the catalysts investigated under our conditions, hydroquinone and catechol were observed as the major products. However the nickel catalysts (**C2**, **C7** and **Ni-MCM-41**) showed higher selectivity for catechol over hydroquinone as compared to the copper systems (**C1**, **C6** and **Cu-MCM-41**). The predominance of catechol over hydroquinone is not unexpected as both metals mediate hydroxylation occurring via a free radical mechanism and the phenol OH is an ortho directing group.<sup>21</sup>

UNIVERSITY of the  
AP E

#### 4.2.7: Heterogeneous versus homogeneous catalyst

##### *i. Phenol conversion*

The activities of the immobilized and unimmobilized catalysts were also compared. In case of the nickel systems, it was observed that the MCM-41 supported catalyst, **Ni-MCM-41**, was more active than the unsupported, **C2**. The low activity of **C2** could be due to possible dimerization of the metal centers or formation of the stable peroxonickel(II) complex. In the case of dimerization the catalyst activity is reduced while when the peroxonickel(II) complex is formed, it's high stability hinders the transfer of the oxygen to the substrate. The increase in activity on immobilization of the mononuclear complex would suggest that the peroxonickel (II) complex is not formed. If this were the case, the activity would not have changed. The immobilization onto MCM-41 prevents the dimerization leading to improved activities in the **Ni-MCM-41** catalyst. This is due to the increased distance between any two metal centers thus reducing the chance of dimerization. The supporting of catalyst on dendrimer was not as effective in



preventing catalyst dimerization. As shown in Tables 4.1 and 4.2, **C1** and **C7** gave lower activities than the **Ni-MCM-41**. This implies that the 1<sup>st</sup> generation diaminobutane-poly (polyleneamine) dendrimer does not offer sufficient distance between any two metal centers to prevent dimerization.

However the opposite is observed in the copper analogues. The unimmobilized, **C1**, is more active than the immobilized one, **CuMCM-41**. This means that the copper catalyst, **C1**, does not undergo dimerization of metal centers or aggregation thus the catalyst life-time is not drastically affected as in the nickel systems. In addition stable homogeneous catalysts are often more active than heterogeneous systems. The MCM-41 nickel system showed an increase in activity compared to the homogeneous system. The activities of the Ni system are similar to what was reported by Maurya *et al.*<sup>12</sup> They observed that the polymer-anchored molybdenum (IV) and vanadium (IV) complexes of salen type ligands showed higher turnover rates than the corresponding unsupported complexes. This was also observed by Lui and co-workers when they compared a homogeneous and MCM-41 supported iron (II)-8-quinolinol complexes.<sup>24</sup> Maurya *et al.*<sup>12</sup> also obtained better selectivity for catechol formation over hydroquinone for both the unsupported as well as polymer supported catalysts.

*ii. Selectivity of hydroxylation products*

On comparing the homogeneous and heterogeneous catalysts, hydroquinone and catechol were observed as major products for both types of catalysts. Catechol was the most favoured of the two products. Nevertheless product distribution was not dependent on the nature of the system, whether homogeneous or heterogeneous, but rather on the pH of the reaction medium. For example **C2** shows 100 % selectivity for catechol over hydroquinone at pH 2 and 6 while at pH 3 a CT: HQ ratio of 2.6:1 was obtained. Maurya *et al.*<sup>12</sup> also obtained better selectivity for catechol formation over hydroquinone for both the unsupported as well as polymer supported catalysts.

#### 4.2.8: Effect of H<sub>2</sub>O<sub>2</sub> concentration on

##### 1. Phenol conversion

The effect of H<sub>2</sub>O<sub>2</sub> concentration on the phenol hydroxylation is shown in Table 4.4. These reactions were carried out at a constant phenol concentration and at pH 3, using 0.01 mmol Cu, **C1**. It was observed that a change of the PhOH:H<sub>2</sub>O<sub>2</sub> ratio from 1:1 to 1:2 exhibited no significant change in activity while a change to 2:1 results in a drastic reduction. Therefore an increase of the hydroxyl radical does not increase the conversion. This suggests that the rate determining step is not the formation OH radical. It appears that phenol concentration rather than H<sub>2</sub>O<sub>2</sub> concentration has a significant impact on the conversion. From Table 4.4 it can be seen that doubling the [PhOH] leads to a dramatic drop in conversion.

Table 4.4: Effect of H<sub>2</sub>O<sub>2</sub> concentration (PhOH:H<sub>2</sub>O<sub>2</sub>) on phenol hydroxylation<sup>a</sup>

PhOH:H <sub>2</sub> O <sub>2</sub>	% phenol conversions	TOF <sup>c</sup>		% selectivity (w/w) <sup>b</sup>		
		CT	HQ	BQ		
1:1	82.00	13.7	66.97	32.23	0.8	
1:2	81.31	13.6	63.64	35.87	0.49	
2:1	59.82	10.0	77.58	21.12	1.31	

<sup>a</sup> 10mL buffer solution, [M] = 1 x 10<sup>-4</sup> molL<sup>-1</sup>, Phenol:M = 100:1, 30% H<sub>2</sub>O<sub>2</sub> as oxidant; 110 °C at 1 atm O<sub>2</sub>

<sup>b</sup> Products , HQ, CT and BQ, distribution is given on a tar free basis

<sup>c</sup> TOF = moles phenol consumed/moles metal/hour

##### 2. Selectivity of hydroxylation products

The concentration of H<sub>2</sub>O<sub>2</sub> also affects the ratio of catechol and hydroquinone. In the case where a PhOH: H<sub>2</sub>O<sub>2</sub> ratio of 1:1 is used, a CT: HQ ratio of 2:1 is obtained. An increase in [H<sub>2</sub>O<sub>2</sub>] only leads to a slight reduction in the ratio to 1.8:1 while the decrease results in greater catechol production.

### 4.3: Conclusion

Six catalysts of Cu and Ni based on N,N-chelate ligands were found to be active for the hydroxylation of phenol. The copper catalysts were found to be more active than the nickel catalysts with the mononuclear copper catalyst, **C1**, being the most active under the conditions used. This was expected as **C1** is a homogeneous system. For all the catalysts the major products detected were catechol and hydroquinone. Nevertheless, these catalysts appear more selective to catechol over hydroquinone.

It can be seen that the MCM-41 immobilized Cu and Ni catalysts were more stable than the homogeneous analogues. They gave relatively steady conversion of phenol apart from at pH 2 where the conversion drastically reduces for the **Ni-MCM-41** catalyst. The product selectivity also remains similar with a ratio of 1:1 at pH 2, and a 2:1 ratio at the other pH values for **Cu-MCM-41** while the **Ni-MCM-41**. The increased amount of hydroquinone formed especially in the **Ni-MCM-41** can be attributed to the shape of the product formed inside the porous channels of MCM-41. The nickel systems were also found to be more sensitive to pH changes.

### 4.4: Experimental

#### 4.4.1: Materials and instrumentation

Disodium tetraborate decahydrate ( $\text{Na}_2\text{B}_4\text{O}_7 \cdot 10\text{H}_2\text{O}$ ) and potassium hydrogen phosphate ( $\text{KH}_2\text{PO}_4$ ) were purchased from B & M Scientific, potassium chloride and acetonitrile from BDH Chemicals Ltd, sodium hydroxide and hydrochloric acid (32 %) were from Kimix Chemicals, while potassium hydrogen phthalate ( $\text{CO}_2\text{H} \cdot \text{C}_6\text{H}_4 \cdot \text{CO}_2\text{K}$ ) was purchased from Nice Chemicals. Phenol, catechol, hydroquinone, benzoquinone and formic acid were obtained from Sigma-Aldrich Ltd and  $\text{H}_2\text{O}_2$  (30 % wt) was from Merck Chemicals Ltd. All chemicals were used without further purification. Oxidation reactions were carried out on a 12 place Radley's Discovery Technologies parallel reactor equipped with glass reaction vessels. High-pressure liquid chromatography (HPLC) was performed on a HP 1090 liquid chromatograph equipped with a ZORBAX<sup>®</sup> C18 column of dimensions 4.6 x 150 mm and a UV visible spectrophotometer. The pH of the buffers was measured at 25 °C using a Metrohm Limited 744 pH meter.

#### 4.4.2: Phenol hydroxylation

Phenol hydroxylation was performed on a 12 place Radley's Discovery Technologies Heated Carousel Reaction Station fitted with a reflux unit as well as a gas distribution system. The reactions were carried out in 45 mL glass reaction vessels under an oxygen atmosphere in deionized water buffered at the appropriate pH. Required amounts of each catalyst giving 0.01 mmol metal, 1 mmol of phenol and 10 mL of buffer solution were added to the glass vessel. The mixture was stirred and heated to 110 °C. Then the resulting mixture was stirred at 110 °C for 15 min. The hydroxylation was initiated by addition of 1 mmol 30 % H<sub>2</sub>O<sub>2</sub> (w/w) and allowed to progress for 6 h under reflux. After 6 h, the reaction mixture was cooled to r. t. and 1 mL portions removed and diluted to 10 mL and filtered through a nylon syringe filter membrane. The products were analyzed with a HP 1100 liquid Chromatograph equipped with a ZORBAX SB-C18 column of dimensions 4.6 x 150 mm at ambient temperature eluted by a two-component gradient programme starting with 0.1 % formic acid. The percentage of the second solvent, CH<sub>3</sub>CN, was increased linearly from 0 to 10 % during the first 5 min, then 40 % during the next 10 min and then reduced to 0 in the last 10 min. Detection of the products was performed with a dual wavelength UV detector (254 and 275 nm). A calibration curve was used to determine the amount of unreacted phenol and products formed. The phenol converted and selectivity of catechol, hydroquinone and benzoquinone were based on molar percentages.

#### 4.5: References

1. F. Luck, *Catal. Today*, **27** (1996) 195.
2. W. Zhao, Y. Luo, P. Deng, Q. Li, *Catal. Lett.*, **73** (2001) 199.
3. J. G. Mei, S. M. Yu, J. Cheng, *Catal. Commun.*, **5** (2004) 437.
4. A. Sorokin, B. Meunier, *Chem. Commun.*, (1994) 1799.
5. K. Zhu, L. Chibiao, W. Yue, *Appl. Catal. B*, **16** (1998) 365.
6. S. Jiang, Y. Kong, J. Wang, X. Ren, Q. Yan, *J. Por. Mater.*, **13** (2006) 341.
7. J. Barrault, J-M. Tatibouët, N. Papayannakos, *C. R. Acad. Sci., Ser. IIC: Chim.*, **3** (2000) 777.

8. J-Q. Xie, J-Z. Li, X-G. Meng, C-W. Hu, X-C. Zeng, *Trans. Met. Chem.*, **29** (2004) 388.
9. J. Zhang, Y. Tang, J-Q. Xie, J-Z. Li, W. Zeng, C-W. Hu, *J. Serb. Chem. Soc.*, **70** (2000) 1137.
10. M. R. Maurya, I. Jain, S. J. J. Titinchi, *Appl. Catal.: A*, **249** (2003) 139.
11. C. R. Jacobs, S. P. Varkey, P. Ratnasamy, *Micropor. Mesopor. Mater.*, **22** (1998) 465.
12. M. R. Maurya, M. Kumar, S. J. J. Titinchi, H. S. Abbo, S. Chand, *Catal. Lett.*, **86** (2003) 97.
13. M. R. Maurya, U. Kumar, P. Manikandan, *J. Chem. Soc., Dalton Trans.*, (2006) 3561.
14. A. Santos, E. Barroso, F. García-Ochoa, *Catal. Today*, **48** (1999) 109.
15. A. Pintar, J. Levec, *J. Catal.*, **135** (1992) 345.
16. A. Pintar, J. Levec, *Chem. Eng. Sci.*, **47**(1992) 2395.
17. A. Santos, P. Yustos, A. Quintanilla, F. García-Ochoa, *Top. Catal.*, **33** (2005) 181.
18. S. Ray, S. F. Mapolie, J. Darkwa, *J. Mol. Cat. A: Chem.*, **267** (2007) 143.
19. A. Alejandre, F. Medina, P. Salagre, A. Fabregat, J. E. Sueira, *Appl. Catal.: B*, **18** (1998) 307.
20. Y. H. Hue, A. Gedeon, J. L. Bonardet, N. Melush, J. B. D'Espinose, J. Fraissard, *Chem. Commun.*, (1999) 1967.
21. J. Wang, J-N. Park, H-C. Jeong, K-S. Choi, X-Y. Wei, S-I. Hong, C. W. Lee, *Energy and Fuels*, **18** (2004) 470.
22. J. L. van Wyk, S. Mapolie, A. Lennartson, M. Håkansson, S. Jagner, Z. *Naturforsch., B: Chem. Sci.*, **62b** (2007) 331.
23. J-M. Tatibouët, E. Guélou, J. Fournier, *Top. Catal.*, **33** (2005) 225.
24. C. Lui, Y. Shan, X. Yang, X. Ye, Y. Wu, *J. Catal.* **168** (1997) 35.

## **Chapter 5 : Summary and Future Work**



### 5.1: Summary

Monofunctional and multifunctional pyrrole-imine ligands have been successfully synthesized and obtained in good yields. The monofunctional ligands were prepared by the condensation of pyrrole-2-carboxylaldehyde with propyl amine, 2,6-diisopropylaniline, and 3-aminopropyl-triethoxysilane. The multifunctional ligand was obtained using the dendrimeric poly(propylene) imine as a synthetic scaffold. These ligands were characterized using a combination of techniques to establish the molecular structure. These include  $^1\text{H-NMR}$ ,  $^{13}\text{C-NMR}$ , and FT-IR spectroscopy and ESI-MS spectrometry. Microanalysis was performed to confirm the purity of the product.

The complexes of the four ligands were prepared from  $\text{Cu}(\text{OAc})_2 \cdot \text{H}_2\text{O}$ ,  $\text{Ni}(\text{OAc})_2 \cdot 4\text{H}_2\text{O}$  and  $\text{Co}(\text{OAc})_2 \cdot 4\text{H}_2\text{O}$ . The complexes were characterized by ESI-MS, FT-IR and their purity confirmed by microanalysis. The monofunctional ligands gave mononuclear complexes while the multifunctional ligand gave binuclear complexes. Single crystal X-ray crystallography of complexes **C3**, **C4** and **C5** was performed to determine the molecular structure. The three structures show that the complexes formed are mononuclear. The structures reveal that the ligands are bidentately coordinated to the metal with a *trans*-geometry. We were unable to obtain the Co complexes of **L2** and **L4**. Various methods reported in the literature with slight modification were employed but all attempts proved to be futile.

The inorganic support MCM-41 was prepared by the hydrolysis of tetraethylorthosilicate in the presence of a templating agent cetyltrimethylammonium bromide. Calcination was done to remove the organic material. The triethoxysilane functionalized complexes of copper and nickel, **C9** and **C10** respectively, were then covalently anchored onto the MCM-41. The obtained catalysts were characterized by FT-IR spectroscopy,  $\text{N}_2$  sorption analysis and X-ray diffraction. Highly crystalline MCM-41 material was obtained and the crystallinity was retained after the immobilization of the metal complexes as evident from the XRD results. The optimal metal loading was observed as 0.74 % for the **Cu-MCM-41** and 0.43 % for **Ni-MCM-41**. The  $\text{N}_2$  sorption study showed that the MCM-41 material synthesized was of high surface area of over  $1\ 200\ \text{m}^2\text{g}^{-1}$  and a pore volume of 1

$\text{cm}^3\text{g}^{-1}$ . These values decrease once the metal complexes are anchored. The **Cu-MCM-41** material surface area reduces to  $1019 \text{ m}^2\text{g}^{-1}$  with a pore volume of  $0.80 \text{ cm}^3\text{g}^{-1}$  while the **Ni-MCM-41** material gave a surface area of  $1086 \text{ m}^2\text{g}^{-1}$  and pore volume of  $0.80 \text{ cm}^3\text{g}^{-1}$ .

These catalysts showed moderate to high activity efficiency in the oxidation of cyclohexene with  $\text{H}_2\text{O}_2$  as oxidant in an oxygen atmosphere. The catalytic activity is highly dependent on the concentration of the metal, substrate and the oxide. The copper catalysts were the most active. However under some of the reaction conditions we used three of the expected products, 2-cyclohexene-1-one 2-cyclohexene-1-ol and cyclohexene-oxide, were obtained. This was also observed for the Co systems. The nickel systems were most selective with only two products, 2-cyclohexene-1-one and cyclohexene oxide, being the only observed products. The homogeneous systems were found to be more active than the heterogeneous ones.

Some of the complexes were also evaluated as catalyst in the oxidation of phenol. It is clear that the catalytic activity of these complexes in the hydroxylation of phenol to the dihydroxylbenzenes (catechol and hydroquinone), is dependent on the pH of the reaction medium. The optimal pH was established to be between 3 and 4 for all the catalysts. At pH lower than 3, all the catalysts showed dramatic reduction in activity while at higher pH the activity reduced then leveled out as the pH was further increased. With regard to selectivity, the catalysts were more selective for catechol over hydroquinone.

## **5.2: Future work**

Future prospects of this work include investigating the nature of the unidentified products in the cyclohexene oxidation. Probing the effects of other reaction conditions such as temperature and other solvents e.g.  $\text{CH}_2\text{Cl}_2$  is recommended. In the case of phenol hydroxylation, evaluation of the cobalt complexes is also important. Other conditions of temperature, basic pH solutions could be carried out. An understanding of the kinetics and the thermodynamic trends of these catalysts is also important. Thus a mechanistic



study involving the interaction of these catalysts and the substrates also needs some attention.

